UNIVERSITY OF CALIFORNIA SAN DIEGO

Pacific climate variability: insights from coral records, Earth System Models, and novel geochemical tracers

A dissertation submitted in partial satisfaction of the
requirements for the degree of

Doctor of Philosophy

in

Oceanography

by

Sara Cassandra Sanchez

Committee in charge:

Christopher Charles (chair)
Jose Carriquiry
James Leichter
Art Miller
Margaret Schoeninger
Shang-Ping Xie

2018

The Dissertation of Sara Cassandra Sanchez is approved, and it is acceptable in quality and form for publication on microfilm and electronically:

Chair

University of California San Diego

2018

EPIGRAPH

Don't panic.
-*D. Adams*

Fortitudine vincimus
By endurance we conquer
-*E. Shackleton*

If I can't scuba, then what's this all been about?
-*C. Bratton*

TABLE OF CONTENTS

LIST OF ABBREVIATIONS

AL	Aleutian Low
CAM	Community Atmosphere Model
CCS	California Current System
CESM	Community Earth System Model
CMIP	Climate Model Intercomparison Project
CPW	Central Pacific Warming
DIC	Dissolved Inorganic Carbon
DJF	December-January-February
ECF	Extracellular calcifying fluid
EPW	Eastern Pacific Warming
ENSO	El Nino Southern Oscillation
EOF	Empirical Orthogonal Function
ETNP	Eastern tropical north Pacific
FR	Fore reef
GCM	Global Climate Model
GPH	Geopotential Height
ITCZ	Intertropical Convergence Zone
JJA	June-July-August
LME	Last Millennium Ensemble
LE	Large Ensemble
MAM	March-April-May

MCA	Maximum Covariance Analysis
MLD	Mixed layer depth
N3	Nino 3
N4	Nino 4
N3.4	Nino 3.4
N1+2	Nino 1+2
NADA	North American Drought Atlas
NEP	Net Ecosystem Production
NEC	Net Ecosystem Calcification
NPO	North Pacific Oscillation
NPGO	North Pacific Gyre Oscillation
PCA	Principal Component Analysis
PDB	Pee Dee belemnite
PDO	Pacific Decadal Oscillation
PDSI	Palmer Drought Severity Index
PMIP	Paleoclimate Model Intercomparison Project
PMM	Pacific Meridional Mode
PNA	Pacific-North America
PSU	Practical salinity unit
RCP	Representation Concentration Pathway
RT	Reef terrace
SOM	Slab ocean model
SON	September-October-November

SSH	Sea surface height
SSS	Sea surface salinity
SST	Sea surface temperature
U	Zonal winds
V	Meridional winds
WES	Wind-Evaporation-Sea Surface Temperature
WTNP	Western tropical north Pacific

LIST OF TABLES

LIST OF FIGURES

ACKNOWLEDGEMENTS

Without the aid of many wonderful people, my Ph.D. would have simply been impossible (not to mention a good deal less interesting and far less fun). Before this spring, I knew that I would have many people to thank for the enormous amount of help I have received over the last 6+ years. However, getting hit by a truck really highlighted just how phenomenal my colleagues, friends, and family are.

First and foremost, I must thank my advisor, Chris Charles, for being a constant source of support throughout my time at Scripps. Chris's ever open office door, extensive familiarity with far flung reaches of scientific literature, and willingness to discuss a whole host of topics, allowed me to tackle a variety of questions and develop this dissertation. Chris's willingness to help in even the most wild of research hangups, patience (courage?) in reading and editing my rough drafts, and encouraging attitude helped me stay motivated and finish this dissertation.

I'd like to thank my other committee members for their help and support. Art, thanks for the encouraging conversations about Pacific climate variability, volcanic eruptions, and wine. Shang-Ping, thank you for being an invaluable source of exciting new ideas about tropical climate dynamics and for your willingness to chat about my research. Jose, thank you for your willingness to collaborate with me early in my graduate school years and for fostering a deep appreciation for the Eastern Tropical North Pacific and coral geochemistry. Jim, thanks for helping with fieldwork in Moorea and providing good discussion about physical processes on coral reefs. Margaret, I thank you for your willingness to talk about the academic process and providing truly interesting North American anthropological context for my paleo work.

Labmates and alumi in the Charles lab deserve significant acknowledgement; Pat, Danny, Niko, Alan, and Riley were critical in adjusting to research and learning the ropes at Scripps. Alan and Riley deserve particular acknowledgement for being deeply involved in my education in carbonate mass spectrometry and the San Diego IPA scene.

Outside of the lab, none of my fieldwork would have been possible without the help of Jessica Carilli or Rich Walsh. Early in graduate school, Jess taught me about coral drilling (despite my never having seen a real coral in the ocean before!), and even generously loaned equipment and equipment specifications. Rich Walsh was incredibly patient and helpful in developing effective methodology in my fieldwork ventures. An enormous thank you is also owed to Rich for accompanying me to French Polynesia in the middle of winter to drill coral cores, and the Smith lab (Amanda, Cailin, Clint, Mike) for aiding in the coral drilling at Palmyra. Also thank you to Christian McDonald for all of the help in planning these expeditions!

The science encouragers of my early years deserve so much appreciation. I'd particularly like to thank Lina Patino and Lisa Rom who were the first to inform me that real people can have a career in scientific research, and heartily encouraged me to get involved in lab work during my undergraduate. I'd also like to thank Julie Cole, Diane Thompson, and Heidi Barnett for mentoring me through said lab work, and for making it fun. Another very important person in my path to science is Michele Dufault. Long conversations at Pie in the Sky and forwarding fictitious, ridiculous grad school applications made the idea of graduate school seem, not just less intimidating or conceivable, but a natural next step to never stop exploring.

So many people at Scripps deserve acknowledgement for keeping science exciting, morale high, and life fun. Sharing a small space with a single person at the end of a dark and fairly ominous hallway could have been straining for nearly seven years, but an enormous thanks

is owed to Yassir for being the best officemate. Other critical thank yous are due to members of the 2011 cohort; the faithful TG and burrito crew; earlier graduate students who instilled a solid understanding of the work-play balance and the importance of getting out in the water; Climate Journal Club regulars; the North Park crew (seriously, thank you Sarah and Maddie for keeping a great sense of humor and donating an outrageous amount of time to transporting me to medical appointments this spring); and many more. Furthermore, I'm very grateful for the thousands of miles of running in the excellent company of the Prado Racing Team, which kept me focused on goals (both inside and outside of science).

My family- Mom, Dad, Anna, Matt- while initially hesitant about the prospect of me leaving for California to dive into the wholly uncharted waters of graduate school (especially if there were sharks involved!), deserve enormous acknowledgement for being extremely supportive throughout this process. I am very lucky to have family that I can call on and put things in perspective. Additionally, I am outrageously lucky to have benefitted from your unwavering belief in my abilities; it has truly been essential to this process. I also must thank Chris, whose humor, keen eye for new running trails, regular reminders about the importance of sleep, and relentless encouragement has been indescribably valuable to the completion of my Ph.D., but also life in general.

I'm extremely grateful for the additional academic and financial support I received while at Scripps. The Center for Marine Biology and Conservation and IGERT Global Change Ecosystems and Society Program were critical in providing funding and pushing me to explore interdisciplinary avenues early on in my Ph.D. I'd also like to thank the San Diego Fellowship, Wyer Family Endowed Fellowship, Krinsk Research Advancement Initiative, SIO Student travel fellowships, TA opportunities and others for allowing to complete this dissertation.

Portions of this dissertation have been published in peer reviewed journals or are in preparation for submission for publication.

Chapter 2, in full, is a reprint of the material as it appears in Geophysical Research Letters 2016. Sanchez, S. C., Charles, C. D., Carriquiry, J. D., & Villaescusa, J. A. (2016). Two centuries of coherent decadal climate variability across the Pacific North American region. *Geophysical Research Letters*, *43*(17), 9208-9216. The dissertation/thesis author was the primary investigator and author of this paper.

Chapter 3, in part, is currently being prepared for submission for publication.
Sanchez, Sara; Amaya, Dillon; Charles, Christopher; Miller, Arthur; Xie, Shang-Ping. "Variability of the Pacific Meridional Mode." The dissertation/thesis author was the primary investigator and author of this material.

Chapter 4, in part, is currently being prepared for submission for publication.
Sanchez, Sara; Charles, Christopher; Rae, James; Stewart, Joseph; Smith, Jennifer; Takeshita, Yuichiro. "Constraining paleo carbonate chemistry: new insights from $\delta^{11}B$ and B/Ca measurements in corals from Palmyra Atoll". The dissertation/thesis author was the primary investigator and author of this material.

VITA

2011 B.S. University of Arizona

2016 M.S. Scripps Institution of Oceanography

2018 Ph.D. Scripps Institution of Oceanography

PUBLICATIONS

Sanchez, S. C., Charles, C. D., Carriquiry, J. D., & Villaescusa, J. A. (2016). Two centuries of coherent decadal climate variability across the Pacific North American region. *Geophysical Research Letters*, *43*(17), 9208-9216.

Rafter, P. A., Sanchez, S. C., Ferguson, J., Carriquiry, J. D., Druffel, E. R., Villaescusa, J. A., & Southon, J. R. (2017). Eastern tropical North Pacific coral radiocarbon reveals North Pacific Gyre Oscillation (NPGO) variability. *Quaternary Science Reviews*, *160*, 108-115.

Sanchez, S. C., Amaya, D.A., Charles, C. D., Miller, A. J., & Xie, S. P. Pacific Meridional Mode over the last Millennium. *In prep.*

Sanchez, S. C., Charles, C. D., Rae, J. B., & Stewart, J. A. (2016). Constraining paleo carbonate chemistry: new insights from $\delta^{11}B$ and B/Ca measurements in monitored corals from Palmyra Atoll. *In prep.*

ABSTRACT OF THE DISSERTATION

Pacific climate variability: insights from coral records, Earth System Models, and novel geochemical tracers

by

Sara Cassandra Sanchez

Doctor of Philosophy in Oceanography

University of California San Diego, 2018

Professor Christopher D. Charles, Chair

This dissertation aims to understand the mechanisms and consequences of the low frequency "unforced" component of variability in the climate system using interannual and decadal variability as a platform to investigate phenomena thought to be sensitive to greenhouse gas emissions. To combat the lack of temporally extended instrumental observations, this

dissertation relies on coral geochemistry and Earth System Models to identify the historical range of Pacific climate variability.

Chapter 2 describes the analysis of a roughly 200 year-long coral record from Clarion Island, in the Revillagigedos Archipelago, Mexico. This record expresses substantial decadal variability in the oxygen isotopes, strongly coherent with other paleoproxies in the central equatorial Pacific and in Southern California, indicative of a coordinated system of ocean-atmospheric interaction. To best resolve the key processes involved, "forward models" are employed to interpret the decadal variability in the coral record.

The **third chapter** complements the first by addressing a mechanism responsible for the modulation of decadal variability in the North Pacific; the Pacific Meridional Mode (PMM). The Community Earth System Model-Last Millennium Ensemble (CESM-LME) is used to estimate the historical range of PMM variability, highlighting the considerable power of natural variability within the system. I investigate the physical processes associated with adjustments in PMM variance, emphasizing that relatively small anomalies in the background state have a significant influence on PMM variability.

Chapter 4 examines the roles of physical and biologically mediated processes on coral calcification from within an equatorial Pacific coral reef. Motivated by the biogeochemical implications of the previous sections, this work examines the manifestation of pH tracers in coral skeletal tissue across a network of diverse, monitored reef sites at Palmyra Atoll. Corals were analyzed for $\delta^{11}B$, trace metal, $\delta^{18}O$, and $\delta^{13}C$ composition. Despite a narrow range in the pH of seawater, high variance in $\delta^{11}B$ were observed between sites, and within single sites, suggesting that individual coral colonies have differential capacities to regulate pH variability and other environmental stressors.

Chapter 1.

Introduction

This chapter serves as an introduction to the dissertation. This dissertation embraces many elements of paleoclimate research to better understand the mechanisms by which various aspects of the ocean/atmosphere system contribute to, or respond to "unforced" climate variability and "forced" climate change. Much emphasis is placed on addressing the questions: "Is the observed variability unprecedented? What governs the behavior of natural variability? Are significant changes be expected with increased greenhouse gas concentrations?" I use interannual-decadal climate variability as a platform to investigate the means by which sensitive systems are projected to change due to a modified background state. Here, the term "sensitive systems" refers to large scale coupled-ocean atmosphere interactions in the subtropical Pacific and, at a much smaller scale, coral reef systems in the tropical Pacific. This dissertation's underlying questions are chiefly motivated by concerns identified in modern observations and forecasted in future projections, such as extremes in decadal climate variability and linkages to

North American hydroclimate; the activity of an important precursor to the El Nino Southern Oscillation, and the ability of corals to tolerate environmental extremes. These questions are addressed using a medley of observations, paleoproxy evidence, and model output and these approaches are outlined briefly below.

This thesis is comprised of three separate sections. The chief focus of chapters 2 and 3 is the analysis of decadal variability in the Northeastern Pacific. Climate variability in this region is thought to be particularly sensitive to climate change. To fully address this topic, an introduction into interannual and decadal Pacific climate variability is necessary.

The two key modes of decadal variability of the Pacific are the Pacific Decadal Oscillation (PDO) and the North Pacific Gyre Oscillation (NPGO). The PDO is defined as the first EOF of sea surface temperature anomalies in the Pacific between 20° and 60° degrees north, and while it spatially resembles the El Nino Southern Oscillation (ENSO), it has a dominant period of 20-30 years (Figure 1.1A). In the atmosphere, the PDO is linked to the strength of the Aleutian Low (AL). The PDO was discovered when salmon fisheries experts noticed large, decadal scale oscillations in fisheries yields [Mantua et al.1997]. This sign change, or "regime shift" has occurred in 1925, 1947, 1976 and 1997 [Mantua et al. 1997, Minobe et al. 1997]. As the spatial signature suggests, the PDO is highly related to canonical ENSO [Shakun and Shaman 2009, Newman et al. 2003, Alexander et al. 2002, DiLorenzo et al. 2010].

The North Pacific Gyre Oscillation (NPGO) is defined as the second EOF of sea surface height in the North Pacific, but represents the second EOF of SST variability, and physically represents the strengthening and weakening of the subtropical gyre [DiLorenzo et al. 2008] (Figure 1.1B). The NPGO is important for ecosystem function as this mode best explains salinity and nutrient variability along the eastern Pacific [DiLorenzo et al. 2009]. The atmospheric

component of the NPGO is the North Pacific Oscillation (NPO), an oscillation with a characteristic dipole structure in sea level pressure, a predominantly decadal periodicity [Walker and Bliss 1932] and a large role on surface temperature and precipitation patterns in the southwestern United States [Linkin and Nigam 2007, Pierce 2005]. The North Pacific Gyre Oscillation has been dynamically linked to the Central Pacific ENSO phenomenon [DiLorenzo et al. 2010, Furtado et al. 2012]. While the relative power of the NPGO is less than that of the PDO in 20th century observations, the strength of the NPGO has been amplifying in the last several decades, perhaps as a result of its relationship with the central Pacific warming events [DiLorenzo et al. 2008, DiLorenzo et al. 2010, DiLorenzo and Mantua 2017].

The North Pacific modes of decadal variability are thought to foster fundamentally different interactions between the tropics and the subtropics in the Northeastern Pacific. Two pathways are highlighted in these exchanges: a quick, yet globalizing role of the atmosphere and a slower, longer persisting role for the ocean. Key mechanisms of tropical-subtropical interactions are the "atmospheric bridge", the "ocean tunnel" and the "meridional mode". In an atmospheric bridge framework, tropical sea surface temperature anomalies excite atmospheric Rossby waves that interact with asymmetries in the zonal mean flow and midlatitude storm tracks that eventually influence remote sea surface temperatures. The anomalies are sustained for longer periods of time through the reemergence mechanism [Alexander et al. 2002]. In an ocean tunnel pathway, the North Pacific's deep mixed layer allows sea surface temperature anomalies to stay below the surface for a summer and either re-emerge the next winter, or travel along isopycnals to be upwelled at the tropics [Gu and Philander 1997]. The Meridional Mode, deeply discussed in this thesis, is a way in which subtropical anomalies can influence the equatorial regions. In this framework of anomalies, extratropical atmospheric anomalies create

sea surface temperature anomalies in the subtropics. These anomalies persist long enough for the trade winds, closer to the tropics, to respond. As the trade winds respond, localized SST anomalies develop via the Wind-Evaporation- Sea surface temperature (WES) feedback [Xie and Philander 1994], prompting further wind anomalies. This feedback of anomalies can influence the development of ENSO events [Vimont et al. 2001, Vimont et al. 2003, Chiang and Vimont 2004].

Canonical ENSO warm events are thought to be initiated in the equatorial regions by westerly wind bursts and the propagation of thermocline anomalies (Figure 1.1C)**, [**Yu et al. 2011]. The El Nino/ La Nina pattern of variability is the first EOF of sea surface temperature anomalies in the tropical Pacific, but can also be calculated using area averaged anomalies in the equatorial Pacific. The anomalies associated with canonical ENSO are focused in the eastern equatorial Pacific and propagate via the atmospheric bridge and coastal Kelvin waves [Chelton and Davis 1982] which can cause long Rossby waves to travel westward across the Pacific [Jacobs 1994]. Canonical ENSO variability has been thought to influence the Pacific Decadal Oscillation [Shakun and Shaman 2009].

While no two El Nino events the same, Central Pacific Warming events are thought to represent a fundamentally different ocean-atmospheric interaction. Central Pacific events are the second EOF of sea surface temperature anomalies in the tropical Pacific and distinguish themselves by the focused anomalies in the central equatorial Pacific, rather than the eastern equatorial Pacific, as is typical with the canonical ENSO events. The Central Pacific events, differ in initiation is well; these anomalies are initiated via the Pacific Meridional Mode (PMM), [Vimont et al. 2015, Vimont et al. 2003, Yu et al. 2010, Yu and Kim 2011]. In this processes, sea surface temperature anomalies are observable southwest of Baja a year to 9-10 months ahead of

the central equatorial Pacific. Central Pacific events have been thought to be related to the NPGO because sea surface temperature anomalies in the central equatorial Pacific excite atmospheric Rossby waves which interact with the southern node of the North Pacific Oscillation [Furtado et al. 2012]. The NPO forces both the NPGO and initiates the "seasonal footprinting" sea surface temperature anomalies (Figure 1.1B). Central Pacific ENSO variability is thought to have become more prevalent since 1979 due to the heightened anthropogenic influence; a modeling study found that in a warmer world, El Nino Modoki becomes five times more common than the canonical, eastern Pacific El Nino due to a weakening of the mean Walker Circulation [Yeh et al. 2009].

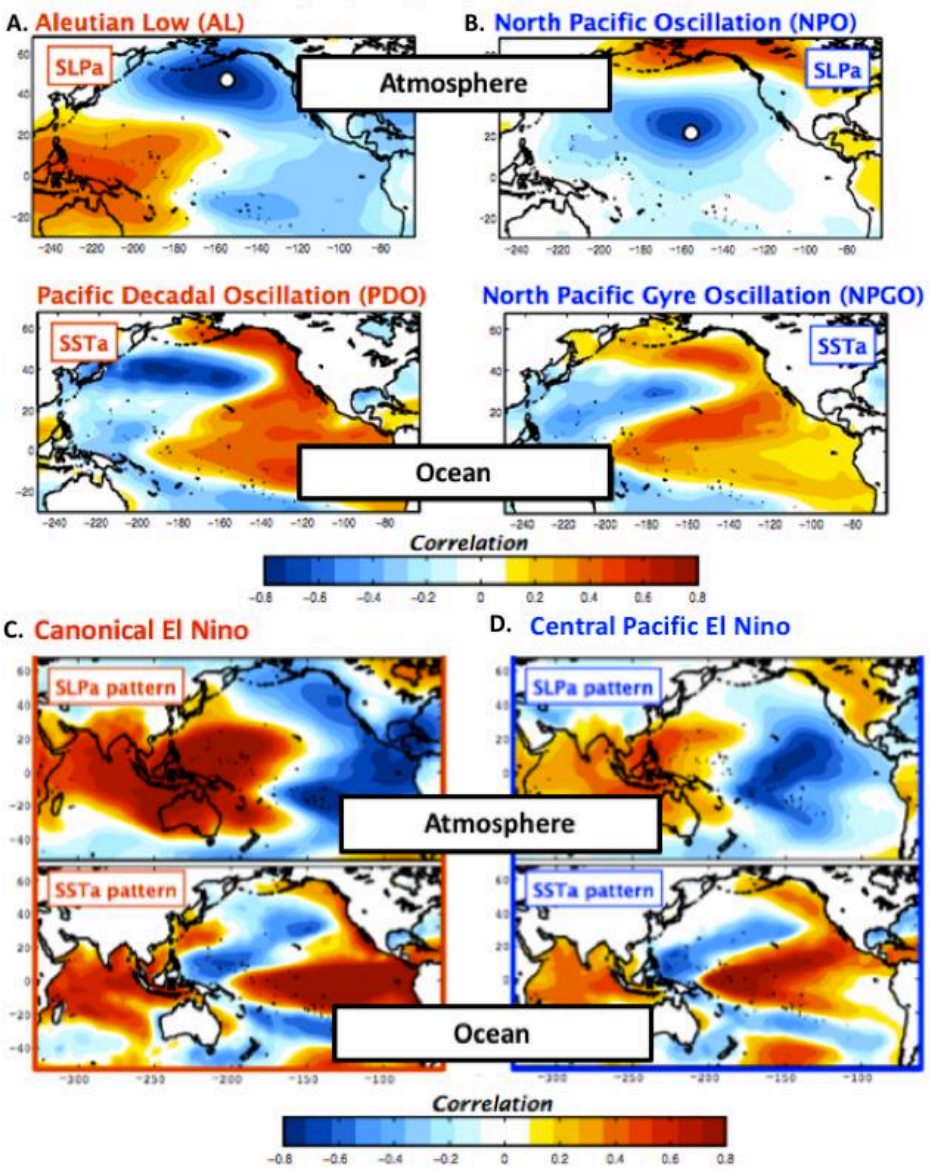

Figure 1.1 Modes of Pacific Climate Variability. Adapted from DiLorenzo and Schneider 2010, spatial representation of the dominant modes of climate variability in the Pacific Ocean. **4A).** The SLP and SST anomalies associated with canonical ENSO, the first EOF of tropical Pacific SST variability. **4B).** The same, but for ENSO Modoki, the second EOF of tropical Pacific SST variability. **4C).** The same but for the Pacific Decadal Oscillation, the first EOF of North Pacific SST variability. **4D).** The same, but for the North Pacific Gyre Oscillation, the second EOF of North Pacific SST variability.

It is still unclear if these flavors of interannual and decadal variability are completely independent of each other; many view the system as a continuum where multiple mechanisms are important [Takahashi et al. 2011, Newman et al. 2011, DiLorenzo et al. 2015, DiLorenzo et al. 2010, Okumura et al. 2017, Ogata et al. 2012, etc].

Uncertainties regarding climate variability highlight one of the most pervasive issues in climate science; a shortage of continuous, high quality, observations. While instrumental observations in the Pacific exist, they are sparse, and observational methods have changed dramatically through time. As an example using SST observations, recent decades are well constrained by satellite coverage, but prior to 1950, observational products struggle to consolidate the differing observational methodologies due to different interpolation/gridding methods, and differing means of dealing with extreme or missing values [Yasunaka and Hanawa 2011]. The diverse methodologies (various types of insulated buckets, engine room intake sensors, ship hull sensors, drifting and moored buoys, and night time marine air temperature) have required bias correction [Kent et al. 2017, Cowtan et al. 2017], but a diversity of bias correction methods have been used, with no clear superior methodology [Comboul et al. 2015]. The significance of these bias corrections are readily observed when comparing datasets in the relatively under-sampled tropical IndoPacific, where long-term trends vary widely [Solomon and Newman 2012, Cowtan et al. 2017, Kent et al. 2017] and bias correction tends to play a larger role due to potential influence of large surface latent heat fluxes [Folland and Parker 1995, Weller and Anderson 1996]. The lack of consistent methodology can distort the estimation of long term trends in the climate system, the magnitude of extreme events, and decadal variability.

Paleoclimate archives provide a means of reconstructing past climates, before the instrumental era. In particular, IndoPacific coral records offer potential to aid in long term climate reconstruction; intervals of their skeletal growth consistently yield geochemical clues, interpretable as environmental metrics. *Porites* corals records grow outwards, adding new layers of aragonite each year. In each layer, the coral incorporates information from the ambient seawater into its skeleton, allowing reconstruction of climatic variables from coral archives.

These coral records span ~70-150 years at roughly monthly resolution, and fossil corals can further extend these geochemical observations back centuries, far beyond the instrumental record. **Figure 1.2** Identifies the location, resolution and length of IndoPacific coral record, previously published or mentioned in this thesis. This thesis uses $\delta^{18}O$, $\delta^{13}C$, $\delta^{11}B$, Li/Ca, B/Ca, Na/Ca, Mg/Ca, Sr/Ca, Ba/Ca, U/Ca measurements to constrain climate variability in the Pacific.

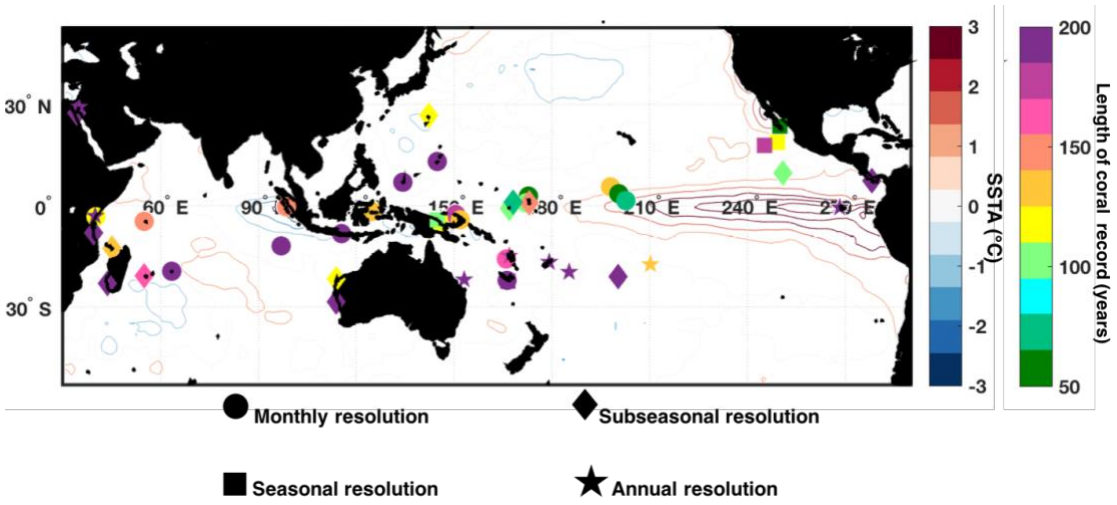

Figure 1.2. Displays the monthly SST anomalies of December of 1997, one of the largest El Nino events in observed history in red-blue contours. The location of 48 SST-relevant coral records from the NOAA paleoclimate archive and personal data are shown in bullets. The color of the bullets corresponds to the length of the available coral record over the 1800-2010 period. The shape of bullets corresponds to the resolution of the individual coral record; 75% of records are at monthly or subseasonal resolution. Records were obtained from the NOAA Paleoclimate archives (https://www.ncdc.noaa.gov/data-access/paleoclimatology-data) or data I have personally handled.

In **Chapter 2**, the generation and analysis of a roughly 200 year-long coral record from Clarion Island, roughly 400 miles southwest of Baja California, Mexico suggests that temperature can only explain a fraction of the substantial decadal variability expressed in the oxygen isotopes. This robust decadal signal is strongly coherent with other paleoproxies in the central equatorial Pacific and hydroclimate records in Southern California, indicative of a coordinated system of high amplitude ocean-atmospheric interaction. To best resolve the key mechanisms controlling the coral's geochemical record, I employ a "forward model" of the

decadal variability in the coral record. Given the location of the coral record, the observations serve to emphasize the importance of the "meridional mode" that connects low and mid-latitude climate variability. I show that the activity of this meridional mode was especially strong during the latter stages of the Little Ice Age (early 19th century).

Chapter 3 is complimentary to the second chapter in that it pursues an evaluation of the variability of Pacific Meridional Mode over the last millennium. Climate models are essential for this purpose because even the network of extended paleoclimatic archives is severely limited in the Eastern Tropical North Pacific. The last millennium serves as a useful experimental platform for this analysis as it features modulations in interannual, decadal, and centennial climate due to the varying influence of solar cycles, volcanic eruptions, introduction of greenhouse gases, land use change, aerosol and ozone emissions, orbital forcing, and natural variability. Additionally, the last millennium has emphasized that unforced aspects of the climate system can be highly sensitive to small shifts in external forcing. In this chapter, I take advantage of recent modelling experiments associated with an array of multiple ensemble members, each prescribed with identical forcing conditions, but marginally different initial conditions. This array of ensemble members allows for a better quantification of the influence of natural variability on climate. In this section, the CESM's Last Millennium Ensemble suggests that the Pacific Meridional Mode has an enormous range of natural variability. Even more, the CESM-LME illustrates commonalities in the background state between periods of historically high and low PMM variance, consistent with the paleoproxy record and some observational studies. While the observed variance of the present day is relatively high, the variance under RCP8.5 forcing is expected to dramatically increase.

Chapter 4 of this thesis uses observations the large 2015-2016 El Nino event as a platform to investigate the roles of physical and biologically mediated processes on coral calcification. For this chapter, I collected and analyzed samples from a diverse network of monitored corals at Palmyra Atoll for the incorporation of traditional and novel geochemical tracers. Particular focus is placed on the relatively new carbonate chemistry tracers; boron isotopes ($\delta^{11}B$) and elemental boron concentrations (B/Ca), but $\delta^{18}O$, $\delta^{13}C$, and trace metal composition were also measured. This chapter documents a highly variable response of coral $\delta^{11}B$ during extreme stress, despite a relatively narrow range of seawater pH, indicating that individual corals differ in ability to moderate the pH of their extracellular calcifying fluid.

In greater detail, during this biomineralization process, corals transport Ca^{2+} and HCO_3^-, or allow the diffusion of uncharged aqueous CO_2, through the layers of tissue and into a layer called the extracellular calcifying fluid (ECF). This extracellular calcifying fluid layer is thought to be a semi-enclosed environment, influenced by seawater, yet susceptible to internal coral regulation. The mechanism by which the coral acquires carbon is yet unsettled. There are three principal pathways by which corals acquire this carbon: a diffusive pathway, an active transport pathway to transport charged ions across a membrane with an ion transporter, and thirdly, infiltration of seawater [Adkins et al. 2003, Allemand et al. 2011]. While it is uncertain the degree to which the coral controls actual mineral growth [Lowenstam 1981], it is agreed upon that corals actively manipulate the chemistry of their calcifying fluid. One relevant example of a coral manipulating its own internal chemistry is the biomineralization process. A coral must maintain a pH higher than that of seawater in this extracellular calcifying fluid to allow for the precipitation of aragonite. This process is more difficult when the pH of the surrounding reef seawater is lower, because it steepens the pH gradient between the seawater and the ECF [Ries et

al. 2011, Kubota et al. 2017, Doney et al. 2009, Hoegh-Guldberg et al. 2007], emphasizing a key danger of ocean acidification on coral reefs.

Boron isotopic composition in coral aragonite could serve as an effective monitor of the regulation of calcifying fluid chemistry. There are two species of dissolved boron in seawater: boric acid and borate, and the speciation varies as a function of pH. The isotopic composition of borate, the species preferentially incorporated into carbonates, therefore also varies with the pH of seawater [Hemming Hanson 1992, McCulloch et al. 2012, Gagnon 2013, Klochko et al. 2006]. Borate is thought to substitute for carbonate ion in coral skeletal formation [Holcomb et al. 2016]. Given the method of incorporation, the boron isotopic ratio, $\delta^{11}B$, shows great promise in capturing variations in seawater pH in biogenic carbonate, but still has unclear biological influences. It is expected that skeletal boron isotope composition would be influenced by the coral "upregulation" of their internal ECF pH, but laboratory experiments have documented that boron isotope incorporation in corals can still reflect the pH of reef seawater through a linear, species dependent offsets [Trotter et al. 2011, Honisch et al. 2004, Honisch and Hemming 2007, Venn 2013].

Some paleoclimatic tracers can provide insight into these biological processes. Some tracers, such as carbon isotopes, or even the annual extension rate have highly documented biological influence [Grottoli et al. 2002, Lough et al. 2014]. Other proxies are less explicitly influenced by these biological processes. The experiment design in Chapter 4 accentuates the different processes imprinting themselves on the coral skeleton; by sampling monitored, yet diverse reef sites it is possible to assess a range of processes from the reef scale to organismal scale. Special emphasis is placed on identifying the individual, small scale differences in reef

environments that influence coral resilience and evaluating the manifestation of their local environment on the suite of geochemical tracers.

Taken together, this thesis highlights the wide range of natural variability within the physical and geochemical components of the climate system. However, in most studies, projections using increased greenhouse gas concentrations suggest that climate change is and will continue to fundamentally alter these systems.

1.1 References

Adkins, J. F., Boyle, E. A., Curry, W. B., & Lutringer, A. (2003). Stable isotopes in deep-sea corals and a new mechanism for "vital effects". *Geochimica et Cosmochimica Acta*, *67*(6), 1129-1143.

Alexander, M. A., Bladé, I., Newman, M., Lanzante, J. R., Lau, N. C., & Scott, J. D. (2002). The atmospheric bridge: The influence of ENSO teleconnections on air-sea interaction over the global oceans. Journal of Climate, 15(16), 2205-2231.

Allemand, D., Tambutté, É., Zoccola, D., & Tambutté, S. (2011). Coral calcification, cells to reefs. In *Coral reefs: an ecosystem in transition* (pp. 119-150). Springer Netherlands.

Chelton, D. B., & Davis, R. E. (1982). Monthly mean sea-level variability along the west coast of North America. *Journal of Physical Oceanography*, *12*(8), 757-784.

Chiang, J. C., & Vimont, D. J. (2004). Analogous Pacific and Atlantic Meridional Modes of Tropical Atmosphere-Ocean Variability*. Journal of Climate, 17(21), 4143-4158.

Comboul, M., Emile-Geay, J., Hakim, G. J., & Evans, M. N. (2015). Paleoclimate sampling as a sensor placement problem. *Journal of Climate*, *28*(19), 7717-7740.

Cowtan, K., Rohde, R., & Hausfather, Z. (2017). Evaluating biases in Sea Surface Temperature records using coastal weather stations. *Quarterly Journal of the Royal Meteorological Society*.

Di Lorenzo, E., Liguori, G., Schneider, N., Furtado, J.C., Anderson, B.T. and Alexander, M.A., 2015. ENSO and meridional modes: A null hypothesis for Pacific climate variability. *Geophysical Research Letters*, *42*(21), 9440-9448.

Di Lorenzo, E. and Mantua, N., 2016. Multi-year persistence of the 2014/15 North Pacific marine heatwave. *Nature Climate Change*, *6*(11),1042-1047.

Di Lorenzo, E., Cobb, K. M., Furtado, J. C., Schneider, N., Anderson, B. T., Bracco, A., Alexander, M.A., & Vimont, D. J. (2010). Central Pacific El Niño and decadal climate change in the North Pacific Ocean. Nature Geoscience, 3(11), 762-765.

Di Lorenzo, E., Fiechter, J., Schneider, N., Bracco, A., Miller, A.J., Franks, P.J.S., Bograd, S.J., Moore, A.M., Thomas, A.C., Crawford, W. and Peña, A., 2009. Nutrient and salinity decadal variations in the central and eastern North Pacific. *Geophysical Research Letters*, *36*(14).

Di Lorenzo, E., Schneider, N., Cobb, K.M., Franks, P.J.S., Chhak, K., Miller, A.J., McWilliams, J.C., Bograd, S.J., Arango, H., Curchitser, E. and Powell, T.M., 2008. North Pacific Gyre Oscillation links ocean climate and ecosystem change. *Geophysical Research Letters*, *35*(8).

Di Lorenzo, E., & Schneider, N. (2010). *An overview of Pacific climate variability*. Technical Report, 1–10.

Doney, S. C., Fabry, V. J., Feely, R. A., & Kleypas, J. A. (2009). Ocean acidification: the other CO2 problem.

Folland, C. K., & Parker, D. E. (1995). Correction of instrumental biases in historical sea surface temperature data. *Quarterly Journal of the Royal Meteorological Society*, *121*(522), 319-367.

Furtado, J. C., Di Lorenzo, E., Anderson, B. T., & Schneider, N. (2012). Linkages between the North Pacific Oscillation and central tropical Pacific SSTs at low frequencies. Climate dynamics, 39(12), 2833-2846.

Gagnon, A. C. (2013). Coral calcification feels the acid. *Proceedings of the National Academy of Sciences*, *110*(5), 1567-1568.

Grottoli, A. G. (2002). Effect of light and brine shrimp on skeletal δ13C in the Hawaiian coral Porites compressa: a tank experiment. *Geochimica et Cosmochimica Acta*, *66*(11), 1955-1967.

Gu, D., & Philander, S. G. (1997). Interdecadal climate fluctuations that depend on exchanges between the tropics and extratropics. Science, 275(5301), 805-807.

Hemming, N. G., & Hanson, G. N. (1992). Boron isotopic composition and concentration in modern marine carbonates. *Geochimica et Cosmochimica Acta*, *56*(1), 537-543.

Hemming, N. G., & Hönisch, B. (2007). Chapter seventeen boron isotopes in marine carbonate sediments and the ph of the ocean. *Developments in Marine Geology*, *1*, 717-734.

Hoegh-Guldberg, O., Mumby, P.J., Hooten, A.J., Steneck, R.S., Greenfield, P., Gomez, E., Harvell, C.D., Sale, P.F., Edwards, A.J., Caldeira, K. and Knowlton, N. (2007). Coral reefs under rapid climate change and ocean acidification. *science*, *318*(5857), 1737-1742.

Holcomb, M., DeCarlo, T. M., Gaetani, G. A., & McCulloch, M. (2016). Factors affecting B/Ca ratios in synthetic aragonite. *Chemical Geology*, *437*, 67-76.

Hönisch, B., Hemming, N., Grottoli, A. G., Amat, A., Hanson, G. N., & Bijma, J. (2004). Assessing scleractinian corals as recorders for paleo-pH: Empirical calibration and vital effects. *Geochimica et Cosmochimica Acta*, *68*(18), 3675-3685.

Jacobs, G. A., Hurlburt, H. E., Kindle, J. C., Metzger, E. J., Mitchell, J. L., Teague, W. J., & Wallcraft, A. J. (1994). Decade-scale trans-Pacific propagation and warming effects of an El Nino anomaly.

Klochko, K., Kaufman, A. J., Yao, W., Byrne, R. H., & Tossell, J. A. (2006). Experimental measurement of boron isotope fractionation in seawater. *Earth and Planetary Science Letters*, *248*(1-2), 276-285.

Kubota, K., Yokoyama, Y., Ishikawa, T., Suzuki, A. and Ishii, M., 2017. Rapid decline in pH of coral calcification fluid due to incorporation of anthropogenic CO 2. *Scientific reports*, *7*(1), p.7694.

Kent, E.C., Kennedy, J.J., Smith, T.M., Hirahara, S., Huang, B., Kaplan, A., Parker, D.E., Atkinson, C.P., Berry, D.I., Carella, G. and Fukuda, Y. (2017). A call for new approaches to quantifying biases in observations of sea surface temperature. *Bulletin of the American Meteorological Society*, *98*(8), 1601-1616.

Linkin, M. E., & Nigam, S. (2008). The north pacific oscillation-west Pacific teleconnection pattern: Mature-phase structure and winter impacts. Journal of Climate, 21(9), 1979-1997.

Lough, J. M., & Cantin, N. E. (2014). Perspectives on massive coral growth rates in a changing ocean. *The Biological Bulletin*, *226*(3), 187-202.

Lowenstam, H. A. (1981). Minerals formed by organisms. *Science*, *211*(4487), 1126-1131.

Mantua, N. J., Hare, S. R., Zhang, Y., Wallace, J. M., & Francis, R. C. (1997). A Pacific interdecadal climate oscillation with impacts on salmon production.Bulletin of the american Meteorological Society, 78(6), 1069-1079.

McCulloch, M., Trotter, J., Montagna, P., Falter, J., Dunbar, R., Freiwald, A., ... & Taviani, M. (2012). Resilience of cold-water scleractinian corals to ocean acidification: Boron isotopic systematics of pH and saturation state up-regulation. *Geochimica et Cosmochimica Acta*, *87*, 21-34.

Minobe, S. (1997). A 50–70 year climatic oscillation over the North Pacific and North America. Geophysical Research Letters, 24(6), 683-686.

Newman, M., Shin, S. I., & Alexander, M. A. (2011). Natural variation in ENSO flavors. Geophysical Research Letters, 38(14).

Newman, M., Compo, G. P., & Alexander, M. A. (2003). ENSO-forced variability of the Pacific decadal oscillation. Journal of Climate, 16(23), 3853-3857.

Ogata, T., Xie, S.P., Wittenberg, A. and Sun, D.Z., 2013. Interdecadal amplitude modulation of El Niño–Southern Oscillation and its impact on tropical Pacific decadal variability. *Journal of Climate*, *26*(18), 7280-7297.

Okumura, Y.M., Sun, T. and Wu, X., 2017. Asymmetric modulation of El Niño and La Niña and the linkage to tropical Pacific decadal variability. *Journal of Climate*, *30*(12),4705-4733.

Pierce, D. W., California Energy Commission., & Scripps Institution of Oceanography. (2005). Effects of the North Pacific Oscillation and ENSO on seasonally averaged temperatures in California: PIER project report. Sacramento, Calif.: California Energy Commission.

Ries, J. B. Skeletal mineralogy in a high-CO_2 world. *J. Exp. Mar. Biol. Ecol.* **403**, 54–64 (2011).

Shakun, J. D., & Shaman, J. (2009). Tropical origins of North and South Pacific decadal variability. *Geophysical Research Letters*, *36*(19).

Solomon, A., & Newman, M. (2012). Reconciling disparate twentieth-century Indo-Pacific ocean temperature trends in the instrumental record. *Nature Climate Change*, *2*(9), 691.

Takahashi, K., Montecinos, A., Goubanova, K., & Dewitte, B. (2011). ENSO regimes: Reinterpreting the canonical and Modoki El Niño. Geophysical Research Letters, 38(10).

Trotter, J., Montagna, P., McCulloch, M., Silenzi, S., Reynaud, S., Mortimer, G., Martin, S., Ferrier-Pagès, C., Gattuso, J.P. and Rodolfo-Metalpa, R., 2011. Quantifying the pH 'vital effect'in the temperate zooxanthellate coral Cladocora caespitosa: Validation of the boron seawater pH proxy. *Earth and Planetary Science Letters*, *303*(3), 163-173.

Venn, A. A., Tambutté, E., Holcomb, M., Laurent, J., Allemand, D., & Tambutté, S. (2013). Impact of seawater acidification on pH at the tissue–skeleton interface and calcification in reef corals. *Proceedings of the National Academy of Sciences*, *110*(5), 1634-1639.

Vimont, D. J., Alexander, M. A., & Newman, M. (2014). Optimal Growth of Central and East Pacific ENSO Events. Geophysical Research Letters.

Vimont, D. J., Battisti, D. S., & Hirst, A. C. (2001). Footprinting: A seasonal connection between the tropics and mid-latitudes. Geophysical research letters,28(20), 3923-3926.

Vimont, D. J., Wallace, J. M., & Battisti, D. S. (2003). The seasonal footprinting mechanism in the Pacific: implications for ENSO*. Journal of climate, 16(16), 2668-2675.

Walker, G. T., & Bliss, E. W. (1932), World weather, V. Mem. Roy. Meteor. Soc., 4, 53-84.

Weller, R. A., & Anderson, S. P. (1996). Surface meteorology and air-sea fluxes in the western equatorial Pacific warm pool during the TOGA Coupled Ocean-Atmosphere Response Experiment. *Journal of Climate*, *9*(8), 1959-1990.

Xie, S. P., & Philander, S. G. H. (1994). A coupled ocean-atmosphere model of relevance to the ITCZ in the eastern Pacific. Tellus A, 46(4), 340-350.

Yasunaka, S., & Hanawa, K. (2011). Intercomparison of historical sea surface temperature datasets. *International Journal of Climatology*, *31*(7), 1056-1073.

Yeh, S. W., Kug, J. S., Dewitte, B., Kwon, M. H., Kirtman, B. P., & Jin, F. F. (2009). El Niño in a changing climate. Nature, 461(7263), 511-514.

Yu, J. Y., & Kim, S. T. (2011). Relationships between extratropical sea level pressure variations and the central Pacific and eastern Pacific types of ENSO. Journal of Climate, 24(3), 708-720.

Yu, J. Y., & Kim, S. T. (2010). Three evolution patterns of central-Pacific El Niño. *Geophysical Research Letters*, *37*(8).

Yu, J. Y., Kao, H. Y., & Lee, T. (2010). Subtropics-related interannual sea surface temperature variability in the central equatorial Pacific. *Journal of Climate*, *23*(11), 2869-2884.

Chapter 2.

Two centuries of coherent decadal climate variability across the Pacific North American region

Abstract

The decadal variability of the Pacific Ocean and North American hydroclimate are subjects of immediate concern for society, yet the length of the instrumental record limits full mechanistic understanding of this variability. Here I introduce a 178 year, seasonally resolved coral oxygen isotopic record from Clarion Island (18°N, 115°W), a region that is strongly influenced by the decadal-scale fluctuations of the North Pacific Gyre Oscillation (NPGO) and a subtropical region that serves as a critical locus for the communication of climate anomalies with the tropics. This Mexican Pacific coral record is highly correlated to coral records from the central tropical Pacific and tree ring records from western North America. Significant changes in the amplitude of oceanic decadal variability in the early 19th century are mirrored in the drought reconstructions in western North America. The spatial manifestation of this relationship was relatively invariant, despite notable changes in the climatic mean state.

2.1 Introduction

The extreme climate of 2012-2015 across the Pacific North American region featured concerted oceanic and atmospheric anomalies spanning nearly the entire Pacific Basin, from the tropics to the subpolar regions. These conditions, estimated to have cost billions of dollars in damage [Howitt et al. 2014], involved i.) a persistent atmospheric ridge of high pressure extending from Alaska to California [Swain et al. 2014] that blocked the moisture-rich midlatitude Pacific storm track, causing exceptional drought on the West Coast [Griffin Anchukaitis 2014, Williams et al. 2015]; and ii.) an adjacent trough that directed Arctic air into East Coast/ Midwest regions, prompting harsh winter conditions [Hartmann et al. 2015, Baxter et al. 2015]; and iii.) record breaking sea surface temperatures in the North Pacific [Bond et al. 2015, Hobday et al. 2016]. Climate models and observations have suggested a variety of hypotheses to explain the origin of these interconnected anomalies. For example, they could be the product of a Rossby wave train emanating from the tropical Pacific [Seager et al. 2014, Wang et al. 2015, Watson et al. 2016] related to an El Nino Southern Oscillation (ENSO) precursor pattern associated with the North Pacific Oscillation (NPO [Wang et al. 2014, Walker and Bliss 1932, Rogers 1981,Wang et al. 2013]). Other studies have suggested that constructive interference from the extratropics, such as low arctic sea ice cover [Lee 2015], could have amplified the anomalies. Alternatively, these anomalies could reflect variations in the subtropical gyre—for example, they might owe their origin to the oceanic component of the NPO known as the North Pacific Gyre Oscillation (NPGO, Appendix A. & Figure A.1, [DiLorenzo et al. 2008, Hartmann 2015, Kilduff et al. 2015]).

Regardless of origin, one of the most extraordinary aspects of these concerted phenomena was their persistence over several consecutive winters. The most common explanations for such resilience involve teleconnecting interactions between the tropics and extratropics [eg. Latif and Barnett 1994, Alexander et al. 2002, Newman et al. 2016]. If so, at least two principal mechanisms could transmit anomalies over such broad regional and temporal scales. Firstly, sea surface temperature anomalies in the central tropical Pacific atmosphere could trigger anomalous convection, driving divergence aloft, exciting atmospheric Rossby waves and disrupting the mean flow [Sardesmukh and Hoskins 1988]. This could influence the extratropics through an atmospheric bridge type mechanism [Alexander et al. 2002] and interaction with the NPO [DiLorenzo et al. 2010, Furtado et al. 2012]. Alternatively, atmospheric variability in the midlatitudes could force anomalous sea surface temperatures and initiate a series of thermodynamic feedbacks between the winds and sea surface. A feedback loop known as the Pacific Meridional Mode [Chiang and Vimont 2004] is initiated when NPO atmospheric variability influences local subtropical sea surface temperatures and, therefore, the local meridional temperature gradient. The strength of the subtropical trade winds is altered via Wind-Evaporation-SST feedback [Xie and Philander 1994], and ultimately, the anomalous winds and sea surface temperatures propagate equatorward.

Observations of such interactions, over multiple decadal cycles and over intervals subject to different radiative forcing, would constitute a critical step for understanding the mechanisms of Pacific North American climate change, including the extreme 2012-2015 conditions. Extended observations would help address whether the conditions of the last several years were purely the result of internal (natural) climate variability [Funk et al. 2015, Seager et al. 2015, Hartmann 2015], or whether the extreme conditions were forced by greenhouse gas-induced

warming, radiative feedbacks and nonlinear responses [Wang et al. 2014, Swain et al. 2014]. Additionally, extended observations could help test whether natural modes of decadal variability such as the NPO, and thus the Pacific Meridional Mode, might be more active with greenhouse gas forcing [Wang et al. 2012, Wang et al. 2014, Furtado et al. 2012, DiLorenzo et al. 2010], thereby modifying the mechanisms by which the subtropics and tropics interact.

Most instrumental records of rainfall, drought, and SST are too brief to capture the full range of natural decadal variability. However, paleoclimatic archives from the appropriate climatic centers of action can complement the temporally limited studies of synoptic scale variability. Here I present a new seasonally resolved record of oxygen isotope variability from a coral collected at Clarion Island (18°N, 115°W), of the Revillagigedo Archipelago, Mexico. This region, known as the "Seasonal Footprinting Region," is characterized by a strong meridional SST gradient and is essential for energizing the Pacific Meridional Mode [Vimont et al. 2001, Vimont et al. 2003, Chiang and Vimont 2004]. In models and observations, sustained SST anomalies in this region propagate southwestward in the direction of the climatological trade winds, through to the Intertropical Convergence Zone and the central equatorial Pacific. Thus, the extended coral record from the region offers potential insight into one of the key mechanisms of decadal variability in the Northeastern Pacific.

I combine this new coral record with previously published tree ring and coral records to document nearly two centuries of coherent decadal-scale climate variability across the Pacific and North America. I provide evidence for historical oceanographic variability similar to the current extreme climate, featuring pronounced interaction between the mid and low latitude Pacific. I also show that the magnitude and recurrence interval of this pattern varied considerably over the past two centuries.

2.2 Methods

The Clarion coral core was sampled every 1 mm and analyzed for its oxygen isotopic composition using a ThermoMAT 253 mass spectrometer equipped with a Kiel IV carbonate preparation device. Long-term analytical reproducibility for $\delta^{18}O$ is 0.08‰, deduced from a pool of ~200 carbonate standards (including NBS-19) analyzed concurrently with the coral samples. The average extension rate of the Clarion coral is 4-6 millimeters per year, implying roughly seasonal resolution. The coral chronology uses the seasonal cycle in the oxygen and carbon isotopic data, and I anchor the extremes to fixed seasons in the year. The calendar age assignments were validated independently by the strong annual density banding (best viewed in X-ray). Thus I estimate that the coral chronology is accurate to within 6 months (no more than 1 year.)

2.3 Site Characteristics

The Clarion coral was collected in July of 1998 (by J.D.C.) from a depth of 8 meters in a well mixed, unrestricted environment with moderate currents and waves in the fore reef zone. Instrumental observations suggest that this site is ideally located to monitor several important aspects of Pacific decadal variability. Firstly, the region is strongly influenced by the variations in sea surface temperature and salinity associated with the NPGO-NPO (Figure 2.1A); sea surface temperature anomalies from Clarion Island location display significant correlation with the NPGO index ($R= -0.24$, $p<0.01$ at monthly resolution, and $R= -0.55$, $p>0.1$ with an 8 year

lowpass filter, using monthly anomalies from NOAA Extended Reconstruction from 1950-2015 [Smith and Reynolds 2003]). This correlation implies that SST at Clarion Island shares a pattern of correlation with North American continental PDSI similar to that of the NPGO–NPO (Figure 2.1B). Clarion Island lies at the termination of the California Current System (CCS); therefore it "feels" the influx of cooler, more saline water during the positive phase of the NPGO, and warmer, fresher water during the negative phase of the NPGO [DiLorenzo et al. 2008]. The Clarion coral differs significantly from other coral-based reconstructions in the eastern tropical North Pacific [Linsley et al. 2000, Tierney et al. 2015, Dunbar et al. 1994] in that it lies in the northeastern end of the Seasonal Footprinting Region. The opportunity to build long continuous records from this part of the subtropical Pacific is extremely rare, but the coral isotopic record presented here provides a record of regional conditions that extends to the early 19th century.

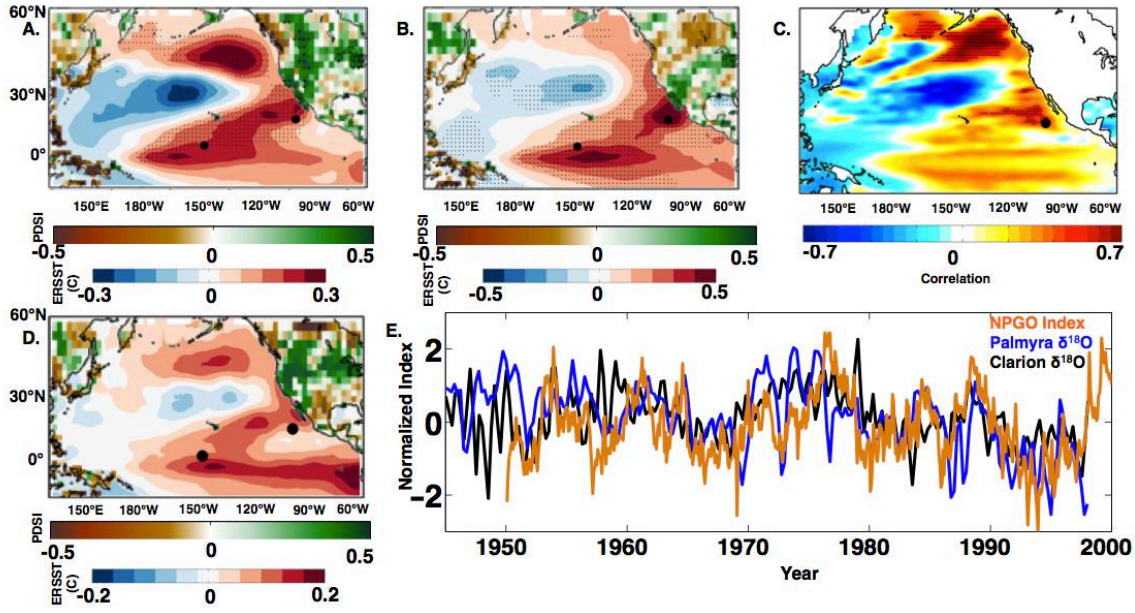

Figure 2.1 Clarion coral $\delta^{18}O$ captures NPGO-like activity. (A.) Regression of monthly mean SST anomalies (NOAA's ERSST v3b, degrees C, 1950-2013, (Smith and Reynolds 2003)) with the negative NPGO index. On the continents: regression of (inverse) NPGO on monthly mean PDSI anomalies (unitless, 1950-2014, [Dai et al. 2004]). For SST, stippling indicates confidence at 95%, and 90% for PDSI accounting for autocorrelation with effective sample size [Bretherton et al. 1999] and field

(Figure 2.1 continued)
significance testing controlled with a False Discovery Rate [Wilks 2016]. The large black circles mark the locations of Clarion Island (18N, 115W) and Palmyra Atoll (6N, 162W). (**B.)** Same as A, but SST and PDSI anomalies are regressed with SST anomalies from the Clarion Island location. (**C.)** Correlation of from AVISO Satellite sea surface height anomalies with the negative NPGO index October 1992 to December 2010. Correlation of Satellite Sea Surface Height (http://www.jason.ocea- nobs.com/) with NPGO index. Clarion Island location is denoted by a black dot, in a region highly correlated with North Pacific Gyre Oscillation SSH variability. Stippling indicates confidence at 95%, accounting for autocorrelation with effective sample size [Bretherton et al. 1999] and field significance testing controlled with a False Discovery Rate [Wilks 2016]. (**D.)** Same as A, but, as an illustration of proxy sensitivity, SST and PDSI anomalies have been seasonally averaged (JFM, AMJ, JAS, OND) and regressed with the (inverse) Clarion coral $\delta^{18}O$ from 1950-1998. **(E.)** Normalized indices of variability from 1950-2000 where the coral oxygen isotopic anomalies have been averaged seasonally. Clarion coral $\delta^{18}O$ in black, R=0.52 with NPGO index over 1950-1998 using annual averages, Palmyra coral $\delta^{18}O$ in blue R=0.54 with NPGO index over 1950-1998 using annual averages, and NPGO in orange. Negative values indicate warm temperature anomalies and positive sea surface height anomalies in the Central and Eastern Tropical North Pacific, while positive values indicate cooler conditions and low SSH anomalies. Note that while the Palmyra record also records El Niño events, the structure of the decadal variability is highly coherent among indices.

The $\delta^{18}O$ anomalies of the Clarion coral record are a product of both SST and SSS anomalies [Epstien et al. 1953, Fairbanks et al. 1997, Nurhati et al. 2011, Thompson et al. 2011]. Available instrumental observations from the region suggest that SSS is perhaps an equally important source of variability for dictating coral oxygen isotopic anomalies (Appendix A., Figure A.2). It should be noted, however, that the salinity observations prior to the ARGO program are sparse [Roemmich et al. 2011], and in the Eastern Tropical North Pacific (ETNP) various salinity reanalysis products do not completely agree with one another [Roden 1972, Kessler 2006, Delcroix et al. 2011, Carton and Giese, 2008]. In the North Pacific, the strengthening or weakening of the subtropical gyre associated with the NPGO is the dominant control of salinity variability, especially in the CCS: both the first principal component of hindcast models and timeseries of salinity anomalies in the Gulf of Alaska and Southern California yield significant correlations with the NPGO index [DiLorenzo et al. 2008, Chhak et al. 2009, DiLorenzo et al. 2009]. SSS and SST at Clarion Island tend to be highly (inversely)

correlated on the timescales of interest (see Appendix A.), and SSH data show that the Clarion region lies within a pole of high correlation to the NPGO index (Figure 2.1C). The relationship between SST, SSS and $\delta^{18}O$ [Epstien et al. 1953, Fairbanks et al. 1997] is such that $\delta^{18}O$ reflects variations in the density of seawater, which is directly related to regional sea surface height. (Low temperatures, high salinity corresponds to high $\delta^{18}O$, high density water masses, and low SSH, while high temperatures and low salinity correspond to low $\delta^{18}O$, low density water masses and positive SSH). Therefore, for discriminating large-scale patterns of variability related to the NPGO, the explicit resolution of temperature and salinity components is not essential to the analysis. I acknowledge, however, that some proposed mechanisms of Pacific decadal variability [e.g. Clement et al. 2009, Bellomo et al. 2014] rely primarily on radiative feedbacks in the subtropics and that the $\delta^{18}O$ proxy addresses such mechanisms only indirectly.

2.4 Results

The complete coral isotopic record spans the years 1819 to 1998 (Figure 2.1D and 2.2*)*. The Clarion coral record features prominent decadal scale variability throughout its length. Oxygen isotopic anomalies over the late 20th century display significant correlation with that of the NPGO index (R=0.52, p=0.01 from 1950-1998, using annual anomalies), as expected from the instrumental observations from the region. Wavelet analysis [Torrence and Compo 1998] of the full Clarion coral record confirms a continuous concentration of variance in the 9-23 year band throughout the past two centuries, and statistically significant power over the period of 1820-1870 (95% level) (Figure 2.2). Statistical significance is assessed relative to stationary red noise with the given autocorrelation of the series. While the pronounced decadal variability is the

defining characteristic of the Clarion record, an especially striking feature of the record is that, relative to the late 20th century, the magnitude of decadal variability was much larger during the early 19th century. The wavelet analysis suggests that the decadal variability of the early nineteenth century was characterized by a slightly longer period than that which prevailed throughout the 20th century (16 years vs. 12-13 years).

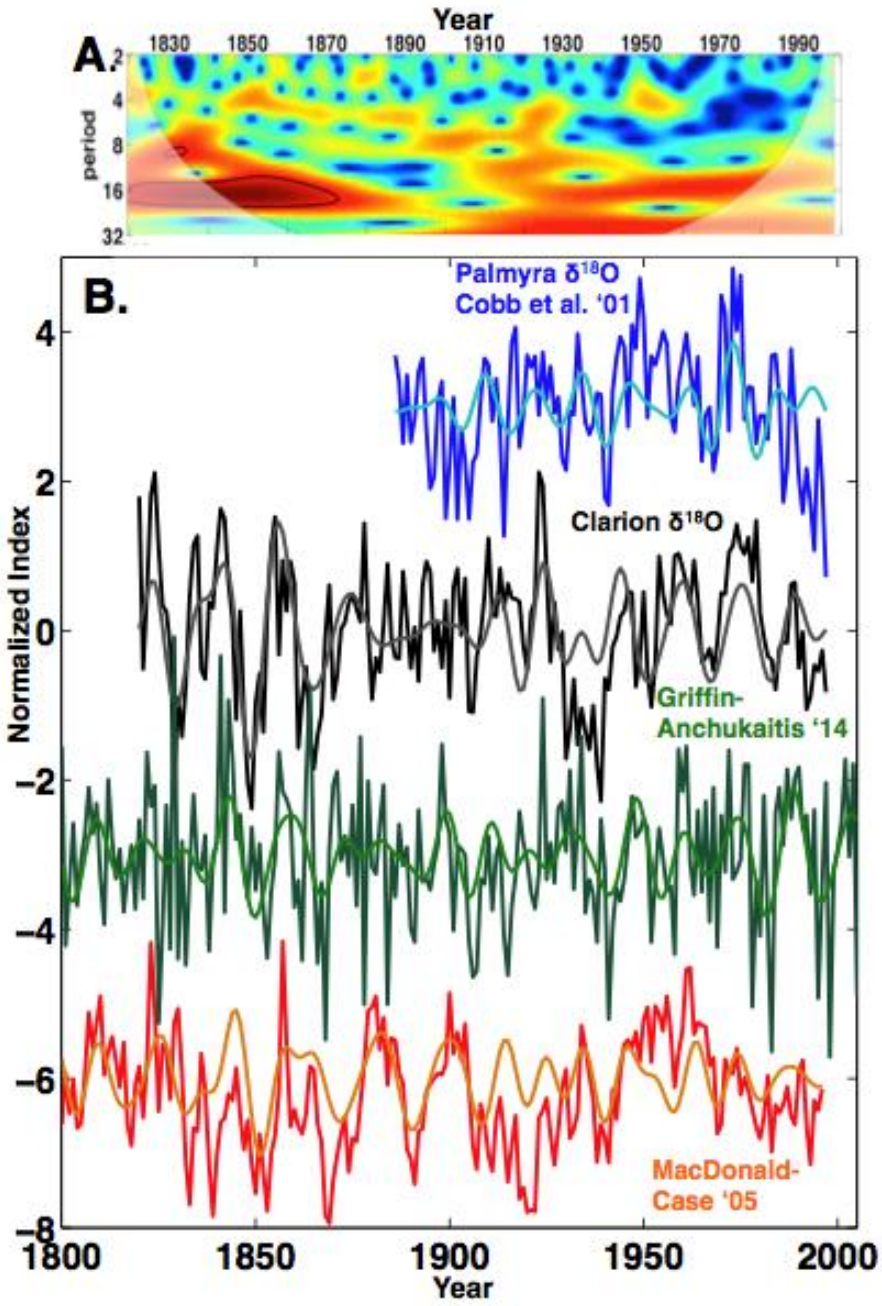

Figure 2.2 Pacific-North American paleoproxies capture amplified decadal variability in the early 19th century. (A.) Morlet mother wavelet power spectrum of Clarion $\delta^{18}O$. Black border shows the 5% significance level test against red noise [Grinstead et al. 2004]. In the Clarion coral, this significance is especially visible in between 1820 and 1870 at periods of roughly 9-23 years. **(B.)** Detrended, normalized paleo-proxy timeseries overlain with a 9-23 year bandpass filter from years 1800-2000, offset by 2 standard deviation units for visibility. The full length Clarion coral $\delta^{18}O$ in black, Griffin-Anchukaitis tree ring index in green, MacDonald-Case tree ring index in orange, Palmyra coral $\delta^{18}O$ in blue. The blue vertical lines highlight the peak of the decadal scale warm SST anomalies, dry-warm continental conditions in the paleo records during the heightened decadal variability in the period from1815-1870.

Despite these changes to the characteristics of the decadal variability, throughout the past two centuries I observe strong similarities in the timing of decadal shifts with other Pacific coral and North American tree ring records. In particular, the Clarion coral $\delta^{18}O$ record exhibits decadal variability in lockstep with that of a central tropical Pacific coral $\delta^{18}O$ record from Palmyra ([Cobb et al. 2001], Figures 2.1D and 2.2, Appendix A. Figure A.4, $R=0.38$, $p<0.01$ between Palmyra $\delta^{18}O$ and Clarion $\delta^{18}O$ from 1887-1998). There are no distinguishable leads or lags between these coral records, but it should be noted that the coral chronologies are not capable of resolving phase offsets shorter than several months. In any case, the strong correlation manifested by these two coral records confirms a strong and persistent link between the northern and southern ends of the North Pacific Seasonal Footprinting Region. On decadal timescales, sea surface temperature variability at Palmyra is strongly correlated with the NPGO ([Nurhati et al. 2011], Palmyra $\delta^{18}O$-NPGO from 1950-1998 using annual anomalies $R=0.54$, $p<0.01$).) The strong correlation between the NPGO and coral records stretching across the southern pole of the NPGO (Figures 2.1D and 2.2), from the Eastern Tropical North Pacific to the Central Tropical Pacific, establishes a means of observing tropical-extratropical communication prior to the instrumental era.

Given the association between North Pacific sea surface temperatures and the current western North American drought, I sought to establish whether such a relationship also extends to the paleoclimatic archives. A number of tree ring indices have been produced to represent hydroclimate variability over the western North American region. Current analysis [Funk et al., 2014; Seager et al., 2014a, 2015; Wang and Schubert, 2014; Wang et al., 2014; Hartmann, 2015, Palmer 2014] suggests that the atmospheric ridge, induced by Pacific SSTAs, primarily acts to halt the transport of warm, moist air over the West Coast of the United States. As California is

one of the most strongly affected regions, the California-based MacDonald and Case 2005 [Macdonald and Case 2005], and Griffin and Anchukaitis 2014 [Griffin and Anchukaitis 2014] indices are used to compare with the coral records (Figure 2.2). The MacDonald and Case 2005 tree ring record was developed using chronologies from San Gorgonio, California and Nordegg, Alberta. The Griffin and Anchukaitis 2014 record is the averaged compilation of Central-Southern California tree ring PDSI. In general, the Clarion and Palmyra coral records are significantly correlated with both tree ring indices on decadal timescales; using a 9-16 year bandpass filter, $R=0.32$, $p=0.22$ between Clarion and Palmyra (1886-1998), $R=-0.73$, $p<0.01$ between Clarion and MacDonald-Case index (1820-1995), and $R=-0.54$, $p<0.01$ between Clarion and Griffin-Anchukaitis PDSI (1820-1998) using annual averages. Importantly, both the Clarion coral and the tree ring records exhibit heightened decadal variability over the interval 1810-1865 AD (~2 standard deviations). There are differences between individual indices, as one might expect from the different regional data sources. For example, the Griffin and Anchukaitis record reveals late 20th century variability of roughly the same magnitude as that of the early 19th century. The MacDonald Case record displays strong decadal variability from the early 19th century until the late 19th century, longer than evidenced in the Clarion, Griffin-Anchukaitis, and Palmyra records. Nevertheless, these proxy records provide evidence for correlated patterns of ocean-atmosphere variability. The coherence between the Clarion coral record and the other records is found to be statistically significant on decadal timescales (at a 5% significance level using a cross wavelet coherence with Monte Carlo methods to generate an ensemble of 1,000 paired datasets with the same AR1 coefficients as the input datasets [Grinstead et al. 2004]). This is particularly the case in the early 19th century (Appendix A., Figure A.4). The coherence between these oceanic and terrestrial records demonstrate that the heightened variability of the

early 19th century was not merely a local phenomenon in the northeastern Pacific, but, rather, was the product of strong, concerted North American hydroclimate-Pacific interaction over the last two centuries.

Along with individual timeseries, the gridded North American Drought Atlas Version 2a (NADA, [Cook et al. 1999, Cook et al. 2004]) are used to explore the spatial expression of the variability associated with each of the individual coral records over the last two hundred years (Figure 2.3*)*. NADA is a gridded dataset of June-July-August PDSI developed from tree ring measurements, but tested and verified against the instrumental PDSI record over the twentieth century. For the purposes of this comparison, the coral records have been annualized using a May-April year and regressed onto the NADA field to maximize the relationship between the winter oceanic variability to the following JJA of the continental NADA archive. The statistical significance of the relationship between the NADA field and the paleo index is assessed, firstly, by altering the number of effective degrees of freedom to account for autocorrelation [Bretherton et al. 1999], and secondly, by implementing a field significance test controlled with a False Discovery Rate [Wilks 2016].

The least squares linear regression of the Clarion coral $\delta^{18}O$ record onto the tree ring NADA PDSI dataset exhibits a strong dipole structure of PDSI between southern California and central Canada (Figure 2.3A). When isolated for the period of heightened decadal variability (1820-1875), the Clarion coral's regression onto the tree ring PDSI maintains nearly identical regional patterns to that of the full record, particularly over Western North America (Figure 2.3B). The regression of the MacDonald-Case record onto the NADA record also shows a similar pattern (Figure 2.3C), as does the Griffin and Anchukaitis record (Appendix A., Figure A.3B). Furthermore, the regression of the annualized Palmyra coral $\delta^{18}O$ record also shows

similar patterns, though Palmyra record does not extend into the period of heightened 19th century variability.

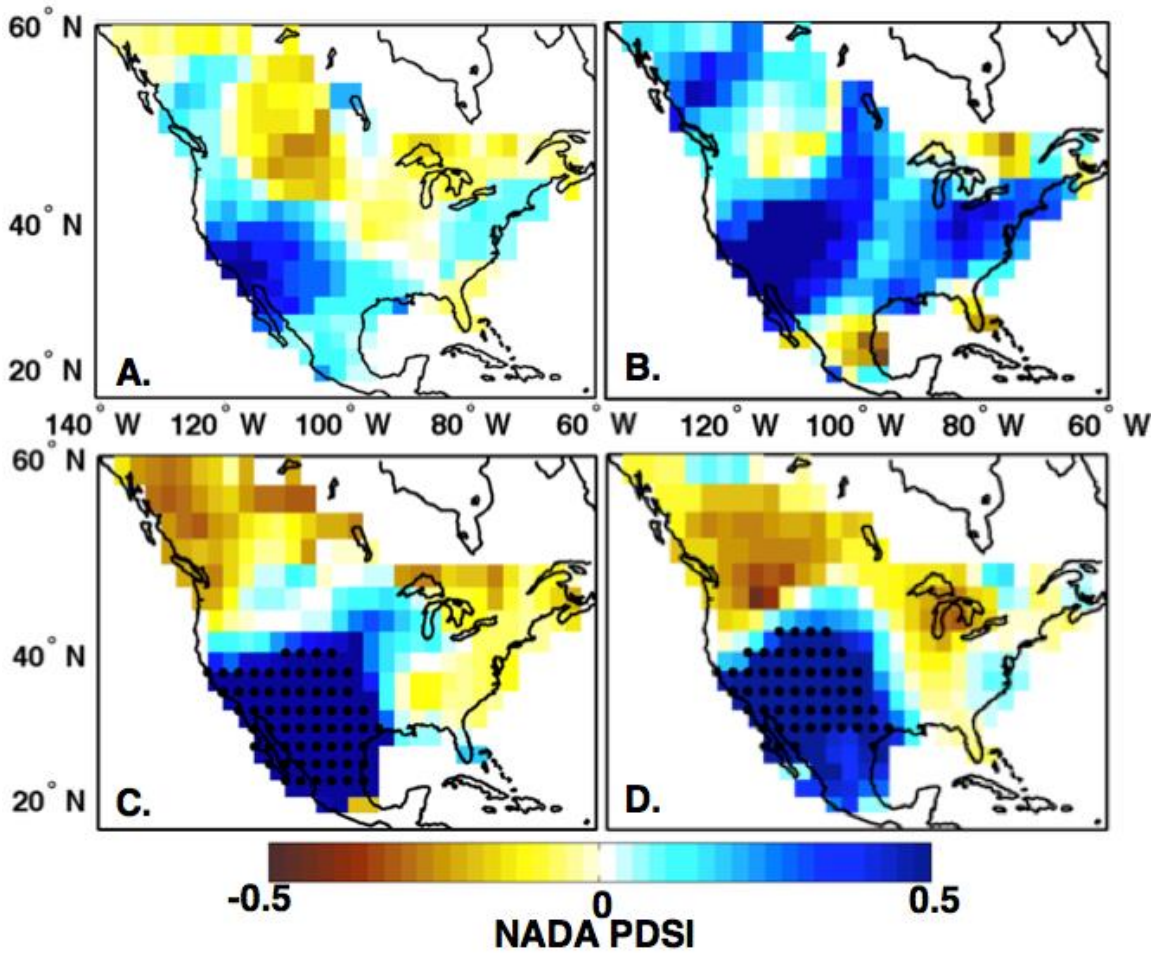

Figure 2.3 Linear regression of the NADA- PDSI data (Cook et al. 1999, Cook et al. 2004) with various paleo proxy indices. When applicable, annual anomalies were calculated over the May-April ENSO year; thus the JJA PDSI regression highlights the relationship with the previous winter SSTs. Stippling indicates confidence at 95% using a two sided student's t-test, accounting for autocorrelation via effective sample size [Bretherton et al. 1999] and field significance testing controlled with a False Discovery Rate [Wilks 2016]. **(A.).** Annual anomalies of (inverse) Clarion $\delta^{18}O$ 1820-1998. The polarity is such that cool-wet (blue) are associated with warm sea surface temperatures in the eastern tropical north Pacific, and dry-warm conditions (brown) are associated with cooler SSTs in the Clarion region. **(B.)** Annual anomalies of Clarion's $\delta^{18}O$ over the period of heightened variability (1820-1875, using the same color scheme as A). **(C.)** Annual anomalies (inverse) Palmyra $\delta^{18}O$ (1886-1998AD), using the same color scheme as A) **(D.)** MacDonald and Case tree ring series (1790-1990) creating a PDO-like index using a dipole of tree ring series from San Gorgonio, California and Nordegg, Alberta.

Interannual (i.e. ENSO) variations account for much of the variance of the Palmyra coral record and the spatial patterns of drought over North America, particularly the north-south dipole structure. Thus, from spatial regression maps alone, it is difficult to distinguish a true decadal mode of variability across the PNA region from a reddened manifestation of ENSO [Newman et al. 2016, Newman et al. 2003]. This differentiation is further complicated by the fact that the NPO, which is potentially responsible for forcing the decadal variability, is itself influenced by ENSO. Thus, a full separation of ENSO from Pacific Decadal Variability is beyond the scope here. However, the Clarion coral record may be relatively unique in illustrating the patterns of decadal variability alone (however independent they may be from ENSO). Firstly, there is very little interannual variability in the instrumental or proxy records from Clarion (Figures 2.1E and 2.2), given its location outside of the direct influence of ENSO. Secondly, the decadal scale changes in salinity monitored by the Clarion coral $\delta^{18}O$ are consistent with the strengthening (weakening) of the subtropical gyre that reflects a mechanistically distinct aspect of the NPGO. The potential discriminatory power of the Clarion record in this regard, is, however, tempered by the fact that none of the grid points in Figure 2.3A and 2.3B meet the p=0.05 threshold for field significance. Inspection of the relevant individual time series suggests that the reduced field significance (with respect to that for Palmyra for example) results directly from the absence of ENSO variance in the Clarion coral and the detrending of the NADA field.

2.5 Discussion

The similarities in the timeseries and the spatial patterns expressed in the coral and tree ring records constitutes strong evidence for synchronous decadal variability, complementing and

extending the inferences drawn from instrumental observations across the Pacific North American region. Prior studies have noted the significant role of the NPO on North American surface temperature and precipitation patterns [Pierce et al. 2004, Linkin and Nigam 2008, Baxter and Nigam 2015]. The impact of the NPO's lower frequency oceanic counterpart, the NPGO, on continental precipitation has only recently been suggested—in part because of the brevity of the instrumental record of this phenomenon. In observations, the extreme negative phase of the NPGO (warm central Pacific and warm ETNP) is associated with a tendency for a weak atmospheric ridge just west of North America, a slight offshore displacement from the winter anomalies of 2014 -2015 (Appendix A., Figure A.5); however, it is also associated with wet conditions on the western North American coast (Figure 2.1A, Appendix A., Figure A.5). This difference from the most recent expression of western North American drought highlights two critical aspects of oceanic forcing of hydroclimate: (i.) isolated modes of oceanic variability typically only account for a fraction of the continental precipitation variability--though oceanic forcing can be significant (30-40% for various regions of the US; [Seager and Hoerling 2014]), high frequency internal atmospheric processes tend to dominate continental weather; (ii.) the phase propagation and interplay between different modes of oceanic variability are important.

To the extent that the Clarion and Palmyra coral records indeed reflect the distinct dynamics of the southern pole of the NPGO, the multiple realizations of decadal fluctuations expressed in these coral archives allow for a more complete assessment of the NPGO influence on continental hydroclimate. While extended drought in North America can stem from a variety of sources [Seager et al. 2014, Seager and Hoerling 2014, Cook et al. 2007, Seager et al. 2009], the shifts from cold/dry to warm/wet conditions in Seasonal Footprinting Region were almost invariably accompanied by a concurrent shift from relative drought to relative moisture surplus

across the western U.S. This connection held regardless of the amplitude or the recurrence interval of the decadal shifts. Thus it is likely that the oceanic forcing during the intervals of northeastern Pacific phase change was powerful enough to guide the higher frequency atmospheric weather that ultimately determined PDSI.

The underlying mechanisms of the NPGO phase changes are currently debatable [Furtado et al. 2012, DiLorenzo et al. 2010], and their discrimination will undoubtedly require an extended network of observations across the various geographic poles. But, at least for the southern pole, the high correlation of the coral records presented here, showing no apparent leads or lags, requires an immediate connection between subtropical anomalies and the tropics. Climate models have shown that seasonal footprinting is an effective means of rapid anomaly propagation in the atmosphere and surface ocean between the subtropics and tropics [Vimont et al. 2001, Vimont et al. 2003]. The coral records strongly suggest that this mechanism played out repeatedly in the real ocean. This connection between subtropical anomalies and the trade winds is also a critical feature in determining the growth of different types of ENSO events [Chiang and Vimont 2004, Vimont et al. 2014, Zhang et al. 2014]. While this analysis focuses strictly on decadal variability, an avenue for future pursuit is to investigate how the strength of this tropical-subtropical connection may have influenced past ENSO variability.

It remains to be established why the decadal variance of the early 19th century was so strong and seemingly characterized by longer recurrence interval (at least with respect to the 20th century). Several studies have linked increasing variance of the NPO to greenhouse induced warming [Wang et al. 2014, DiLorenzo et al. 2010, DiLorenzo et al. 2008, DiLorenzo et al. 2015], while other studies suggest that large-scale droughts will be more prevalent in a warmer world [Swain et al. 2014, Delworth et al. 2015, Diffenbaugh et al. 2015, Williams 2015]. Perhaps

the early 19th variability was an example of unforced natural variability, but this was also a time of a dynamic radiative balance. The Northern Hemisphere experienced the close of the Little Ice Age; and the Tambora eruption in 1815 led directly to the "year without a summer" in 1816 [Wagner and Zorita 2005]. The origin of these changes is quite different from the modern radiative imbalance caused by anthropogenic greenhouse gas emissions. The fact that the spatial expression, particularly over the California region, remains much the same across these stronger decadal oscillations implies that many of physical linkages between regions remain intact, irrespective of forcing.

In conclusion, the new Clarion coral oxygen isotopic record links large scale continental hydroclimate variability to the ocean, providing evidence for concerted ocean-atmospheric interaction across the Pacific basin over the last two hundred years. The heightened variability of the early 19th century implies that the 20th century decadal scale climate swings—that, among other things, provided a baseline for water policy and use in the western U.S.--were in fact relatively mild. Thus the seeming severity of the current climate must be understood in a more comprehensive historical context.

2.6 References

Alexander, M. A., I. Blade, M. Newman, J. R. Lanzante, N. C. Lau, and J. D. Scott (2002), The atmospheric bridge: The influence of ENSO teleconnections on air-sea interaction over the global oceans, J. Clim., 15(16), 2205–2231.

Baxter, S., and S. Nigam (2015), Key Role of North Pacific Oscillation/West Pacific Pattern in Generating the Extreme 2013-2014 North American Winter, J Clim, 28(20), 8109-8117, doi:10.1175/JCLI-D-14-00726.1.

Bellomo, K., Clement, A., Mauritsen, T., Rädel, G., & Stevens, B. (2014), Simulating the role of subtropical stratocumulus clouds in driving Pacific climate variability, J Clim, 27(13), 5119-5131, doi: http://dx.doi.org/10.1175/JCLI-D-13-00548.1.

Bond, N. A., Cronin, M. F., Freeland, H., & Mantua, N. (2015), Causes and Impacts of the 2014 Warm Anomaly in the NE Pacific, Geophys Res Lett, 42(9): 3414–3420,doi:10.1002/2015GL063306.

Bretherton, C. S., Widmann, M., Dymnikov, V. P., Wallace, J. M., & Bladé, I. (1999), The effective number of spatial degrees of freedom of a time-varying field, J Clim, 12(7):1990-2009,doi:10.1175/1520-0442(1999)012<1990:TENOSD>2.0.CO;2.

Carton, J. A. , and B. S. Giese (2008), A reanalysis of ocean climate using Simple Ocean Data Assimilation (SODA), Mon. Weather Rev., 136,2999–3017, doi:10.1175/2007MWR1978.1.

Chhak, K. C., E. Di Lorenzo, N. Schneider and P. F. Cummins, 2009: Forcing of Low-Frequency Ocean Variability in the Northeast Pacific. J Clim, 22(5) 1255-1276, doi:10.1175/2008jcli2639.1.

Chiang, J. C., & Vimont, D. J. (2004), Analogous Pacific and Atlantic Meridional Modes of Tropical Atmosphere-Ocean Variability, J Clim, 17(21): 4143-4158,doi:10.1175/JCLI4953.1.

Clement, A, Burgman, R., Norris, J. (2009), Observational and model evidence for positive low-level cloud feedback, Science,325(5939),460-464, doi: 10.1126/science.1171255.

Cobb, K. M., Charles, C. D., & Hunter, D. E. (2001), A central tropical Pacific coral demonstrates Pacific, Indian, and Atlantic decadal climate connections, Geophys Res Lett, 28(11): 2209-2212,doi:10.1029/2001GL012919.

Cook, E. R., C. A. Woodhouse, C. M. Eakin, D. M. Meko, and D. Stahle (2004), Long-term aridity changes in the western United States, Science, 306(5698): 1015–1018, doi:10.1126/science.1102586.

Cook, E. R., Seager, R., Cane, M. A., & Stahle, D. W. (2007), North American drought: reconstructions, causes, and consequences, Earth-Sci, Rev. 81(1): 93-134,doi:10.1016/j.earscirev.2006.12.002.

Cook, E.R., D.M. Meko, D.W. Stahle, and M.K. Cleaveland (1999), Drought reconstructions for the continental United States, J Clim, 12:1145-1162,doi:10.1175/1520-0442(1999)012<1145:DRFTCU>2.0.CO;2.

Dai, A., K. E. Trenberth, and T. Qian (2004), A global data set of Palmer Drought Severity Index for 1870-2002: Relationship with soil moisture and effects of surface warming, J. Hydrometeorol, 5:1117–1130,doi: http://dx.doi.org/10.1175/JHM-386.1.

Delworth, T. L., Zeng, F., Rosati, A., Vecchi, G. A., & Wittenberg, A. T. (2015), A link between the hiatus in global warming and North American drought, J Clim, 28(9): 3834-3845,doi:10.1175/JCLI-D-14-00616.1.

Delcroix, T., Alory, G., Cravatte, S., Corrège, T., & McPhaden, M. J. (2011), A gridded sea surface salinity data set for the tropical Pacific with sample applications (1950–2008), Deep-sea Res PT I, 58(1): 38-48, doi:10.1016/j.dsr.2010.11.002.

Di Lorenzo, E., Cobb, K. M., Furtado, J. C., Schneider, N., Anderson, B. T., Bracco, A., Alexander, M.A., & Vimont, D. J. (2010). Central Pacific El Niño and decadal climate change in the North Pacific Ocean. Nature Geoscience, 3(11), 762-765.

Di Lorenzo, E., Fiechter, J., Schneider, N., Bracco, A., Miller, A.J., Franks, P.J.S., Bograd, S.J., Moore, A.M., Thomas, A.C., Crawford, W. and Peña, A., 2009. Nutrient and salinity decadal variations in the central and eastern North Pacific. *Geophysical Research Letters*, *36*(14).

Di Lorenzo, E., Schneider, N., Cobb, K.M., Franks, P.J.S., Chhak, K., Miller, A.J., McWilliams, J.C., Bograd, S.J., Arango, H., Curchitser, E. and Powell, T.M., 2008. North Pacific Gyre Oscillation links ocean climate and ecosystem change. *Geophysical Research Letters*, *35*(8).

Di Lorenzo, E., G. Liguori, J. Furtado, N. Schneider, B. T. Anderson and M. Alexander (2015), ENSO and Meridional Modes: a null hypothesis for Pacific climate variability, Geophys Res Lett, 42, doi:10.1002/2015GL066281.

Diffenbaugh, N. S., Swain, D. L., & Touma, D. (2015), Anthropogenic warming has increased drought risk in California, Proc Natl Acad Sci, 112(13): 3931-3936,doi:10.1073/pnas.1422385112.

Dunbar, R. B., Wellington, G. M., Colgan, M. W., & Glynn, P. W. (1994), Eastern Pacific sea surface temperature since 1600 AD: The δ18O record of climate variability in Galápagos corals, Paleoceanography, 9(2), 291-315, doi: 10.1029/93PA03501.

Epstein, S. , et al. (1953),Revised carbonate-water isotopic temperature scale, Geol. Soc. Am. Bull.,64(11), 1315–1326, doi:10.1130/0016-7606(1953)64[1315:RCITS]2.0.CO;2.

Fairbanks, R. G., M. N. Evans, J. L. Rubenstone, R. A. Mortlock, K. Broad, M. D. Moore, and C. D. Charles, 1997: Evaluating climate indices and their geochemical proxies measured in corals. Coral Reefs, 16, S93–S100, doi:10.1007/s003380050245.

Funk, C., A. Hoell, and A. Stone (2014), Examining the contribution of the observed global warming trend to the California droughts of 2012/13 and 2013/14, Bull. Am. Meteorol. Soc., 95, S11–S15.

Furtado, J. C., Di Lorenzo, E., Anderson, B. T., & Schneider, N. (2012), Linkages between the North Pacific Oscillation and central tropical Pacific SSTs at low frequencies, Cli Dyn, 39(12): 2833-2846,doi:10.1007/s00382-011-1245-4.

Griffin, D., & Anchukaitis, K. J. (2014), How unusual is the 2012–2014 California drought?, Geophyis Res Lett, 41(24): 9017-9023, doi:10.1002/2014GL062433.

Grinsted, A., Moore, J. C., & Jevrejeva, S. (2004), Application of the cross wavelet transform and wavelet coherence to geophysical time series, Nonlinear Process Geophys, 11(5/6): 561-566, doi:10.5194/npg-11-561-2004.

Hartmann, D. L. (2015), Pacific sea surface temperature and the winter of 2014, Geophys Res Lett, 42(6): 1894–1902,doi:10.1002/2015GL063083.

Hobday, A. J., L. V. Alexander, S. E. Perkins-Kirkpatrick, D. A. Smale, S. C. Straub, and E. C. J. Oliver. 2016. A hierarchical approach to defining marine heatwaves. Prog. Oceanogr. 141:227–238.

Howitt, R., J. Medellin-Azuara, D. MacEwan, J. Lund, *and* D. A. Sumner *(*2014*),* Economic analysis of the 2014 drought for California agriculture*, UC Davis Cent. for Watershed Sci., Davis, Calif. [Available at https://watershed.ucdavis.edu/files/biblio/DroughtReport_23July2014_0.pdf.]*

Kilduff, D. P., Di Lorenzo, E., Botsford, L. W., & Teo, S. L. (2015), Changing central Pacific El Niños reduce stability of North American salmon survival rates, Proc Natl Acad Sci 112(35): 10962–10966, doi:10.1073/pnas.1503190112.

Kessler, W. S. (2006), The circulation of the eastern tropical Pacific: A review, Prog Oceanogr69(2), 181-217, doi:10.1016/j.pocean.2006.03.009.

Latif, M., and T. P. Barnett (1994), Causes of decadal climate variability over the North Pacific and North America, Science, 266 (5185),635–637, doi:10.1126/science.266.5185.634

Lee, M.-Y., C.-C. Hong, and H.-H. Hsu (2015), Compounding effects of warm sea surface temperature and reduced sea ice on the extreme circulation over the extratropical North Pacific and North America during the 2013–2014 boreal winter, Geophys. Res. Lett., 42, 1612–1618, doi:10.1002/2014GL062956.

Linkin, M. E., & Nigam, S. (2008), The North Pacific Oscillation-West Pacific teleconnection pattern: Mature-phase structure and winter impacts, J Clim, 21(9): 1979-1997,doi:10.1175/2007JCLI2048.1.

Linsley, B. K., Wellington, G. M., & Schrag, D. P. (2000), Decadal sea surface temperature variability in the subtropical South Pacific from 1726 to 1997 AD, Science, 290(5494), 1145-1148, doi: 10.1126/science.290.5494.1145.

MacDonald, G. M., & Case, R. A. (2005), Variations in the Pacific Decadal Oscillation over the past millennium, Geophyis Res Lett, 32(8): L0873,doi:10.1029/2005GL022478.

Newman, M., Compo, G. P., & Alexander, M. A. (2003) ENSO-forced variability of the Pacific decadal oscillation, J Clim, 16(23), 3853-3857. http://dx.doi.org/10.1175/1520-0442(2003)016<3853:EVOTPD>2.0.CO;2

Newman, M., Alexander, M.A., Ault, T.R., Cobb, K.M., Deser, C., Di Lorenzo, E., Mantua, N.J., Miller, A.J., Minobe, S., Nakamura, H. and Schneider, N., 2016. The Pacific decadal oscillation, revisited. *Journal of Climate*, *29*(12), 4399-4427.

Nurhati, I. S., Cobb, K. M., & Di Lorenzo, E. (2011), Decadal-scale SST and salinity variations in the central tropical Pacific: Signatures of natural and anthropogenic climate change, J Clim, 24(13), 3294-3308, doi: 10.1175/2011JCLI3852.1.

Palmer, T. (2014), Record-breaking winters and global climate change, Science, 344(6186), 803–804, doi:10.1126/science.1255147.

Pierce, D. W., California Energy Commission., & Scripps Institution of Oceanography. (2005), Effects of the North Pacific Oscillation and ENSO on seasonally averaged temperatures in California: PIER project report, Sacramento, Calif.: California Energy Commission, CEC-500-2005-002.

Reynolds, R.W., N.A. Rayner, T.M. Smith, D.C. Stokes, and W. Wang. (2002): An improved in situ and satellite SST analysis for climate, J. Clim, 15, 1609-1625, doi: 10.1175/1520-0442(2002)015<1609:AIISAS>2.0.CO;2.

Roden, G. I. (1972), Thermohaline structure and baroclinic flow across the Gulf of California entrance and in the Revilla Gigedo Islands region, J. Phys. Oceanogr, 2(2), 177-183.

Roemmich, D., and J. Gilson (2011), The global ocean imprint of ENSO, Geophys. Res. Lett., 38, L13606, doi:10.1029/2011GL047992.

Rogers, J. C. (1981), The North Pacific oscillation. Int J Climatol 1(1): 39-57.

Sardeshmukh, P. D., andB. J. Hoskins (1988), The generation of global rotational flow by steady idealized tropical divergence, J. Atmos. Sci.,45, 1228–1251, doi: http://dx.doi.org/10.1175/1520-0469(1988)045<1228:TGOGRF>2.0.CO;2

Seager, R., & Hoerling, M. (2014) Atmosphere and Ocean Origins of North American Droughts, J Clim, 27(12): 4581-4606,doi:10.1175/JCLI-D-13-00329.1.

Seager, R., M. Hoerling, S. Schubert, H. Wang, B. Lyon, A. Kumar, J. Nakamura, and N. Henderson (2014), Causes and predictability of the 2011–14 California drought, Rep., 40 pp., doi:10.7289/V7258K7771F.

Seager, R., Tzanova, A., & Nakamura, J. (2009), Drought in the southeastern United States: causes, variability over the last millennium, and the potential for future hydroclimate change, J Clim, 22(19): 5021-5045, doi:10.1175/2009JCLI2683.1.

Smith, T.M., and R.W. Reynolds (2003), Extended Reconstruction of Global Sea Surface Temperatures Based on COADS Data (1854-1997), J Clim, 16(10): 1495-1510, doi:10.1175/1520-0442-16.10.1495.

Swain, D., M. Tsiang, M. Haughen, D. Singh, A. Charland, B. Rajarthan, and N. Diffenbaugh (2014),The extraordinary California drought of 2013/2014: Character, context and the role of climate change, in Explaining Extreme Events of 2013 From a Climate Perspective, Bull. Am. Meteorol. Soc., edited by S. C. Herring, et al., pp. S3–S6, Am. Meteorol. Soc., Boston, Mass., doi:10.1175/1520-0477-95.9.S1.1.

Thompson, D. M. , T. R. Ault , M. N. Evans , J. E. Cole , and J. Emile-Geay (2011), Comparison of observed and simulated tropical climate trends using a forward model of coral $\delta^{18}O$, Geophys. Res. Lett., 38, L14706, doi:10.1029/2011GL048224.

Tierney, J.E., Abram, N.J., Anchukaitis, K.J., Evans, M.N., Giry, C., Kilbourne, K.H., Saenger, C.P., Wu, H.C. and Zinke, J., 2015. Tropical sea surface temperatures for the past four centuries reconstructed from coral archives. *Paleoceanography*, *30*(3), 226-252.

Torrence, C., & Compo, G. P. (1998), A practical guide to wavelet analysis, Bull Am Meteorol Soc, 79(1): 61-78,doi:10.1175/1520-0477(1998)079<0061:APGTWA>2.0.CO;2.

Vimont, D. J., Alexander, M. A., & Newman, M. (2014), Optimal growth of Central and East Pacific ENSO events, Geophyis Res Lett, 41(11): 4027-4034,doi:10.1002/2014GL059997.

Vimont, D. J., Battisti, D. S., & Hirst, A. C. (2001), Footprinting: A seasonal connection between the tropics and mid-latitudes, Geophyis Res Lett, 28(20): 3923-3926,doi:10.1029/2001GL013435.

Vimont, D. J., Wallace, J. M., & Battisti, D. S. (2003), The seasonal footprinting mechanism in the Pacific: implications for ENSO*, J Clim, 16(16): 2668-2675,doi:10.1175/1520-0442(2003)016<2668:TSFMIT>2.0.CO;2.

Wagner, S., & Zorita, E. (2005), The influence of volcanic, solar and CO2 forcing on the temperatures in the Dalton Minimum (1790–1830): a model study, Clim Dyn, 25(2-3): 205-218,doi:10.1007/s00382-005-0029-0.

Walker, G. T., & Bliss, E. W. (1932), World weather, V. Mem. Roy. Meteor. Soc., 4, 53-84.

Wang, H., and S. Schubert (2014), Causes of the extreme dry conditions over California during early 2013, Bull. Am. Meteorol. Soc., 95, S7–S11.

Wang, S. Y., L. Hipps, R. R. Gillies, and J.-H. Yoon (2014), Probable causes of the abnormal ridge accompanying the 2013–2014 California drought: ENSO precursor and anthropogenic warming footprint, Geophys Res Lett, 41(9): 3220–3226,doi:10.1002/2014GL059748.

Wang, S. Y., L'Heureux, M., Chia, H. H. (2012), ENSO prediction one year in advance using western North Pacific sea surface temperatures, Geophys Res Lett, 39(5): L05702,doi:10.1029/2012GL050909.

Watson, P. A. G., A. Weisheimer, J. R. Knight, and T. N. Palmer (2016), The role of the tropical West Pacific in the extreme Northern Hemisphere winter of 2013/2014, J. Geophys. Res. Atmos., 121, 1698–1714, doi:10.1002/2015JD024048.

Williams, A.P., R. Seager, J. Abatzoglou, B.I. Cook, J.E. Smerdon and E.R. Cook (2015), Contribution of anthropogenic warming to California drought during 2012-2014, Geophys Res Lett, 42(16), 6819-6828, doi:10.1002/2015GL064924.

D.S. Wilks (2016), "The stippling shows statistically significant gridpoints": How Research Results are Routinely Overstated and Over-interpreted, and What to Do About It. Bull. Amer. Meteor. Soc. , 0, doi: 10.1175/BAMS-D-15-00267.1.

Xie, S. P., & Philander, S. G. H. (1994), A coupled ocean-atmosphere model of relevance to the ITCZ in the eastern Pacific, Tellus A, 46(4): 340-350,DOI: 10.1034/j.1600-0870.1994.t01-1-00001.x.

Zhang, H., Clement, A., & Di Nezio, P. (2014), The South Pacific meridional mode: A mechanism for ENSO-like variability, J Clim, 27(2): 769-783, doi:10.1175/JCLI-D-13-00082.1.

2.7 Acknowledgements

Chapter 2, in part, has been published in Geophysical Research Letters:

Sanchez, S. C., Charles, C. D., Carriquiry, J. D., & Villaescusa, J. A. (2016). Two centuries of coherent decadal climate variability across the Pacific North American region. *Geophysical Research Letters*, *43*(17), 9208-9216. The dissertation author was the primary investigator and author of this paper.

Additional elements of this publication can be found in Appendix A.

Chapter 3.

Pacific Meridional Mode over the last millennium

Abstract

The Pacific Meridional Mode, a coupled ocean-atmospheric interaction responsible for propagating subtropical anomalies to the tropics via thermodynamic mechanisms, features prominently in discussions of the response of climate variability to climate change. However, it is presently unclear how and why the variance in PMM might change, or even if greenhouse gas forcing might lead to heightened activity. Here, PMM variance over the last millennium is assessed in the Community Earth System Model (CESM) Last Millennium Ensemble (LME). The model reproduces the main spatial characteristics of the PMM in the modern ocean in agreement with observations. With this basis, I assess the magnitude of the PMM variance over the past millennium, subject to forcing from a variety of sources. Internal (unforced) variability dominates the PMM variance in the LME, but prolonged periods of strong or weak PMM variance are found to be associated with characteristic spatial patterns, consistent across ensemble members and forcing experiments. The pattern of strong PMM variance features a cooler north Pacific, weaker Walker circulation, and a southward-shifted ITCZ. This pattern also suggests that equatorial anomalies can influence the southern node of the North Pacific Oscillation, and, further, that this interaction has a role in sustaining PMM variability in the model. Comparison with a slab ocean model suggests that equatorial ocean dynamics are necessary to sustain the statistically significant multidecadal variability. With respect to the last millennium, present greenhouse forcing does not promote exceptional PMM variance. However, the PMM variability projected in the RCP8.5 scenario exceeds the thresholds expressed with the forcings applied over the Last Millennium. Aside from multidecadal variability, the model observations also bear on ENSO variability and the sensitivity of climate variability to external forcing.

3.1 Introduction

The Pacific Meridional Mode (PMM) is a form of tropical ocean-atmospheric interaction, independent of ENSO, that can create coherent anomalies through an interplay of wind speed and surface evaporation. This mode has been increasingly recognized as an influential component of climate variability, effective in channeling extratropical anomalies to the equatorial ocean-atmosphere system [Chiang and Vimont 2004]. The PMM is reinforced by a thermodynamic feedback involving varying wind speed, evaporation, and sea surface temperatures (WES feedback; [Xie and Philander 1994, Chang et al. 1997]). Central to this mode, extratropical atmospheric variability acts to warm (cool) local sea surface temperatures in the subtropical North Pacific, adjusting the mean surface wind field and spurring lesser (greater) evaporative cooling; this particular mechanism has been termed "seasonal footprinting" [Vimont et al. 2001, Vimont et al. 2003]. These positive (negative) sea surface temperature anomalies, typically initiated southwest of Baja California in the Eastern Tropical North Pacific, induce further weakening (strengthening) of the trade winds by relaxing the meridional surface temperature gradient. These weakened trade winds further reduce (increase) evaporation rates, allowing the sea surface temperature anomalies to propagate southwestward to the equatorial Pacific. The "meridional mode" framework is important as it links El Niño Southern Oscillation (ENSO) variability to internal extratropical atmospheric variability.

Indeed, the PMM was initially hypothesized as an important precursor to ENSO [Chiang and Vimont 2004)]. This hypothesized connection has been supported in subsequent observational and modelling studies. For example, using instrumental observations between 1958 and 2000, Chang et al. 2007 found that more than 70% of El Niños followed a positive PMM

event. This strong relationship has similarly been observed in National Center for Atmospheric Research Community Climate System Model, version 3 (CCSM3, [Zhang et al. 2009a], and in version 4(CCSM4, [Larson and Kirtman 2013]), and other CMIP5 models [Lin et al. 2015]. The PMM also seems to be important for the formation of central Pacific El Niños [Vimont 2015, DiLorenzo et al. 2010, Yu et al. 2011, Yu and Kim 2011, Kim and Yu 2012], and, accordingly, the increase in prevalence of the Central Pacific El Niño events over the past few decades has been attributed to an intensification of the thermodynamic coupling mechanism central to the PMM [DiLorenzo et al. 2015, DiLorenzo et al. 2016]. The PMM has further been identified as an important feature in Pacific cyclone suppression/ enhancement [Zhang et al. 2016], is thought to have played a role in the extreme drought, and sea surface temperatures, and resilience of a mid-level atmospheric high pressure system of 2012-2016 [Wang et al. 2014, Hartman et al. 2015], the associated marine heat wave [DiLorenzo and Mantua 2016, Joh and DiLorenzo 2017], and is an important means of attenuating low frequency variability in the tropics [DiLorenzo 2015].

While the PMM has proven to be an important feature in the climate system, the recent amplification of PMM variability (Figure 3.1C.), deserves careful consideration. It is still unknown if and why the Pacific Meridional Mode might be intensifying. The apparent increase in variance might simply be the result of unforced modulations in the climate system. Alternatively, this intensification may have been induced by a changing mean state associated with anthropogenic global warming. The background state could influence the PMM through a number of processes: 1. The effectiveness of WES feedback could fluctuate via changes in the mean surface temperature and wind fields [DiLorenzo et al. 2015, DiLorenzo et al. 2016, Vimont et al. 2009], 2. the characteristics of stochastic wind forcing in the extratropics can be

modified due to variations in atmospheric circulation [Chiang et al. 2006, Chiang et al. 2009], and 3. The structure and location of the Intertropical Convergence Zone (ITCZ) could change, potentially allowing for greater propagation of anomalies from the subtropics to the tropics [Zhang et al. 2014, Martinez-Villa Lobos et al. 2016]. Instrumental records are simply not long enough to capture the full range of variability of the PMM and to test these alternatives.

Over the last millennium, Earth's radiative budget has fluctuated as a result of a variety of natural and anthropogenic forcings: volcanic eruptions, solar cycles, orbital variation, land use change, greenhouse gas and aerosol emissions. These shifts provide a means of investigating how sensitive is the PMM to subtle variations in the mean state and provide greater context to understand the extent the natural variability. In principle, therefore, the last millennium represents a valuable experimental platform. Paleoclimatic proxy records (e.g. from corals) provide some indication of PMM variance (e.g. Sanchez et al. 2016), but, as yet, are too geographically sparse to pinpoint mechanisms of PMM variability beyond the instrumental record. Thus, temporally extended model integrations are required to make use of the experimental platform. In this study, the Community Earth System Model- Last Millennium Ensemble (CESM-LME) is used to better understand the extent of PMM variability. My explanation of climate behavior in the CESM-LME seeks to address the following questions: How has modeled PMM changed over the last millennium? Has the PMM always operated in a physical framework similar to that of today? What causes the PMM to vary? Does the PMM respond to forced change? Do variations in the variability of the PMM influence ENSO?

3.2 Datasets and Methodology

Several of the Community Earth System Model 1.1.1. (CAM5) experiments are explored to assess the low frequency variability of the PMM, outlined in Table 3.1 The Last Millennium Ensemble (CESM-LME, [Otto-Bleisner et al. 2015]) and the Large Ensemble (CESM-LE, [Kay et al. 2015]) experiments use the same coupled physical model of ocean, atmosphere (the Community Atmosphere Model version 5), land, and sea ice. However, the experiments differ in grid cell resolution and forcing employed: the CESM LME has a coarser land and atmosphere resolution (~2° atmosphere and land, ~0.3°-1° ocean and sea ice coupled model), while the CESM LE has a 1° atmosphere model. In addition, the experiments consist of a number of realizations to capture a fuller extent of internal variability in the model behavior. The LME is forced with varying solar intensity, volcanic aerosol emissions, greenhouse gas concentrations, land use changes, orbital variations, aerosols and ozone calibrated with values from observations and high resolution paleoclimate reconstructions. Each LME ensemble member spans 1256 years, beginning in year 850 and extending to 2006 (more information available in Otto-Bliesner et al. 2015). The LME is therefore an especially useful platform for forcing-response diagnosis, given that there are multiple ensemble members within each prescribed forcing regime. Here, twelve of the all-forcing experiments, five volcanic-only forcing experiments, one control run, and four RCP8.5 future ensemble members are used. The "all forcing" experiments include all relevant radiative forcing (volcanic, greenhouse gases, ozone-aerosols, land use change, solar intensity, and orbital), while, as the name implies, volcanic forcing-only ensemble members have only been forced with historical volcanic eruptions. The control (unforced) run provides a measure of internal variability within the model. Finally, the future projections are an extension

of four of the all forcing scenario ensemble members (#2,3,8, and 9), following the RCP 8.5 forcing pathway. This multitude of ensemble members provides the unique opportunity to not only account for the range of natural variability, but also to pinpoint the common and robust characteristics of the modelled Pacific Meridional Mode. I additionally assess two long unforced control runs in the Community Earth System Model Large Ensemble (CESM-LE, [Kay et al. 2015]) to gauge the role of ocean dynamics in the variability of the PMM. One control run comes from the fully coupled model (CESM-LE), the other control run comes from a slab ocean experiment using the CAM5 model (CESM-LE-SOM).

Table 3.1. Characteristics of model experiments.

Model	**Years**	**Ensemble Members**	**Applied Forcing**
CESM LME Control *Bleisner et al. 2015*	850-2006	1	None
CESM LME Volcanic-Only *Bleisner et al. 2015*	850-2006	5	Volcanic
CESM LME All Forcing *Bleisner et al. 2015*	850-2006	12	Greenhouse gases, ozone-aerosols, volcanic, land use change, solar intensity, and orbital volcanic, greenhouse gases, ozone-aerosols, land use change, solar intensity, and orbital
CESM LME RCP8.5 *Bleisner et al. 2015*	2006-2100	4	Greenhouse gases, ozone-aerosols, volcanic, land use change, solar intensity, and orbital volcanic, greenhouse gases, ozone-aerosols, land use change, solar intensity, and orbital
CESM LE Control *Kay et al. 2015*	1-1000	1	None
CESM LE SOM Control *Kay et al. 2015*	1-900	1	None

Observations of the present day sea surface temperature, surface winds and precipitation were obtained from NOAA's Extended Reconstruction version 3B (ERSSTv3b, [Smith and Reynolds 2008]) and NCEP-NCAR Reanalysis version 1 [Kalnay et al. 1996] to provide an observationally bound reference to the CESM's PMM.

3.3 Results

3.3.1 Model Validation

The Pacific Meridional Mode is calculated as in Chiang and Vimont 2004; monthly means of sea surface temperatures and 1015mb zonal and meridional winds from 21°S-32°N, 175°-265°E are removed and three month moving average is applied before taking the Maximum Covariance Analysis (MCA) of the three variables. As in observations, the Pacific Meridional Mode in CESM-LME is the second mode of maximum covariance between winds and SST after ENSO, and it is characterized by large sea surface temperature and wind anomalies southwest of Baja California, extending southwestwards towards the dateline (Figure 3.1). In the Last Millennium Ensemble, the magnitudes of the SST and wind anomalies associated with the PMM are comparable to observations; however, with respect to observations, the mean spatial pattern of SST and wind anomalies is shifted westward and into the Western Pacific Warm Pool region. The correlation of the SST and wind expansion coefficients are slightly stronger in the model than in observations (R=0.86 vs R=0.70, respectively), implying marginally stronger air-sea coupling in CESM.

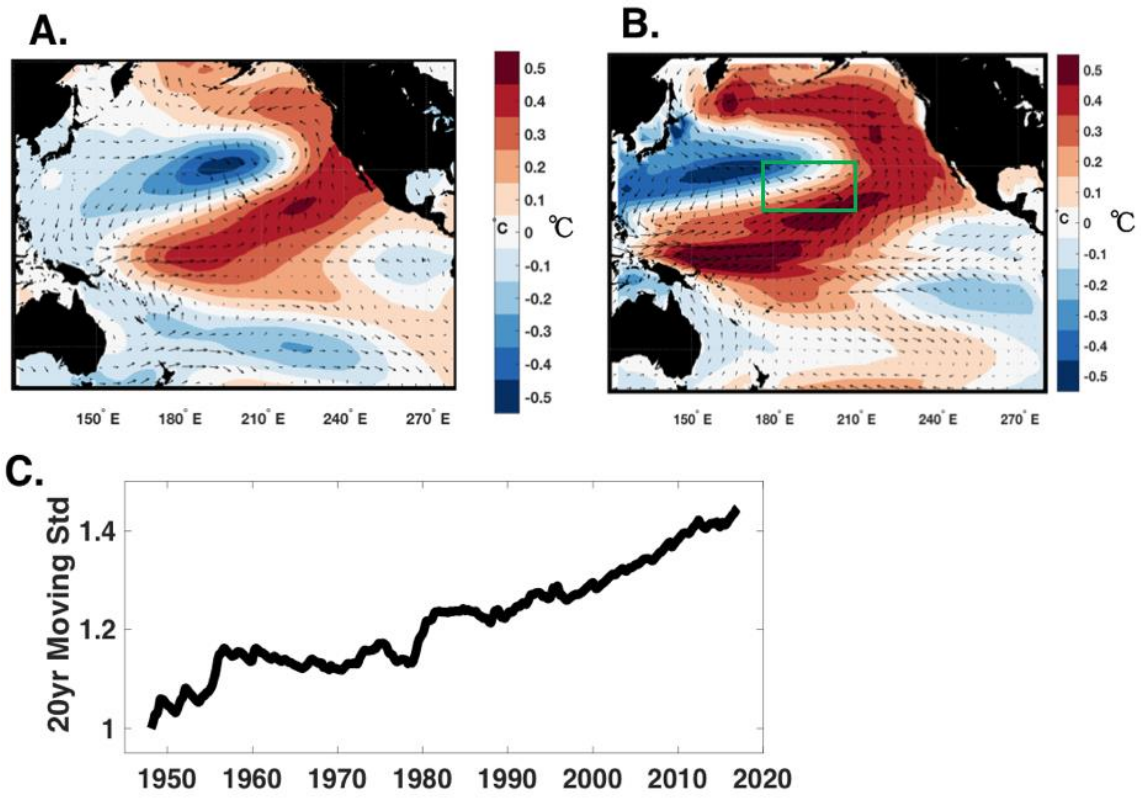

Figure 3.1 Linear regression maps between PMM and SST and surface wind vector anomalies (**A.)** in observations, using years 1948-2006 from NOAA ERSST and NCEP winds and (**B.)** a single ensemble member the CESM-LME using years 1948-2006. The green box outlined highlights the region of NPO DJF zonal wind forcing used in Figure 3.6 (**C.)** The moving 20year standard deviation (using a centered window) of the Pacific Meridional Mode index in observations (relative to the 1948-1968 mean), highlighting the often discussed trend for increasing variance.

The NPO, calculated as the 2nd EOF of sea level pressure in the North Pacific, defined as 180°W-110°W, 25°N-62°N [Walker and Bliss 1932, Rodgers 1981, Linkin and Nigam 2008], forces the PMM in the preceding DJF [Anderson et al. 2003, Vimont et al. 2003, Vimont et al. 2015]. Approximately 2-3 months before the PMM peaks, wind anomalies associated with the NPO imprint a pattern of SST anomalies. The monthly variance of the PMM is maximized in March-April-May and can initiate ENSO activity in the following DJF (9 months later Figure

3.2A and 3.2B). That ENSO activity is described by the Niño 3 index, the area averaged SST anomaly for the region 5°S-5°N, 150°W-90°W. While the standard deviation of the Niño 3 region is directly related to the variability of the PMM (Figure 3.2C), it is not as tightly coupled to the variability of the NPO. The NPO-PMM-ENSO chain of events is much weaker in any other configuration, ex. ENSO-PMM-NPO, or ENSO-NPO-PMM. In general, the physical consistency of the model with observations allows us to refer to the variability within CESM-LME to investigate both the internal and forced variability of the PMM.

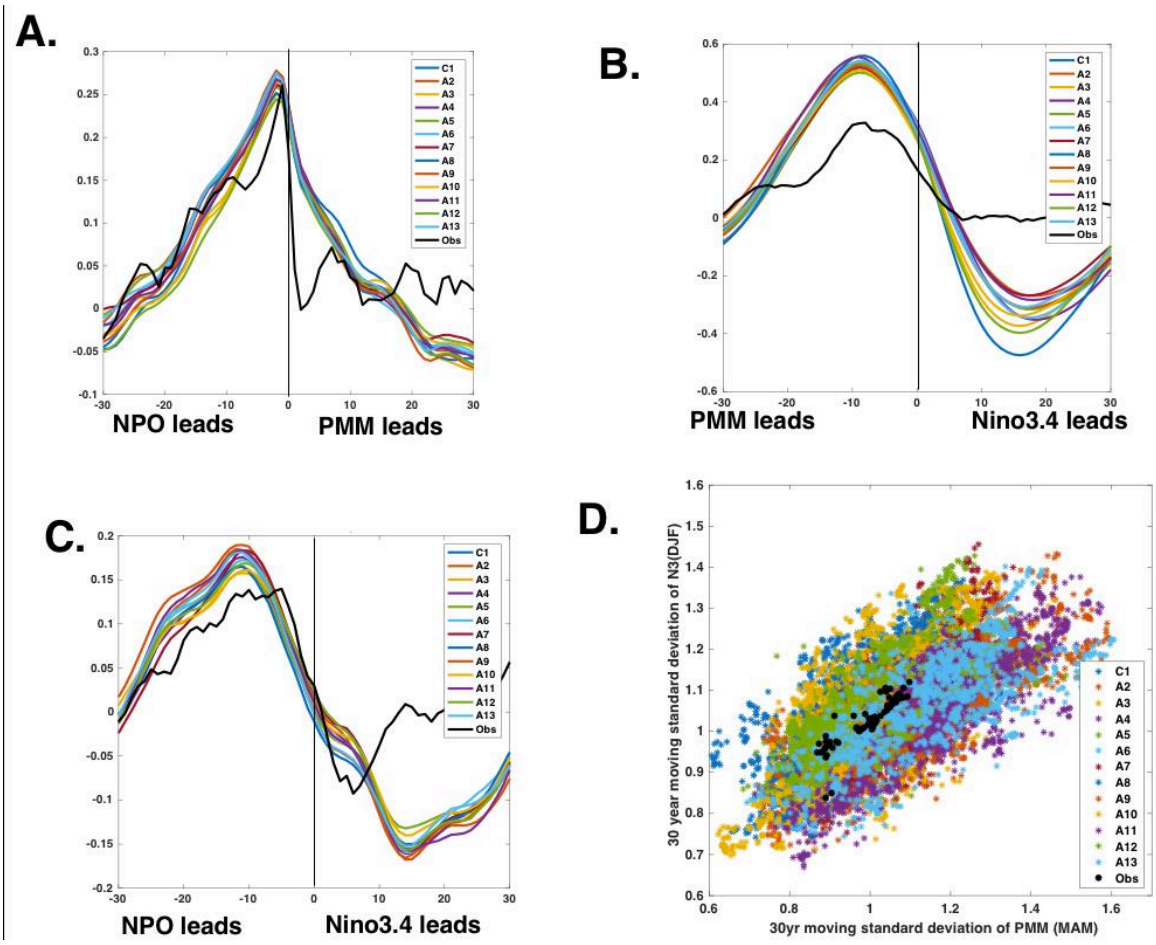

Figure 3.2 The model PMM is physically consistent with observations. (**A.)** lead-lag plot in the Control and 12 All Forcing experiments (colors) and observations (black) between the PMM and the NPO Index (calculated as the second EOF of SLP in the North Pacific); maximum correlation is found when NPO leads by 2 months), (median maximum correlation, R=0.27). (**B.)** PMM and Nino 3.4 index; a maximum correlation is found when ENSO follows the PMM by 9 months, (median maximum correlation, R=0.57). Observations here use the wind component of the PMM. (**C.)** For comparison's

sake, I also show the relationship between the North Pacific Oscillation and the Nino 3.4 As the strength of the correlations are much weaker than that of the NPO-PMM, or PMM-Nino 3.4, this highlights the important role of the PMM (median maximum correlation, R=0.17 when the NPO leads by 12 months). **(D.)** Scatterplot of the moving standard deviations of the PMM (MAM) and the following Nino 3 (DJF).

There are two commonly used metrics for describing the strength of the Pacific Meridional Mode. One metric is the 30 year moving standard deviation of the SST expansion coefficient of the PMM MCA index in March-April-May (the months of highest variance, as in DiLorenzo et al. 2016, Wang et al. 2014). The other is the 30 year moving correlation between the wind and SST expansion coefficients from the maximum covariance analysis (used in other MCA analysis to show greater coupling between variables, as in Amaya et al. 2016, Lin et al. 2015). In the observational record, both metrics have shown an increase in variability or coupling strength from years 1950 to the present (Figure 3.2C), implying an increase in variance and in the air-sea coupling affiliated with the PMM.

A 30 year moving standard deviation of the PMM is calculated in the unforced control run (Figure 3.3A) to provide a baseline expectation for the internal variability observed in the model. In the unforced control run, the 30 year moving standard deviation fluctuates roughly by a factor of two and experiences a wider range in variability than that of the forced runs. In CESM-LME, the variability in the correlation between the wind and SST expansion coefficients is minimal, even in the forced experiments. However, the rare deviations in the correlation coefficient of the expansion coefficients skew highly negatively, implying that the surface SST or winds are temporarily decoupled. This type of deviation is most common immediately following volcanic eruptions in single ensemble members, but is not found in ensemble averages. For these reasons, the analyses are confined to ensemble average behavior.

3.3.2 Unforced variability

The term "internal" variability describes unforced processes intrinsic to the climate system, unprompted by any variations in Earth's radiative balance, as in Deser et al. 2012. The term "forced" variability describes processes that occur as a result of a change that alters Earth's radiative balance. Common examples of forced change are the introduction of greenhouse gasses, aerosols, land use change even volcanic eruptions, which occur naturally. Internal variability in the climate system dominates the variance of the PMM in each individual ensemble member. In single ensemble members from each particular forcing experiment, the most pronounced form of variability is the low frequency variability, also readily observed in the control run. In each of the forced experiments, the internal variability is comparable to that of the control run and causes the standard deviation of the PMM to vary by about a factor of two. However, when ensemble members from single forcing experiments are averaged together, the high amplitude internal variability is smoothed out and not observable, as internal variability should not be coherent between ensemble members. This provides a means of identifying forced responses as periods when the ensemble averaged PMM index is above a particular threshold. It is expected that forced variability would create coherent anomalies of the same sign between ensemble members, regardless of their internal variability. Figure 3.3 illustrates the range of the ensemble members in each forcing scenario.

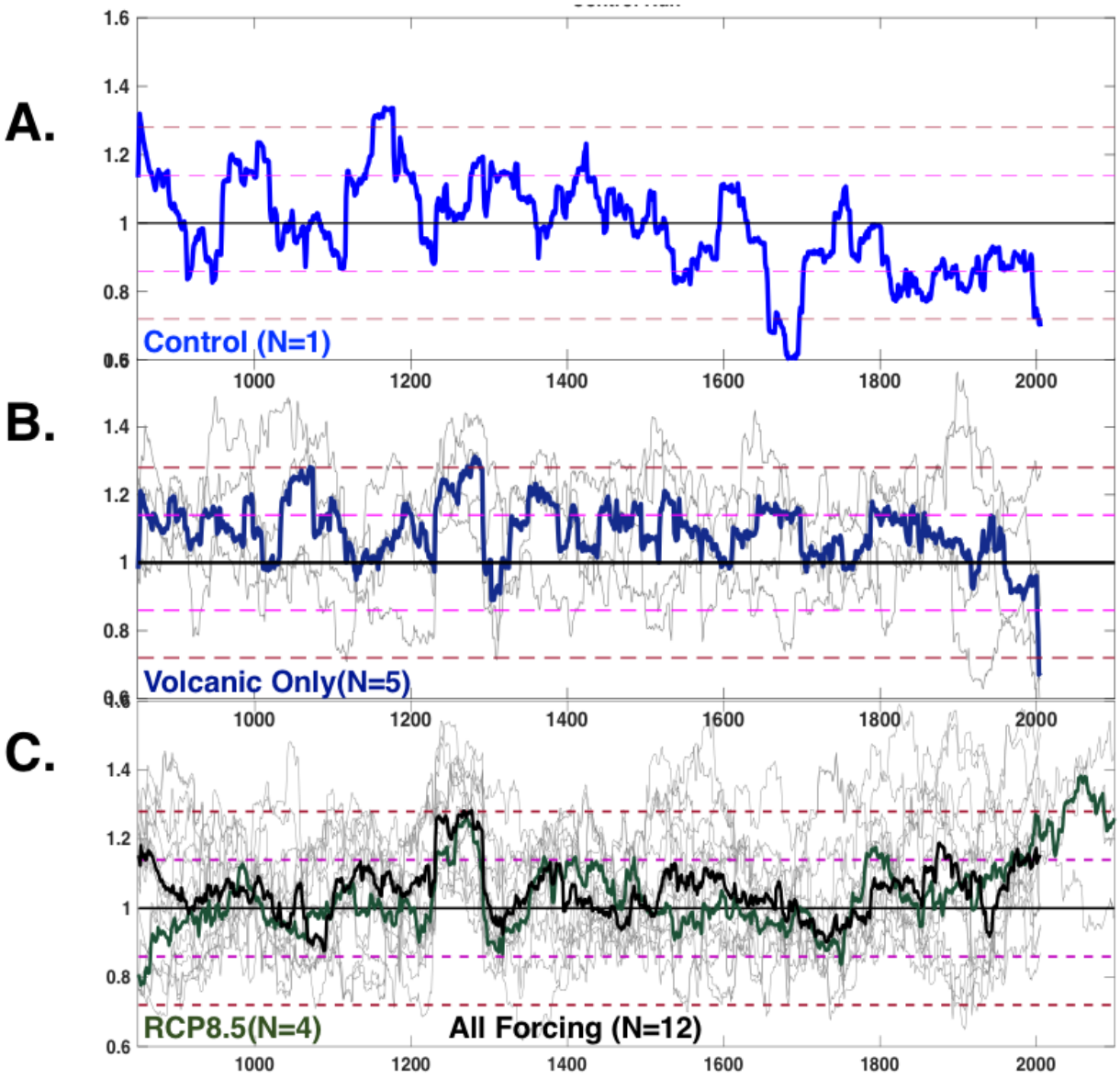

Figure 3.3. A moving 30-year standard deviation (centered window) is used on a variety of indices to assess the variability of the PMM over the last millennium. In **(A.)** A moving 30-year standard deviation is used on the unforced control run to get a range of variability and set the mean standard deviation of the control run to 1. The 1 sigma mark is dashed in magenta, and the 2 sigma mark is dashed in rust-red. In **(B.)** Each ensemble member from the volcanic-only forcing experiment is plotted in gray to highlight the range of natural variability within the model. The median of the 5 "Volcanic-Only" experiments is in navy. In **(C.)** same as B, but using 12 "All Forcings" experiments (median in black) and the four RCP8.5 experiments (median in dark green). The RCP8.5 experiments are merely a continuation of four of the "All forcing" experiments, specifically ensemble members #2, 3, 8 and 9.

That said, the time series of PMM activity suggest an influence of radiative forcing.

Volcanic eruptions tend to amplify the variability of the PMM in the ensemble mean, increasing

the variance of the SST expansion coefficient. For example, the Samalas event of 1257[Lavigne et al. 2013, Gulliet et al. 2017], the largest volcanic eruption in the last 2500 years [Lavigne et al. 2013], created a short lived, but high amplitude signal, prompting the epoch of highest averaged variance in the last millennium (Figure 3.3B, 3.3C). The thirty year moving standard deviation calculation results in an artificially prolonged sixty-year period of high variance (excluding the years 1260,1261,1262, with an outstanding ensemble average 5 standard deviation anomaly, the variance of the 30 year moving average falls within the typical range throughout the last millennium (Appendix B., Figure B.1).

Also, in the twelve All Forcing scenarios, an increase in Pacific Meridional Mode variance is observed through the late 20th century (through the year 2006 in the CESM simulations). The variance in the "present" is above average, but does not exceed the bounds of that simulated over the last millennium. In a single ensemble member, the variance rises above all previous values, but the mean trend suggests that there is no clear difference in the variability of the late 20th century from the variability witnessed over the last millennium

3.3.3 Pattern of Variance

Modifications in the background climate have been hypothesized to amplify or dampen the variability of the Pacific Meridional Mode. The three leading hypotheses describing the ways in which the mean climate might influence the PMM are: 1). The mean location of the ITCZ can influence the extent to which subtropical anomalies can influence equatorial regions [Zhang et al. 2014, Martinez-Villalobos and Vimont 2016]. 2). The sensitivity of latent heat fluxes to the variations in wind speed are expected to change with the mean background temperature [DiLorenzo et al. 2015, Vimont et al. 2009]. 3). Finally, variations in "noisiness" in the

extratropical atmosphere directly impact the North Pacific Oscillation and are sensitive to variations in the mean atmospheric circulation [Chiang et al. 2009, Chiang et al. 2010]. To investigate the mean state's influence on the PMM, I identify the characteristic conditions that accompany periods of extreme PMM variance. There is no reason to expect a clear background pattern of variability, but the existence of a pattern might help address the mechanisms responsible for altering the variance of the Pacific Meridional Mode.

A least squares linear regression of relevant climate fields is calculated on the thirty year moving standard deviation of the Pacific Meridional Mode (MAM) index. Each of these moving standard deviation time series consists of 1156 model years from each of the 12 "All forcing" ensemble members. A consistent pattern of variability emerges in each ensemble member (Figure 3.4). Additionally, when creating a composite of the 20% most extreme events highly similar patterns in the climate fields (see the Appendix B.). Periods of high variance are characterized by anomalously cool North Pacific sea surface temperatures (of about 0.2° Celsius for 1 standard deviation) and cooler warm pool region, while the eastern equatorial Pacific and Kuroshio region shows a slight warming tendency. The surface wind field and precipitation response are also consistent with a weaker Walker circulation during periods of higher variance, while lower PMM variance tends to be characterized by a strengthened Walker Cell and warmer North Pacific. The precipitation response during periods of high PMM variance also features a contracted, southward shifted ITCZ. The same analysis is performed with Pacific mixed layer depth and results in a consistent pattern in the background state associated with PMM variance; high variance is associated with a deepening of the western Pacific and far eastern Pacific mixed layer depth and shoaling of central equatorial mixed layer depth, with shoaled flanks extending

eastward in the extratropics (Figure 3.4). The PMM variance pattern is a robust feature in CESM, regardless of forcing experiment.

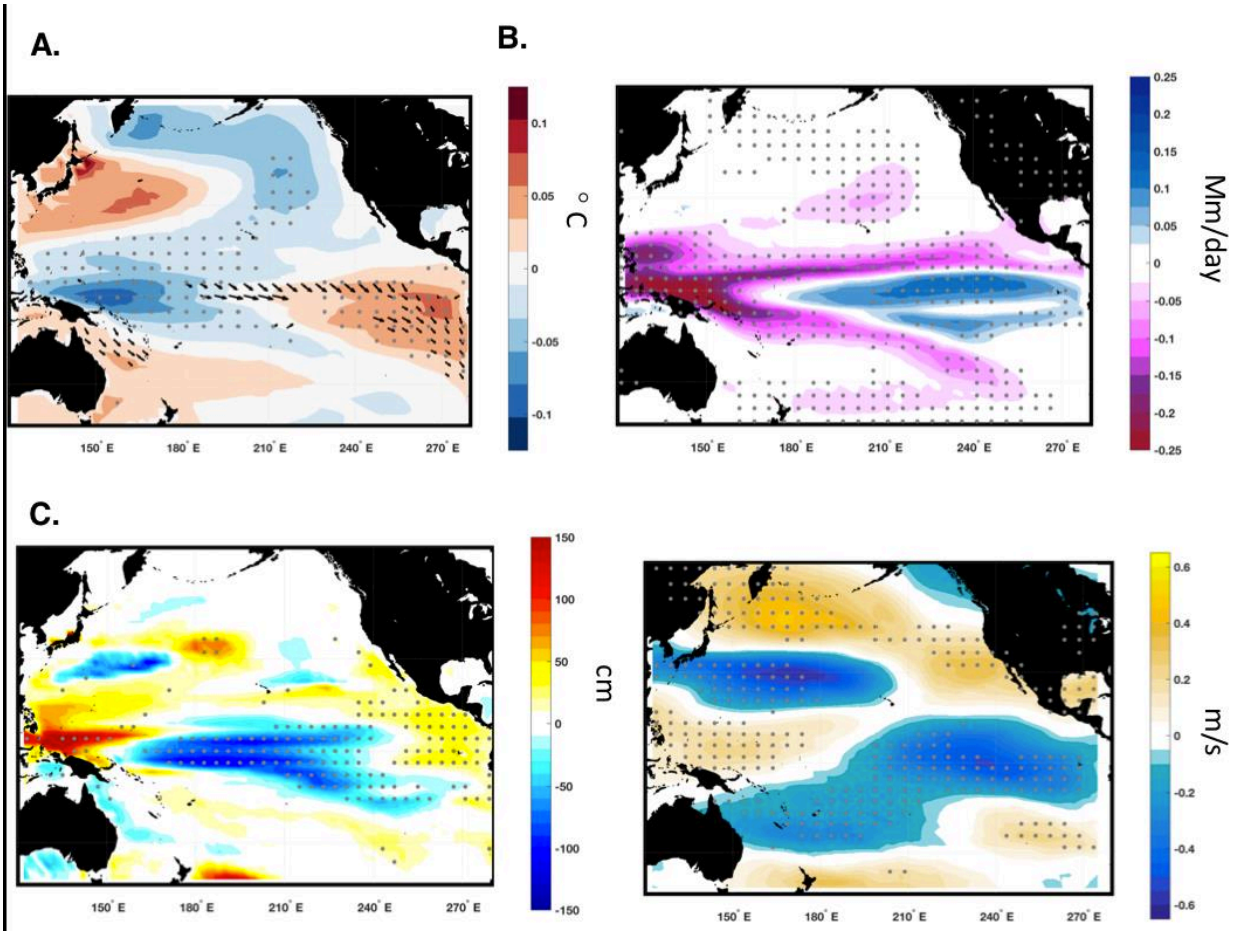

Figure 3.4. Least squares linear regression of the following DJF fields on the 30-year moving standard deviation of the PMM index from year 850 to 2006 in each of the twelve model ensemble member. The following plots show the median linear regression pattern between all 12 ensemble members, encompassing 13,872 model years. Stippling indicates sign agreement in 100% of ensemble members. Extremely similar patterns are also found when compositing the most extreme 20% of years (See Appendix B.). Fields evaluated are (**A.**) SST and surface wind anomalies, (**B.**) Precipitation anomalies, (**C.**) Mixed layer depth anomalies, and (**D.**) 200mb zonal wind anomalies

There is some agreement with this background pattern associated with the internal variability of the Pacific Meridional Mode and the previously hypothesized mechanisms of PMM change. Periods of high PMM activity are accompanied by a southward shifted ITCZ and a

weaker Walker circulation. Recent work has found that the PMM is particularly sensitive to ITCZ shifts in intensity and location (using a simple linear coupled model, [Martinez-Villalobos and Vimont 2016]. Other studies have suggested that the location of the ITCZ might inhibit or help types of Meridional Modes from occurring [Zhang et al. 2014]. However, the magnitude of the meridional shift in ITCZ position in the CESM LME simulations is small enough to preclude drawing conclusions of causality.

Minor variations in the sensitivity of latent heat flux are found in the western tropical North Pacific associated with the PMM variance. I calculate this sensitivity of latent heat flux to zonal winds, or Wind-Evaporation-Sea-Surface-Temperature Parameter, or "WES" parameter ($\propto$), using a linearized approximation as in Czaja et al. 2002 and Vimont et al. 2009.

$$-\propto (y) = \frac{\partial LH}{\partial u} = L_v C_e \rho \left(q_{sat}(T_s) - RH q_{sat}\left(T_{ref}\right)\right)\frac{u}{w} = LH\frac{u}{\overline{w}^2}$$

Where LH is latent heat, U is zonal wind, overbar w is wind speed ($\overline{w} = \sqrt{u^2 + v^2 + \widehat{w}^2}$), $\widehat{w}$ is a background wind speed used to account for higher frequency variance, $\widehat{w} = 4\mathrm{m}s^{-1}$ [Czaja et al. 2002], and $\propto$ has units of W s m^{-3}. These variations are small in magnitude, and in regions not particularly important for the activation of the Pacific Meridional Mode. In contrast, the change in latent heat flux sensitivity to the mean zonal winds expected under RCP8.5 forcing creates a far greater magnitude change; roughly a 20% increase in the mean WES feedback parameter (Figure 3.5).

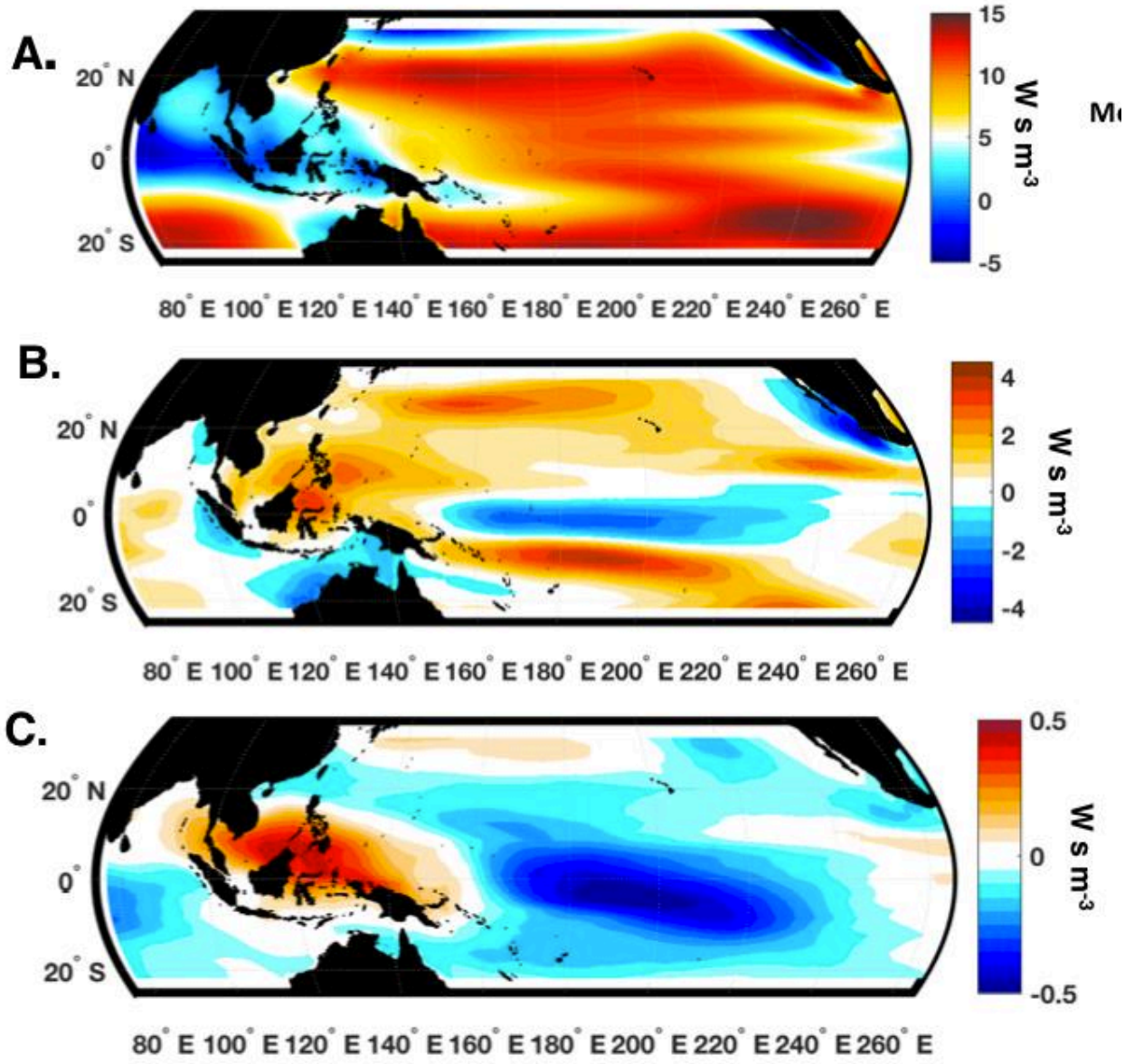

Figure 3.5. Relationship between WES parameter and the Pacific Meridional Mode. (**A**.) Mean WES feedback parameter field in W s m^{-3} over the 1950 to 2000 period in all 12 "All Forcing" ensemble members. In **(B.)** The 2080-2100 average under RCP 8.5 forcing are compared to the present day mean (1950-2000) with the four available ensemble members (#2,3,8,9). In (**C.)** The linear regression pattern associated with the natural variability of the Pacific Meridional Mode, methodology identical to climatological fields in Figure 3.4.

Finally, using a simplified calculation for the strength of the jet stream (200mb zonal wind averaged over wind speed between 20°N to 45°N and 110°E to 180°E at 200mb in jet exit

region over western Asia, a significant correlation is found between PMM activity and weakness of the jet stream, R= -0.45, $p<0.01$. Such an association is expected on general principles: when the jet stream is stronger (westerlies exceed 45 m/s), baroclinic eddy activity diminishes with reduced atmospheric noise [Nakamura et al. 2002, Luo et al. 1994]. Thus, when there is a stronger jet, eddies are advected away more quickly, causing a suppression of the North Pacific Oscillation that ultimately forces the Pacific Meridional Mode [Chiang et al. 2009, Chiang et al. 2010]. This correlation is apparent in Figure 3.4: the slower the jet stream, the more energetic the variance of the Pacific Meridional Mode, and vice versa. Again, as with the other hypothesized sources of PMM, the variations in wind speed found in the CESM LME are so small, they cannot be prime drivers for PMM behavior. Thus, while each of the prior hypotheses cannot be discounted by the CESM-LME results, no single mechanism can be responsible for the internal variability of the Pacific Meridional Mode described here.

3.3.4 Mechanisms driving variance pattern

It is difficult to assess the fidelity of the background climatic pattern associated with the variance of the model PMM with the instrumental record, because observations are too short. We, thus, rely on the CESM-LME to take another approach, asking: Where does this variance mode come from? What physical drivers are associated with this background pattern affiliated with PMM variance? I take a new approach to identify the processes responsible for maintaining the low frequency variability associated with this pattern by separate roles of the potential thermodynamic and dynamic mechanisms. Are ocean dynamics fundamental in the pattern of variance associated with the PMM, or can such epochs of extreme variance exist from atmospheric variability alone?

The CESM-LME control and two unforced control runs from the CESM Large Ensemble (using a 1° latitude/longitude version of CAM5, [Kay et al. 2015]) are used to discriminate the role of the dynamical and thermodynamic mechanisms. In general, the CESM LENS was not meant to model variability over the last millennium; instead, the project sought to create a multitude of ensemble members over the industrial era and future projections, including a fully coupled controlled experiment and a slab ocean experiment, used here. The variability of the PMM and the NPO are assessed in both the fully coupled CESM Last Millennium Ensemble Control (1155 years), the fully coupled CESM Large Ensemble Control (1000 years), and the CESM Large Ensemble Slab Ocean Control (900 years).

By definition, the slab ocean model does not have an SST variable, so in this experiment the PMM is calculated using surface temperatures instead of SST; otherwise the treatment is identical to the previously described MCA method. In other experiments, the correlation between the surface temperature and sea surface temperature over the PMM region are highly correlated. I find consistency between the fully coupled and slab ocean experiments in the standard metrics of the PMM. In the slab ocean experiment, the correlation of the wind and SST expansion coefficient, or degree of air-sea connectivity, is 0.8675, while both coupled model experiments observed values of 0.86 (observations R=0.7). In each simulation, the PMM follows NPO variability and experiences maximum variance in March-April-May.

In each experiment, the March-April-May portion of the PMM index is normalized to have a unit variance and perform multitaper mean spectrum analysis [Thomson1982, Percival and Walden 1993, Ghil et al. 2002]. Both the LME and LE coupled ocean model experiments have statistically significant PMM variability in the 26-32 year bands at 95% significance (using 4 tapers, but still significant over a range of 2 to 8 tapers). However, there is no significant

multidecadal variability observed in the slab ocean model (Figure 3.6). This result is not influenced by the number of tapers. This fundamental difference in behavior of the slab ocean model implies that the decadal frequencies observed in the PMM cannot be explained by an attenuation of stochastic white noise and ocean thermodynamics alone; some dynamical oceanic mechanism is required.

To further assess the roles of thermodynamical and dynamical mechanisms responsible for the low frequency PMM variability, I explore the atmospheric component that forces the PMM activity, the North Pacific Oscillation. The North Pacific Oscillation (NPO) is the principal driver of PMM variability through modifying the surface wind field in the DJF and imprinting the characteristic PMM SST anomaly pattern in the Eastern Tropical North Pacific the following MAM through anomalous latent heat fluxes. In the Last Millennium Ensemble, the ensemble mean correlation between the PMM (MAM) and preceding NPO (DJF) indices is R=0.52 at seasonal resolution in the All-Forcing Ensemble members. The region where NPO zonal wind forcing is most influential on zonal winds is identified, (175E-205W, 15-30N,) and an index using the area averaged zonal wind components is created to assess any differences in the actual forcing of the PMM. Once again multitaper mean spectrum analysis is performed on the DJF NPO's zonal wind forcing in the three control experiments and find that there is no significant difference in the low frequency (>10 years) component (Figure 3.6). Neither the coupled model experiments nor the slab ocean model experiments exhibit statistically significant variability. Thus, the statistically significant decadal variability in the coupled models cannot be attributed to a low frequency component of atmospheric forcing. As the atmospheric forcing component in both the coupled and slab ocean models are similar, the significant decadal variability must be due to some feedback process between the atmospheric forcing and equatorial ocean dynamics.

Mechanisms for such oceanic feedbacks have been hypothesized, such as rectification of interannual variability onto thermocline stratification [Ogata et al. 2013, Rodgers 2004].

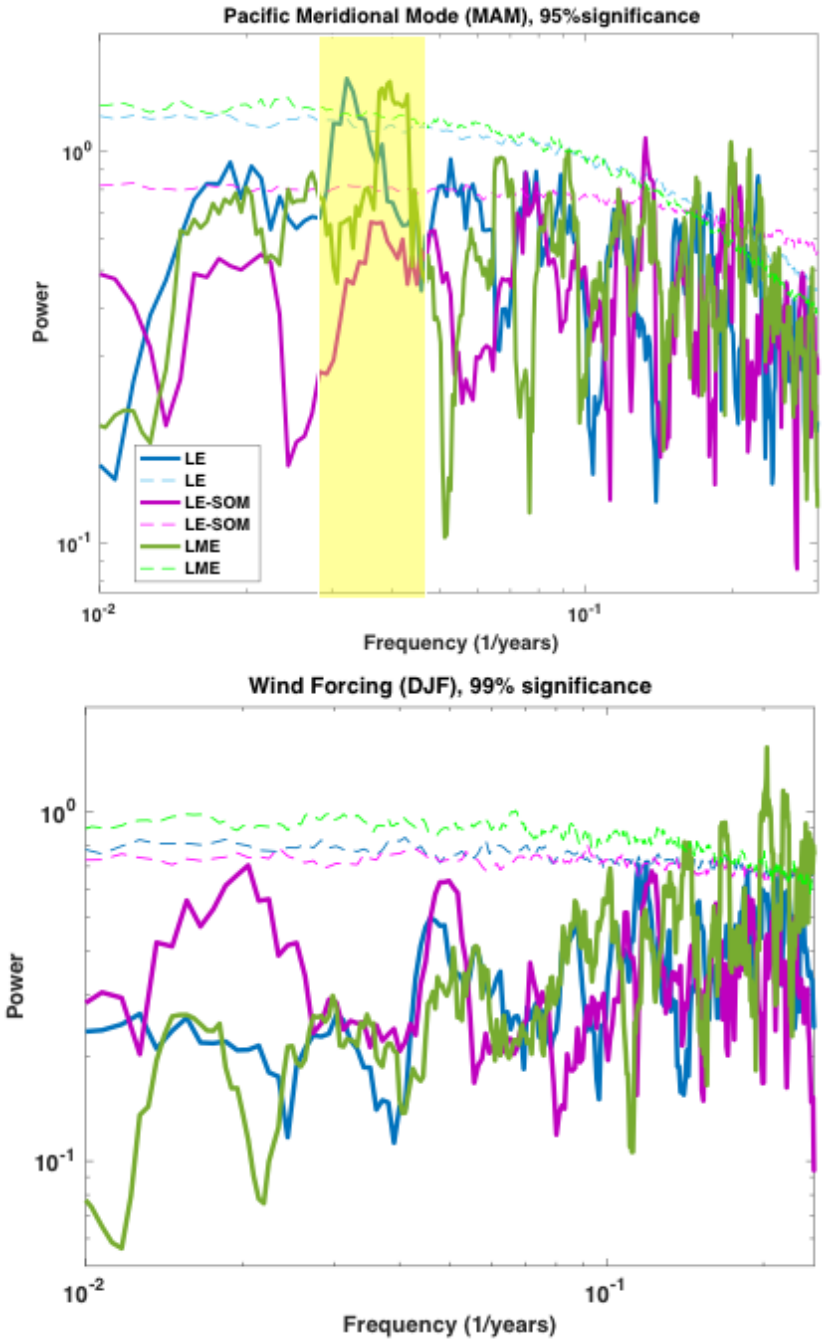

Figure 3.6 Assessment of the necessity of ocean dynamics through contrasting experiments with and without an interactive ocean. I use the 1. Control from the CESM-Last Millennium Ensemble (green, 1156 years), 2. Control from the CESM Large Ensemble (to ensure that there are no critical differences when changing our spatial resolution between the LME and LE, blue, 1000 years) and

(Figure 3.6 Continued)
2). A slab ocean model with no ocean dynamics (pink, 999 years). I use multitaper spectral analysis (4 tapers) to assess the dominant frequencies in (**A.)** the Pacific Meridional Mode index and (**B.)** averaged zonal winds in the region most influential on the PMM (In CESM it is U averaged over 15°N to 30°N, 175° to 205°E, slightly westward of that in the observational record, highlighted in green in Figure 3.1).

3.4 Discussion

3.4.1 Feedbacks within the background state

Modifications in the background climate have been hypothesized to alter the variability of the Pacific Meridional Mode. The work presented here does not disprove the most prominent hypotheses (ITCZ structure, sensitivity of latent heat flux to zonal winds, and North Pacific storminess); however, no single process mentioned here appears to dominate the unforced internal variation of the model PMM. Still, a background climatological pattern associated with the Pacific Meridional Mode variance emerges in the CESM Last Millennium Ensemble. This background state is characterized by cooler North Pacific sea surface temperatures, and Weaker Walker circulation in the equatorial Pacific during periods of high PMM variance. This variability is statistically significant at multidecadal timescales and requires oceanic feedbacks to maintain this significance. This oceanic feedback is suspected to be dominated by equatorial thermocline variability.

The equatorial thermocline has a potentially important role in the natural modulation of the Pacific Meridional Mode. My analysis has shown that 1. Ocean dynamics are fundamental in setting the timescales observed in PMM variability, and 2. robust modulations in the subsurface equatorial Pacific occur in association with variations in the amplitude of the Pacific Meridional Mode. Thermocline variability has an important role in determining the interdecadal amplitude of ENSO [Ogata et al. 2013, Rodgers et al. 2004, Dewitte et al. 2007, Borlace et al. 2013].

During periods of high ENSO variance, a sharpening of the thermocline is observed, which translates to a deepening of the western equatorial Pacific thermocline [Ogata et al. 2013]. A sharper thermocline increases the sensitivity of surface SST to thermocline displacement, which supports a positive feedback between ENSO and tropical Pacific decadal variability. However, it is important to note that the pattern in the CESM mixed layer depth associated with PMM variance does not explicitly resemble the canonical ENSO response.

Previous studies have noted the dynamical ink between the Western North Pacific and the North Pacific Oscillation [Linkin and Nigam 2008, Baxter and Nigam 2015, Wang et al. 2012, Wang et al. 2014, Hartmann 2015] whereby anomalous convection in the Western Tropical North Pacific (WTNP) will generate atmospheric Rossby waves that can influence the NPO during the influential winter season (Wang et al. 2014, Furtado et al. 2012]. The southern node of the NPO is thought to be highly influenced by tropical wave train activity from the equatorial Pacific [Furtado et al. 2012, DiLorenzo et al. 2010]. However, our study suggests that in CESM, this tropical atmospheric interaction is not the driving factor maintaining the statistically significant decadal variability in the PMM system. While the atmospheric component of the slab ocean experiment is statistically indistinguishable from model runs with active ocean dynamics, the slab ocean simulations of the PMM do not feature significant decadal variability, implying that the source of the significant decadal variability stems from the oceanic feedback. Given the high loading in the equatorial Pacific found in the fully coupled experiments; ENSO dynamics are likely necessary to maintain this decadal variability.

These results support prior studies showing distinct, yet necessary roles for both subtropical atmospheric noise and equatorial dynamics in maintaining decadal variability [DiLorenzo et al. 2015, Okumura et al. 2017]. DiLorenzo et al. 2015 neatly divided the influence

of "meridional" and "zonal" modes on decadal variability, noting that the Meridional Mode can supply decadal and multidecadal variability to the tropics, while ENSO dynamics are important to amplify that variability through global teleconnections. Okumura et al. 2017 further illustrated that influences from other regions, particularly the South Pacific, might have an important role in mediating interdecadal Pacific variability. This pattern in the background state is associated with physical characteristics that makes the PMM more receptive to forcing from the North Pacific Oscillation.

The background state of the Pacific has long been thought to have the potential to influence on the amplitude of tropical variability. However, here I illustrate the range of internal PMM variability and attempt to show how it may have varied over the last millennium. Previous works have hypothesized mechanisms responsible for the low frequency modulation of ENSO [Li et al. 2011, Ogata et al. 2013, Chowdary et al. 2012, Rodgers et al. 2004, Meehl et al. 2001]. Many of these works suggest that ENSO variance is enhanced during periods of decreased zonal SST contrast, deeper eastern equatorial Pacific thermocline, and weaker Walker circulation [Meehl et al. 2001, Imada and Kimoto 2008, Kirtman and Schopf 1998; Kleeman et al. 1999; Barnett et al. 1999; Ogata et al. 2013**].** Complimentary to the work presented here, Okumura et al. 2017 found that both ENSO and extratropical variability are important in setting prominent decadal variability in CCSM4. The pattern associated with the interdecadal amplitude modulation of ENSO in CCSM4 resembles the PMM variance pattern in CESM-LME.

3.4.2 Interdecadal amplitude modulation of PMM and ENSO

The Pacific Meridional Mode is distinct from ENSO, but modulation of PMM behavior nevertheless may have important consequences for ENSO (Figure 3.2D). This work connects the

variance of the NPO, PMM, and Niño 3 in the CESM LME, showing that variations in the PMM are an influential means by which ENSO responds to forced change, thereby connecting ENSO variability to nonlocal stochastic variability. This result is supported by Chiang et al. 2009, 2010, which showed that a dampening of ENSO during the mid-Holocene could be attributed to weakened PMM variability, potentially due to a stronger jet stream, minimizing atmospheric noise through the mid-winter suppression mechanism [Nakamura et al. 1992]. An outstanding question is if the PMM's ability to influence decadal variability and ENSO has varied throughout time, independent of changes in the variance of the PMM.

While the instrumental record is too short to directly compare observations with these model based results, there is evidence in the observational record that central Pacific El Niño events, dynamically linked to the PMM, become more prevalent during colder North Pacific conditions [Xiang et al. 2011, McPhaden 2010, Chung and Li 2013, Choi et al. 2011]. McPhaden [2010] pointed out that the central equatorial Pacific El Niño events were becoming more prevalent during a period with a cooler, negative Pacific Decadal Oscillation phase, in contrast to the prevailing theories suggesting that Central Pacific El Niño events were becoming more powerful due to the anthropogenic warming. Further studies cited mechanisms of zonal advective feedback, thermocline feedback, and mean suppressed convection theory to explain this enhancement of Central Pacific El Niño events [Xiang et al. 2011, Chung and Li 2013, Choi et al. 2011]. However, it is possible to assess these forced changes though the past in the PMM framework.

3.4.3 Paleoarchives

While instrumental records lack the length to capture century-scale changes in the mean state, paleoclimate proxies have recorded the variations in the climate system over the last millennium. For example, during a period known as the Little Ice Age, years 1400-1850, paleoclimate proxies suggest that while mean global temperature may no have varied much (IPCC AR4), the Northern Hemispheric surface temperatures were 0.6°-0.8°C cooler [Mann et al. 1998, Mann et al. 2009], the ITCZ was displaced southward by as much as 5° [Sachs et al. 2009] or significantly different in structure [Denniston et al. 2016, and Lechleitner et al. 2017], southwestern Pacific salinity increased [Hendy et al. 2002]. The exact cause of these departure from "average" is thought to be a combination of intense volcanism and reduced solar forcing [Atwood et al. 2017]. It is interesting to note that physically constrained general circulation models have a difficult time reproducing the magnitude of the anomalies expressed in paleoclimate proxies during this Little Ice Age event. This may be due partially to inaccuracies in model physics, and partially due to the interpretation of limited samples the paleoproxy record. However, the comparison between paleoclimate proxies and models allows for a highly effective means of constraining past climate dynamics. While it is premature to compare the Little Ice Age in the Last Millennium Ensemble to the relevant paleoclimate proxies, I can describe some of the expected changes in the mean state. In paleoclimate proxies, there is evidence that PMM variability could have responded to subtle changes in the mean state. During the Little Ice Age, a period renowned for northern hemispheric cooling [Mann et al. 1998] and lower ITCZ [Sachs et al. 2009], heightened decadal variability associated with the PMM has been observed [Sanchez et al. 2016]. Other proxies in regions of PMM influence also show

heightened decadal variability during the early 19th century [Halfar et al. 2011, Hertzinger et al. 2011 MacDonald and Case 2005, Griffin and Anchukaitis 2014]. However, it should be noted that equatorial upwelling is thought to have been intensified [Druffel et al. 2015], implying a stronger Walker Circulation, directly at odds with our implication of Weaker Walker Circulation during periods of high PMM activity. Additionally, ENSO reconstructions [Li et al. 2013, Emile-Geay et al. 2013] do not show an intensification of ENSO variability, or a preponderance for an El Niño-like state during this time. The response of the PMM to the Little Ice Age in the CESM LME is not assessed because the magnitude of the mean state anomalies in the model are much weaker than the evidence suggested by high resolution paleoclimate archives.

3.4.4 Anthropogenic Change and Forced Variability

In the CESM LME, unforced, internal variability alone is found to modulate the moving standard deviation of the PMM by a factor of two. In single ensemble members, this internal variability dominates, while forced changes have a less substantial impact on the PMM. Four simulations forced by an "All Forcing" scenario were continued through year 2100 with RCP8.5 greenhouse gas forcing. The RCP8.5 scenarios demonstrate that truly unprecedented change can occur. A 33% increase in standard deviation of the PMM relative to the 2006 average by year 2100 is found, similar to the result found by Liguori and DiLorenzo 2018. In the RCP 8.5 scenarios, the correlations between expansion coefficients do not change, implying that no increase or decrease in air-sea coupling that accompanies the warming trend. Figure 3.3C shows the range of the ensemble members in the All forcing and RCP8.5 forcing scenarios. This forced change in PMM variability is distinct from the unforced, internal modulation described in depth here. This study also shows that suggests that at the "present" 2006, the variance observed is not

outstanding given the context of the last millennium. Our study also demonstrates that volcanic eruptions can influence the PMM, but the link is not extremely robust (Appendix B. Figure B.3).

3.5 Conclusion

I set out to address how the Pacific Meridional Mode may have changed over the last millennium. In CESM Last Millennium Ensemble, the PMM has operated in a physical framework similar to modern observations. I show that the model PMM has the ability to influence ENSO, particularly in the N3 region.

Our results demonstrate that PMM responds to forced change. Ensemble averages produce consistent responses to greenhouse gas forcing and some large volcanic eruptions. However, deviations in PMM variability not due to forced changes are the largest source of variability over the last millennium and can modify the standard deviation of the PMM by a factor of two. Furthermore, projected end-of-21^{sst} century changes under the RCP8.5 pathway are larger than for any episode over the last millennium.

In the CESM LME, I have found a common pattern associated with the magnitude of the variance of the Pacific Meridional Mode. Epochs of high variability are associated with weaker Walker Circulation, cooler North Pacific sea surface temperatures, and a more southerly ITCZ. Conversely, epochs of low variance have nearly opposite traits. These epochs of high or low variance persist for decades, and ocean dynamics appear to be fundamental in setting the timescale. However, additional thermodynamic feedbacks between the Western Tropical North Pacific sea surface temperatures and the extratropics are likely to be important.

My results reinforce a complexity of previously-proposed hypotheses for the generation and persistence of the PMM, instead of invalidating any single hypothesis. Without disentangling causality, I have shown the southward ITCZ shift, atmospheric noise in the extratropics, and strength of the WES feedback are all positively associated with PMM variability. At the very least, the results also allow us to interpret and test paleoclimate observations in new light, particularly during the Little Age when Northern Hemispheric temperatures are thought to have been cooler, the ITCZ thought to have been shifted further south. This work also opens new questions: How does the unforced "variance mode" actually enhance the PMM? Is the relationship between ENSO and the Pacific Meridional Mode constant? What factors are most important?

3.6 References

Amaya, D. J., DeFlorio, M. J., Miller, A. J., & Xie, S. P. (2017). WES feedback and the Atlantic Meridional Mode: observations and CMIP5 comparisons. *Climate Dynamics*, *49*(5-6), 1665-1679.

Anderson, B. T. (2003). Tropical Pacific sea-surface temperatures and preceding sea level pressure anomalies in the subtropical North Pacific. *Journal of Geophysical Research: Atmospheres*, *108*(D23).

Atwood, A. R., Battisti, D. S., Wittenberg, A. T., Roberts, W. H. G., & Vimont, D. J. (2016). Characterizing unforced multi-decadal variability of ENSO: a case study with the GFDL CM2. 1 coupled GCM. *Climate Dynamics*, 1-18.

Alexander, M. A., Vimont, D. J., Chang, P., & Scott, J. D. (2010). The impact of extratropical atmospheric variability on ENSO: Testing the seasonal footprinting mechanism using coupled model experiments. *Journal of Climate*, *23*(11), 2885-2901.

Baxter, S., & Nigam, S. (2015). Key role of the North Pacific Oscillation–west Pacific pattern in generating the extreme 2013/14 North American winter. *Journal of Climate*, *28*(20), 8109-8117.

Barnett, T. P., Pierce, D. W., Latif, M., Dommenget, D., & Saravanan, R. (1999). Interdecadal interactions between the tropics and midlatitudes in the Pacific basin. *Geophysical Research Letters*, *26*(5), 615-618.

Bischoff, T., & Schneider, T. (2014). Energetic constraints on the position of the intertropical convergence zone. *Journal of Climate*, *27*(13), 4937-4951.

Borlace, S., Cai, W., & Santoso, A. (2013). Multidecadal ENSO amplitude variability in a 1000-yr simulation of a coupled global climate model: Implications for observed ENSO variability. *Journal of Climate*, *26*(23), 9399-9407.

Chang, P., Zhang, L., Saravanan, R., Vimont, D.J., Chiang, J.C., Ji, L., Seidel, H. and Tippett, M.K., 2007. Pacific meridional mode and El Niño—Southern oscillation. *Geophysical Research Letters*, *34*(16).

Chang, P., Ji, L., & Li, H. (1997). A decadal climate variation in the tropical Atlantic Ocean from thermodynamic air-sea interactions. *Nature*, *385*(6616), 516.

Chiang, J. C., & Bitz, C. M. (2005). Influence of high latitude ice cover on the marine Intertropical Convergence Zone. *Climate Dynamics*, *25*(5), 477-496.

Chiang, J. C. H., Fang, Y., & Chang, P. (2009). Pacific climate change and ENSO activity in the mid-Holocene. *Journal of Climate*, *22*(4), 923-939.

Chiang, J. C., & Fang, Y. (2010). Was the North Pacific wintertime climate less stormy during the mid-Holocene?. *Journal of Climate*, *23*(14), 4025-4037.

Chiang, J. C., & Vimont, D. J. (2004). Analogous Pacific and Atlantic meridional modes of tropical atmosphere–ocean variability. *Journal of Climate*, *17*(21), 4143-4158.

Choi, J., An, S. I., & Yeh, S. W. (2012). Decadal amplitude modulation of two types of ENSO and its relationship with the mean state. *Climate dynamics*, *38*(11-12), 2631-2644.

Chowdary, J. S., Xie, S. P., Tokinaga, H., Okumura, Y. M., Kubota, H., Johnson, N., & Zheng, X. T. (2012). Interdecadal variations in ENSO teleconnection to the Indo–western Pacific for 1870–2007. *Journal of Climate*, *25*(5), 1722-1744.

Chung, P. H., & Li, T. (2013). Interdecadal relationship between the mean state and El Niño types. *Journal of climate*, *26*(2), 361-379.

Czaja, A., Van der Vaart, P., & Marshall, J. (2002). A diagnostic study of the role of remote forcing in tropical Atlantic variability. *Journal of Climate*, *15*(22), 3280-3290.

Denniston, R.F., Ummenhofer, C.C., Wanamaker, A.D., Lachniet, M.S., Villarini, G., Asmerom, Y., Polyak, V.J., Passaro, K.J., Cugley, J., Woods, D. and Humphreys, W.F., 2016. Expansion and contraction of the Indo-Pacific tropical rain belt over the last three millennia. *Scientific reports*, *6*, p.34485.

Deser, C., Phillips, A.S., Tomas, R.A., Okumura, Y.M., Alexander, M.A., Capotondi, A., Scott, J.D., Kwon, Y.O. and Ohba, M., 2012. ENSO and Pacific decadal variability in the Community Climate System Model version 4. *Journal of Climate*, *25*(8), 2622-2651.

Deser, C., Phillips, A., Bourdette, V., & Teng, H. (2012). Uncertainty in climate change projections: the role of internal variability. *Climate Dynamics*, *38*(3-4), 527-546.

Dewitte, B., Yeh, S. W., Moon, B. K., Cibot, C., & Terray, L. (2007). Rectification of ENSO variability by interdecadal changes in the equatorial background mean state in a CGCM simulation. *Journal of climate*, *20*(10), 2002-2021.

Di Lorenzo, E., Liguori, G., Schneider, N., Furtado, J. C., Anderson, B. T., & Alexander, M. A. (2015). ENSO and meridional modes: A null hypothesis for Pacific climate variability. *Geophysical Research Letters*, *42*(21), 9440-9448.

Di Lorenzo, E., & Mantua, N. (2016). Multi-year persistence of the 2014/15 North Pacific marine heatwave. *Nature Climate Change*.

Di Lorenzo, E., Cobb, K. M., Furtado, J. C., Schneider, N., Anderson, B. T., Bracco, A., Alexander, M.A., & Vimont, D. J. (2010). Central Pacific El Niño and decadal climate change in the North Pacific Ocean. Nature Geoscience, 3(11), 762-765.

Donohoe, A., Marshall, J., Ferreira, D., & Mcgee, D. (2013). The relationship between ITCZ location and cross-equatorial atmospheric heat transport: From the seasonal cycle to the Last Glacial Maximum. *Journal of Climate*, *26*(11), 3597-3618.

Druffel, E. R., Griffin, S., Vetter, D., Dunbar, R. B., & Mucciarone, D. M. (2015). Identification of frequent La Niña events during the early 1800s in the east equatorial Pacific. *Geophysical Research Letters*, *42*(5), 1512-1519.

Emile-Geay, J., Cobb, K. M., Mann, M. E., & Wittenberg, A. T. (2013). Estimating central equatorial Pacific SST variability over the past millennium. Part II: Reconstructions and implications. *Journal of Climate*, *26*(7), 2329-2352.

Furtado, J. C., Di Lorenzo, E., Anderson, B. T., & Schneider, N. (2012). Linkages between the North Pacific Oscillation and central tropical Pacific SSTs at low frequencies. *Climate dynamics*, *39*(12), 2833-2846.

Ghil, M., Allen, M.R., Dettinger, M.D., Ide, K., Kondrashov, D., Mann, M.E., Robertson, A.W., Saunders, A., Tian, Y., Varadi, F. and Yiou, P., 2002. Advanced spectral methods for climatic time series. *Reviews of geophysics*, *40*(1).

Griffin, D., & Anchukaitis, K. J. (2014). How unusual is the 2012–2014 California drought?. *Geophysical Research Letters*, *41*(24), 9017-9023.

Guillet, S., Corona, C., Stoffel, M., Khodri, M., Lavigne, F., Ortega, P., Eckert, N., Sielenou, P.D., Daux, V., Churakova, O.V. and Davi, N., 2017. Climate response to the Samalas volcanic eruption in 1257 revealed by proxy records. *Nature Geoscience*, *10*(2), p.123.

Halfar, J., Williams, B., Hetzinger, S., Steneck, R.S., Lebednik, P., Winsborough, C., Omar, A., Chan, P. and Wanamaker Jr, A.D., 2011. 225 years of Bering Sea climate and ecosystem dynamics revealed by coralline algal growth-increment widths. *Geology*, *39*(6), 579-582.

Hartmann, D. L. (2015). Pacific sea surface temperature and the winter of 2014. *Geophysical Research Letters*, *42*(6), 1894-1902.

Hendy, E. J., Gagan, M. K., Alibert, C. A., McCulloch, M. T., Lough, J. M., & Isdale, P. J. (2002). Abrupt decrease in tropical Pacific sea surface salinity at end of Little Ice Age. *Science*, *295*(5559), 1511-1514.

Hetzinger, S., Halfar, J., Mecking, J.V., Keenlyside, N.S., Kronz, A., Steneck, R.S., Adey, W.H. and Lebednik, P.A., 2012. Marine proxy evidence linking decadal North Pacific and Atlantic climate. *Climate Dynamics*, *39*(6), 1447-1455.

Imada, Y., & Kimoto, M. (2009). ENSO amplitude modulation related to Pacific decadal variability. *Geophysical Research Letters*, *36*(3).

Change, I. C. (2007). The Fourth Assessment Report of the Intergovernmental Panel on Climate Change. *Geneva, Switzerland*.

Joh, Y., & Di Lorenzo, E. (2017). Increasing Coupling Between NPGO and PDO Leads to Prolonged Marine Heatwaves in the Northeast Pacific. *Geophysical Research Letters*, *44*(22).

Kalnay, E., Kanamitsu, M., Kistler, R., Collins, W., Deaven, D., Gandin, L., Iredell, M., Saha, S., White, G., Woollen, J. and Zhu, Y., 1996. The NCEP/NCAR 40-year reanalysis project. *Bulletin of the American meteorological Society*, *77*(3), 437-471.

Kay, J.E., Deser, C., Phillips, A., Mai, A., Hannay, C., Strand, G., Arblaster, J.M., Bates, S.C., Danabasoglu, G., Edwards, J. and Holland, M., 2015. The Community Earth System Model (CESM) large ensemble project: A community resource for studying climate change in the presence of internal climate variability. *Bulletin of the American Meteorological Society*, *96*(8), 1333-1349.

Kim, Seon Tae, and Jin-Yi Yu. "The two types of ENSO in CMIP5 models." *Geophysical Research Letters* 39.11 (2012).

Kirtman, B. P., & Schopf, P. S. (1998). Decadal variability in ENSO predictability and prediction. *Journal of Climate*, *11*(11), 2804-2822.

Kleeman, R., McCreary, J. P., & Klinger, B. A. (1999). A mechanism for generating ENSO decadal variability. *Geophysical Research Letters*, *26*(12), 1743-1746.

Larson, S. M., & Kirtman, B. P. (2014). The Pacific meridional mode as an ENSO precursor and predictor in the North American multimodel ensemble. *Journal of Climate*, *27*(18), 7018-7032.

Larson, S., & Kirtman, B. (2013). The Pacific Meridional Mode as a trigger for ENSO in a high-resolution coupled model. *Geophysical Research Letters*, *40*(12), 3189-3194.

Lavigne, F., Degeai, J.P., Komorowski, J.C., Guillet, S., Robert, V., Lahitte, P., Oppenheimer, C., Stoffel, M., Vidal, C.M., Pratomo, I. and Wassmer, P., 2013. Source of the great AD 1257 mystery eruption unveiled, Samalas volcano, Rinjani Volcanic Complex, Indonesia. *Proceedings of the National Academy of Sciences*, *110*(42), 16742-16747.

Lechleitner, F.A., Breitenbach, S.F., Rehfeld, K., Ridley, H.E., Asmerom, Y., Prufer, K.M., Marwan, N., Goswami, B., Kennett, D.J., Aquino, V.V. and Polyak, V., 2017. Tropical rainfall over the last two millennia: evidence for a low-latitude hydrologic seesaw. *Scientific Reports*, *7*, p.45809.

Li, J., Xie, S.P., Cook, E.R., Morales, M.S., Christie, D.A., Johnson, N.C., Chen, F., D'Arrigo, R., Fowler, A.M., Gou, X. and Fang, K., 2013. El Niño modulations over the past seven centuries. *Nature Climate Change*, *3*(9), p.822.

Liguori, G., & Di Lorenzo, E. (2018). Meridional Modes and Increasing Pacific decadal variability under anthropogenic forcing. *Geophysical Research Letters*.

Lin, C. Y., Yu, J. Y., & Hsu, H. H. (2015). CMIP5 model simulations of the Pacific meridional mode and its connection to the two types of ENSO. *International Journal of Climatology*, *35*(9), 2352-2358.

Linkin, M. E., & Nigam, S. (2008). The North Pacific Oscillation–west Pacific teleconnection pattern: Mature-phase structure and winter impacts. *Journal of Climate*, *21*(9), 1979-1997.

MacDonald, G. M., & Case, R. A. (2005). Variations in the Pacific Decadal Oscillation over the past millennium. *Geophysical Research Letters*, *32*(8).

Mann, M. E., Bradley, R. S., & Hughes, M. K. (1998). Global-scale temperature patterns and climate forcing over the past six centuries. *Nature*, *392*(6678), 779.

McPhaden, M. J., Lee, T., & McClurg, D. (2011). El Niño and its relationship to changing background conditions in the tropical Pacific Ocean. *Geophysical Research Letters*, *38*(15).

Martinez-Villalobos, C., & Vimont, D. J. (2016). The Role of the Mean State in Meridional Mode Structure and Growth. *Journal of Climate*, *29*(10), 3907-3921.

Mann, M.E., Zhang, Z., Rutherford, S., Bradley, R.S., Hughes, M.K., Shindell, D., Ammann, C., Faluvegi, G. and Ni, F., 2009. Global signatures and dynamical origins of the Little Ice Age and Medieval Climate Anomaly. *Science*, *326*(5957), 1256-1260.

McGee, D., Donohoe, A., Marshall, J., & Ferreira, D. (2014). Changes in ITCZ location and cross-equatorial heat transport at the Last Glacial Maximum, Heinrich Stadial 1, and the mid-Holocene. *Earth and Planetary Science Letters*, *390*, 69-79.

Meehl, G. A., Gent, P. R., Arblaster, J. M., Otto-Bliesner, B. L., Brady, E. C., & Craig, A. (2001). Factors that affect the amplitude of El Niño in global coupled climate models. *Climate Dynamics*, *17*(7), 515-526.

Nakamura, H. (1992). Midwinter suppression of baroclinic wave activity in the Pacific. *Journal of the Atmospheric Sciences*, *49*(17), 1629-1642.

Ogata, T., Xie, S. P., Wittenberg, A., & Sun, D. Z. (2013). Interdecadal amplitude modulation of El Niño–Southern Oscillation and its impact on tropical Pacific decadal variability. *Journal of Climate*, *26*(18), 7280-7297.

Okumura, Y. M., Sun, T., & Wu, X. (2017). Asymmetric modulation of El Niño and La Niña and the linkage to tropical Pacific decadal variability. *Journal of Climate*, *30*(12), 4705-4733.

Otto-Bliesner, B.L., Brady, E.C., Fasullo, J., Jahn, A., Landrum, L., Stevenson, S., Rosenbloom, N., Mai, A. and Strand, G., 2016. Climate variability and change since 850 CE: an ensemble approach with the community earth system model. *Bulletin of the American Meteorological Society*, *97*(5), 735-754.

Percival, D. B., and A. T. Walden, *Spectral Analysis for Physical Applications*, 583, Cambridge Univ. Press, New York, 1993.

Rogers, J. C. (1981). The north Pacific oscillation. *International Journal of Climatology*, *1*(1), 39-57.

Rodgers, K. B., Friederichs, P., & Latif, M. (2004). Tropical Pacific decadal variability and its relation to decadal modulations of ENSO. *Journal of Climate*, *17*(19), 3761-3774.

Sachs, J. P., Sachse, D., Smittenberg, R. H., Zhang, Z., Battisti, D. S., & Golubic, S. (2009). Southward movement of the Pacific intertropical convergence zone AD 1400–1850. *Nature Geoscience*, *2*(7), 519-525.

Sanchez, S. C., Charles, C. D., Carriquiry, J. D., & Villaescusa, J. A. (2016). Two centuries of coherent decadal climate variability across the Pacific North American region. *Geophysical Research Letters*, *43*(17), 9208-9216.

Schneider, T., Bischoff, T., & Haug, G. H. (2014). Migrations and dynamics of the intertropical convergence zone. *Nature*, *513*(7516), 45-53.

Smith, T. M., Reynolds, R. W., Peterson, T. C., & Lawrimore, J. (2008). Improvements to NOAA's historical merged land–ocean surface temperature analysis (1880–2006). *Journal of Climate*, *21*(10), 2283-2296.

Stevenson, S., Otto-Bliesner, B., Fasullo, J., & Brady, E. (2016). "El Niño Like" Hydroclimate Responses to Last Millennium Volcanic Eruptions. *Journal of Climate*, *29*(8), 2907-2921.

Sullivan, A., Luo, J. J., Hirst, A. C., Bi, D., Cai, W., & He, J. (2016). Robust contribution of decadal anomalies to the frequency of central-Pacific El Niño. *Scientific Reports*, *6*, 38540.

Thomas, E. E., & Vimont, D. J. (2016). Modeling the Mechanisms of Linear and Nonlinear ENSO Responses to the Pacific Meridional Mode. *Journal of Climate*, *29*(24), 8745-8761.

Thomson, D. J., Spectrum estimation and harmonic analysis, *Proc. IEEE*, **70**, 1055– 1096, 1982.

Vimont, D. J., Battisti, D. S., & Hirst, A. C. (2001). Footprinting: A seasonal connection between the tropics and mid-latitudes. *Geophysical research letters*, *28*(20), 3923-3926.

Vimont, D. J., Wallace, J. M., & Battisti, D. S. (2003). The seasonal footprinting mechanism in the Pacific: Implications for ENSO. *Journal of Climate*, *16*(16), 2668-2675.

Vimont, D. J. (2005). The contribution of the interannual ENSO cycle to the spatial pattern of decadal ENSO-like variability. *Journal of Climate*, *18*(12), 2080-2092.

Vimont, D. J., Alexander, M., & Fontaine, A. (2009). Midlatitude excitation of tropical variability in the Pacific: the role of thermodynamic coupling and seasonality. *Journal of Climate*, *22*(3), 518-534.

Vimont, D. J. (2010). Transient growth of thermodynamically coupled variations in the tropics under an equatorially symmetric mean state. *Journal of Climate*, *23*(21), 5771-5789.

Vimont, D. J., Alexander, M. A., & Newman, M. (2014). Optimal growth of central and east Pacific ENSO events. *Geophysical Research Letters*, *41*(11), 4027-4034.
Walker, G. T., & Bliss, E. W. (1932) World weather. V. Mem. Roy. Meteor. Soc., 4, 53-84.

Wang, S. Y., L'Heureux, M., & Chia, H. H. (2012). ENSO prediction one year in advance using western North Pacific sea surface temperatures. *Geophysical Research Letters*, *39*(5).

Wang, S. Y., L'Heureux, M., & Yoon, J. H. (2013). Are greenhouse gases changing ENSO precursors in the western North Pacific?. *Journal of Climate*, *26*(17), 6309-6322.

Wang, S. Y., Hipps, L., Gillies, R. R., & Yoon, J. H. (2014). Probable causes of the abnormal ridge accompanying the 2013–2014 California drought: ENSO precursor and anthropogenic warming footprint. *Geophysical Research Letters*, *41*(9), 3220-3226.

Xiang, B., Wang, B., & Li, T. (2013). A new paradigm for the predominance of standing central Pacific warming after the late 1990s. *Climate dynamics*, *41*(2), 327-340.

Xie, S. P., & Philander, S. G. H. (1994). A coupled ocean-atmosphere model of relevance to the ITCZ in the eastern Pacific. *Tellus A*, *46*(4), 340-350.

Yu, J. Y., & Kim, S. T. (2011). Relationships between extratropical sea level pressure variations and the central Pacific and eastern Pacific types of ENSO. *Journal of Climate*, *24*(3), 708-720.

Yu, J. Y., Kao, H. Y., & Lee, T. (2010). Subtropics-related interannual sea surface temperature variability in the central equatorial Pacific. *Journal of Climate*, *23*(11), 2869-2884.

Zhang, H., Clement, A., & Di Nezio, P. (2014). The South Pacific meridional mode: A mechanism for ENSO-like variability. *Journal of Climate*, *27*(2), 769-783.

Zhang, H., Deser, C., Clement, A., & Tomas, R. (2014). Equatorial signatures of the Pacific Meridional Modes: Dependence on mean climate state. *Geophysical Research Letters*, *41*(2), 568-574.

Zhang, L., Chang, P., & Ji, L. (2009). Linking the Pacific meridional mode to ENSO: Coupled model analysis. *Journal of Climate*, *22*(12), 3488-3505.

Zhang, W., Vecchi, G. A., Murakami, H., Villarini, G., & Jia, L. (2016). The Pacific meridional mode and the occurrence of tropical cyclones in the western North Pacific. *Journal of Climate*, *29*(1), 381-398.

3.7 Acknowledgements

Portions of this Chapter 3 are being prepared for submission for publication.

Sanchez, Sara; Amaya, Dillon; Charles, Christopher; Miller, Arthur; Xie, Shang-Ping. The dissertation author was the primary investigator and author of this paper.

Additional elements of this submission can be found in Appendix B.

Chapter 4.

Constraining paleo carbonate chemistry: new insights from $\delta^{11}B$ and B/Ca measurements in monitored corals from Palmyra Atoll

Abstract

Limited observations from diverse coral reef systems highlight uncertainties in the relative importance of various small scale physical oceanographic, reef, and organismal processes that contribute to coral health. Here I present observations of skeletal carbon chemistry tracers in a network of *Porites* corals from Palmyra Atoll, a virtually pristine location in the central equatorial Pacific. The chemical and isotopic analysis of the coral skeletons spanning the growth years 2014-2017 overlaps with high resolution *in situ* observations from sensor packages immediately adjacent to the coral colonies sampled. This direct comparison provides a unique opportunity to test the fidelity of these proxies in different reef environments while also capturing the response to a large El Nino event. The coral records suggest differential ability to modify internal calcifying fluid chemistry, and, in particular, large excursions in the boron isotopic composition are found in some (but not all) corals coincident with a documented bleaching event and maximum temperature stress. The comparison of boron isotopes with other geochemical tracers is used to investigate the variables that control the ability of a coral to upregulate its internal calcifying fluid.

4.1 Introduction

Of all the potential risks associated with progressive acidification of tropical oceans, the decreased vitality of the coral reef ecosystems ranks among the most prominent and important. Yet, despite the intense interest in, and research effort devoted to the issue, there remains a fundamental disconnect between the regional oceanographic understanding of the ocean acidification phenomenon and the ultimate projections of the effects on coral calcification. The source of this disconnect is at least three-fold:

(1) The regional trends in carbon uptake delineated by WOCE surveys and analogous international programs (e.g. [Doney et al., 2009; Feely et al., 2004; 2013]) do not necessarily capture the various scales of pH variability that actually occur on reefs. While the unidirectional anthropogenically forced trends in the mean state are often the principal focus of carbon cycling projections, natural variations in seawater carbon parameters in isolated coral reef ecosystems typically dwarf the magnitude of expected mean trends for even the most extreme projections of tropical open ocean pH (e.g. RCP 8.5 forcing scenario). For example, diurnal pH range from 7.82 to 8.42 units were observed in a Molaki reef [Yates and Halley 2006], and diurnal variability of up to 0.6-0.9 pH units were found in various reef environments around Moorea [Hoffman et al., 2011, Rivest et al. 2014]. Thus, while open ocean pH may provide an important baseline of the pH of seawater in coral reefs, local seawater pH in reef systems--the direct influence on coral physiology and vitality—can vary independently of open ocean trends.

(2) Secondly, various reef processes on the community scale that dictate the relative balance of net calcification, photosynthesis and respiration could effectively filter the primary oceanographic forcing in ways that might either exacerbate or mitigate the anthropogenic pH

variability. [eg. Cryonak et al. 2018, DeCarlo et al. 2016, Yeakel et al. 2015, DeCarlo et al. 2015, Andersson et al., 2013, Shaw et al. 2012, Cryonak et al. 2014, Shamberger et al. 2014, Takeshita 2016, Nicole Price 2012, Yates and Halley 2006, Blackford and Gilbert 2007, Feely et al.2008, Salisbury et al. 2008]. The details of this "filtering" by reef communities are not likely to be universal among all reefs, and, therefore, it is difficult to extrapolate the observations from experimental aquaria or other mesocosm installations across the tropics.

(3) Thirdly, on an organismal scale, the possibility exists for varying degrees of intracellular regulation of calcifying fluid pH. In order to precipitate calcium carbonate, corals must actively modulate their internal chemistry by pumping out H^{2+} and pumping in Ca^{2+}. Though it is well-established that the pH of the coral calcifying fluid is elevated above that of ambient seawater, the actual mechanisms of the regulatory process--the ion transport and enzymatic pathways, and the internal pH monitor that ultimately dictates the traffic of these pathways (e.g. [Barott et al., 2013, 2017])--is largely unknown. This lack of understanding makes it essentially impossible to articulate *a priori* the expected response to pH perturbations across coral taxa. The most common assumption is that the coral internal calcifying fluid varies in conjunction with that of the surrounding seawater [Trotter et al. 2011, McCulloch e al. 2012, Venn et al. 2013, Holcomb et al. 2014], an assumption that is supported by at least some experimental observations [Venn et al. 2011]. The implication of this assumption is that if the seawater pH drops, the coral must expend more energy to upregulate its internal pH to precipitate aragonite and form its skeleton under this higher pH differential [McCulloch et al. 2012]. Since preindustrial times, mean seawater pH has dropped ~0.1 units, but it is estimated to drop another 0.1-0.4 pH units by the end of the 21st century [Bopp et al. 2013]. On the other hand, other evidence suggests that calcifying fluid

chemistry can vary uniquely within each coral, and even within calcifying centers in an individual coral.

These considerations all underscore the importance of establishing long-term monitoring systems for as many reef systems as possible. As straightforward as this recognition might seem, the practical limitations of *in situ* sensor installations has meant that there are only a few continuous *in situ* instrumental time series of reef pH spanning more than a season (e.g. [Bates et al., 2010]). And though the number of *in situ* installations has increased significantly in recent years [Hoffman et al., 2011; Cyronak et al. 2018], observations sufficient for comprehensive assessment of interannual-decadal variability from such installations will not be realized for another two decades. Furthermore, these sensor data do not, by themselves, speak to the pH variability at the site of coral calcification; coral skeletal characteristics must be interrogated for that insight.

Consequently, there is a clear and immediate role for the alternative approach of looking backward with "retrospective" monitoring systems that make use of skeletal tracers archived in cores from massive coral colonies. Here I make use of one such experimental platform afforded by coral skeletal samples collected from Palmyra Atoll, a central Pacific reef setting that is largely free of direct human disturbance, but that lies close to the center of action for the El Niño phenomenon. I investigate the record of carbon chemistry tracers in several massive *Porites* corals at multiple sites that have been the subject of multi-year ecological surveys that included instrumentation with *in situ* pH sensors. Furthermore, the coral skeletal samples capture the response of the large 2015/2016 El Nino event that witnessed a globally widespread and locally significant bleaching event.

A particular focus of the study was to characterize the boron concentration and the boron isotopic variability in the coral skeletal samples. In seawater, boron has a long residence time,

yielding a rather consistent, worldwide boron isotopic composition [Spivak and Edmond 1987, Taylor and McLennan 1985]. There are two species of dissolved boron in seawater: boric acid and borate, and this speciation varies as a function of pH. Only the borate species is involved in incorporating boron into the carbonate structure [Hemming and Hanson 1992]. The isotopic composition of borate, also varies with the pH of seawater [Hemming Hanson 1992, McCulloch et al. 2012, Gagnon 2013]. The boron concentration of biogenic carbonate has been used to infer the carbonate ion concentration of seawater or of the calcifying fluid [McCulloch et al. 2017, Yu and Elderfield 2007, Rae et al. 2011]. Boron isotopes offer a favorable signal to noise ratio as measurement reproducibility is roughly 0.02 pH units. A number of laboratory studies have verified a relationship between boron isotopes in corals and seawater [Honisch et al. 2004, Reynaud et al. 2004], and there are a few publications using boron isotopes in corals to construct a long climate record in a paleoclimate context [Pelejero et al. 2005, Wei et al. 2009, Shinjo et al. 2013]. However, the laboratory experiments lack many of the biophysical dynamics of the real ocean, while the reconstructions of boron isotopes in fossil corals lack a rigorous comparison to contemporaneous instrumental measurements of seawater pH. Here, I take advantage of the borate-boric acid system in seawater, by measuring boron isotopes and trace metal concentrations in the monitored Palmyra corals. This in situ calibration experiment, across a relatively undisturbed reef system and across a large ENSO event, allows us to investigate the role of the local environment perturbations and coral physiology in governing not only the pH proxy systematics, but also, more generally, coral vitality.

4.2 Site Characteristics and Experiment Design

Palmyra Atoll (5.8° N, 162.0° W) lies in the central equatorial Pacific and is a remote, essentially uninhabited marine protected area. As a result, the island experiences minimal direct human influences in the form of runoff, fishing, and sedimentation. This offers a unique environment to study the impacts of climate change on coral reef systems. As such, many ecological studies have taken place at Palmyra, using it as a reference for "healthy" coral ecosystem [Stevenson et al. 2007, Dinsdale et al., 2008; Sandin et al., 2008, Williams et al. 2013].

Palmyra Atoll is also ideally positioned to document the influence of the El Nino Southern Oscillation (ENSO) phenomenon. For example, coral skeletal tracers from this site have been used to document ENSO's character over the last millennium [Cobb et al. 2001, Cobb et al. 2003]. At Palmyra Atoll, El Nino events are regularly characterized by anomalously warm sea surface temperatures, increased rainfall, changes in ocean circulation, a weakening of the prevailing trade winds, and occasionally coral bleaching. Globally, the 2015 and 2016 period stand out as the two warmest years in the instrumental record; the El Nino event was one of the largest documented, and associated with widespread bleaching and coral mortality [Hughes et al. 2017, Hughes et al. 2018].

Four short cores of *Porites* were collected in October 2016 (in the recovery phase of the 2015/2016 El Niño event) from three sites off of the western terrace of the atoll using a small, hand held pneumatic drill. Coring sites were targeted on the basis of proximity to one of the network of Honeywell Durafet® SeapHOx sensors [Martz et al. 2010, Bresnahan et al. 2014], that have been deployed and maintained, beginning in 2009, as part of a long term ecological

study (by Jennifer Smith, SIO). These *in situ* sensors continuously record seawater pH, SST, and SSS. The record from these sensors was sampled in 15 minute intervals, though periodic sensor failure resulted in discontinuous time series at the various locations. Coring sites were further selected to maximize local differences in site depth, rugosity, and coral cover (see Table 4.1 for characteristics of each site, Figure 4.1 for map of coral locations).

Table 4.1 Coring site characteristics.

Site	Cores Analyzed	Depth	Characteristics	Percent Hard Coral Cover	Growth rate over 2014-2016 period (mm/year)	SST Standard Deviation(insitu sensor, 15 min sampling interval)
Reef Terrace 10	RT10	15ft, 4.6m	Well protected, high rugosity, typically very clear water.	~58%	14mm/year	0.55°C
Reef Terrace 4	RT4 & RT4 Side	18ft,5.5m	mixing with lagoon and open ocean common, occasionally cloudy.	~62%	14mm/year and 14mm/year	0.52°C
Fore Reef 3	FR3	42ft, 12.8m	Well mixed with open ocean. Subject to strong currents.	~60%	14mm/year	0.43°C

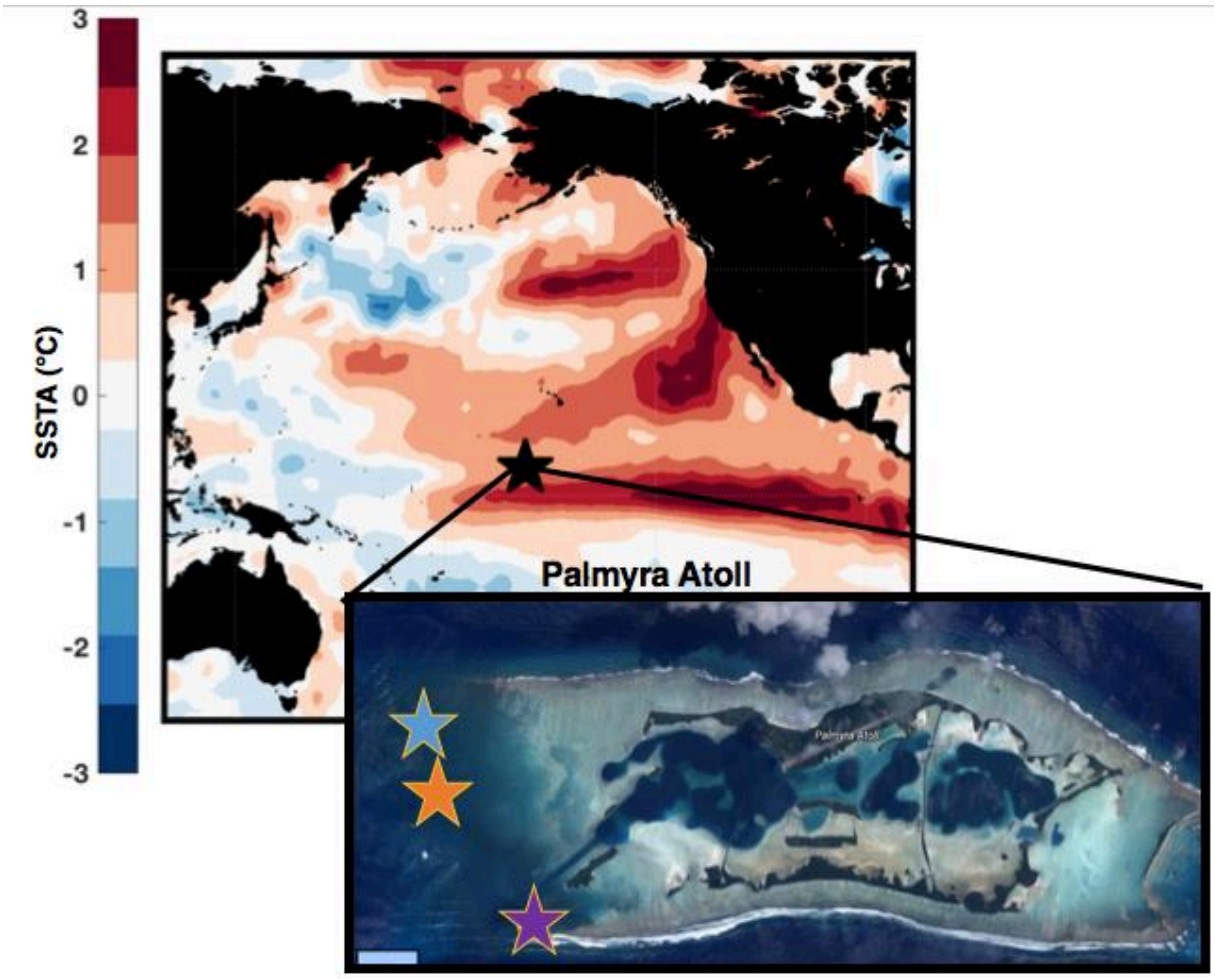

Figure 4.1 Sea surface temperature anomalies in September 2015 from NOAA Optimum Interpolation SST product (OISST). The study site, Palmyra Atoll (5.85N, 162.08W) is denoted with a black star and individual site locations are found in the bottom plot. Individual sites are denoted with stars; RT10 (blue), RT4 (orange), and FR3 (purple).

Two of the sampled sites are from the western reef terrace, characterized by shallow depth (3.8 meters at RT10, 4.7 meters at RT4), high rugosity, and some protection from the open ocean. However, there are some notable differences between the RT4 and RT10 sites. The RT10 site is the most protected, with exceptional water clarity and high coral cover. The RT4 site experiences more regular mixing with the inner lagoon and open ocean, with higher amounts of surge, occasionally causing cloudy conditions. The third site was in the fore reef, at 13.5 meters

depth. This location has very little three-dimensional structure and is regularly subject to strong currents, thus promoting vigorous exchange with the open ocean.

4.3 Methods

Corals were collected using a ~1.5 in diameter handheld pneumatic drill under permit #12533-16024 from The Nature Conservancy in September/October of 2016. Corals were x-rayed at UCSD Thornton Hospital to assess the annual banding of high and low skeletal density. Cores were then sampled every 1 mm along the primary growth axis and analyzed for $\delta^{13}C$ and $\delta^{18}O$ on the Finnegan MAT 253 at Scripps Institution of Oceanography. ThermoMAT 253 mass spectrometer equipped with a Kiel IV carbonate preparation device. Long-term analytical reproducibility for $\delta^{18}O$ is 0.08‰ and 0.06‰ for $\delta^{13}C$. Along with the annual density bands, these analyses helped to established the coral chronology, as detailed below. Coral powder was saved in clean Teflon centrifuge tube at Scripps Institution of Oceanography.

Boron isotope and trace metal analysis was conducted at the University of St. Andrews Stable Isotope and Geochemistry (StaIG lab), in Class-100 metal free clean rooms. Analytical techniques follow Foster et al. 2008 (and [Rae et al. 2011, Stewart et al. 2016]). Coral samples from the clean centrifuge tubes were weighed for 2.5 to 4mg of sample, then were prepared for oxidative cleaning. Oxidative cleaning entailed warm 1% H_2O_2 (buffered in ammonium hydroxide) to remove remaining organic matter. A weak acid leach was then applied (0.0005 M HNO_3) to remove any re-adsorbed ions. Afterwards, the cleaned samples were dissolved in a minimal volume of 0.5M HNO_3 before centrifuging and transferring into clean vials.

Prior to boron isotopic analysis, ~7% of each sample solution was reserved for trace elemental analysis using the Agilent Quadrupole ICP-MS. Each aliquot was diluted to have an equal concentration of Ca and was bracketed by well-characterized, matrix-matched synthetic standard solutions to yield B/Ca, Mg/Ca, Sr/Ca and U/Ca ratios for samples and to assess external reproducibility. This step yielded the trace metal (Li/Ca, B/Ca, Na/Ca, Mg/Ca, Sr/Ca, Ba/Ca, U/Ca) data.

In the remaining sample solutions, boron was separated from the samples' carbonate matrix using 20 µl micro-columns containing Amberlite IRA 743 boron-specific anionic exchange resin (Kiss, 1988). Samples are loaded in a 2M sodium acetate–0.5 M acetic acid buffer, rinsed with MilliQ water, and collected in 450 µl of 0.5 M HNO3. Column yields, checked by isotope dilution, are N95% [Foster, 2008] and the elution tail of every sample is checked with an extra acid rinse to ensure no significant amount of sample boron remains. $\delta^{11}B$ of purified boron samples were measured in triplicate on a Thermo Scientific Neptune multi-collector (MC)-ICPMS against NIST RM 8301c [Stewart et al. in prep] and JCp-1 [Okai et al. 2002]. Quality control was monitored by the standard deviation of the triplicate measurements of $\delta^{11}B$, by the concentration of boron in the elution tails (ensuring > 99% of sample boron was recovered in the sample), and measurements of the blanks and standards.

4.4 Results

The *in situ* sensor records of SSS and SST document high correlation between sites and, at monthly timescales, the records correlate strongly with large gridded SST products (such as ARGO drifting floats [Roemmich et al. 2003], NOAA ERSST [Huang et al. 2014], and NOAA

OISST [Banzon et al. 2016]). At higher frequencies, the reef terrace sites are characterized by significant (+/- 2°C) SST and (+/- 1PSU) SSS variability about the monthly mean, while the fore reef site features less variability on diurnal-fortnightly timescales. The similarities among all the sites in the monthly mean SST and SSS variability manifest themselves in the coral skeletal proxies that are commonly taken as monitors of the physical variables. For example, despite the markedly different site locations and local environmental conditions, the coral records have virtually identical mean and seasonal-interannual variability in $\delta^{18}O$ and Sr/Ca. The high apparent correlation of $\delta^{18}O$ and Sr/Ca with the observed SST and SSS is used to assign a monthly chronology to coral skeletal growth (Figure 4.2). There are limitations to the use of Sr/Ca as a strict SST proxy (e.g. [Alpert et al. 2016]), but the strong correlation with instrumental observations over the seasonal cycle provides a relatively tight constraint on the chronology (with an approximate uncertainty of +/- one month for any given coral record).

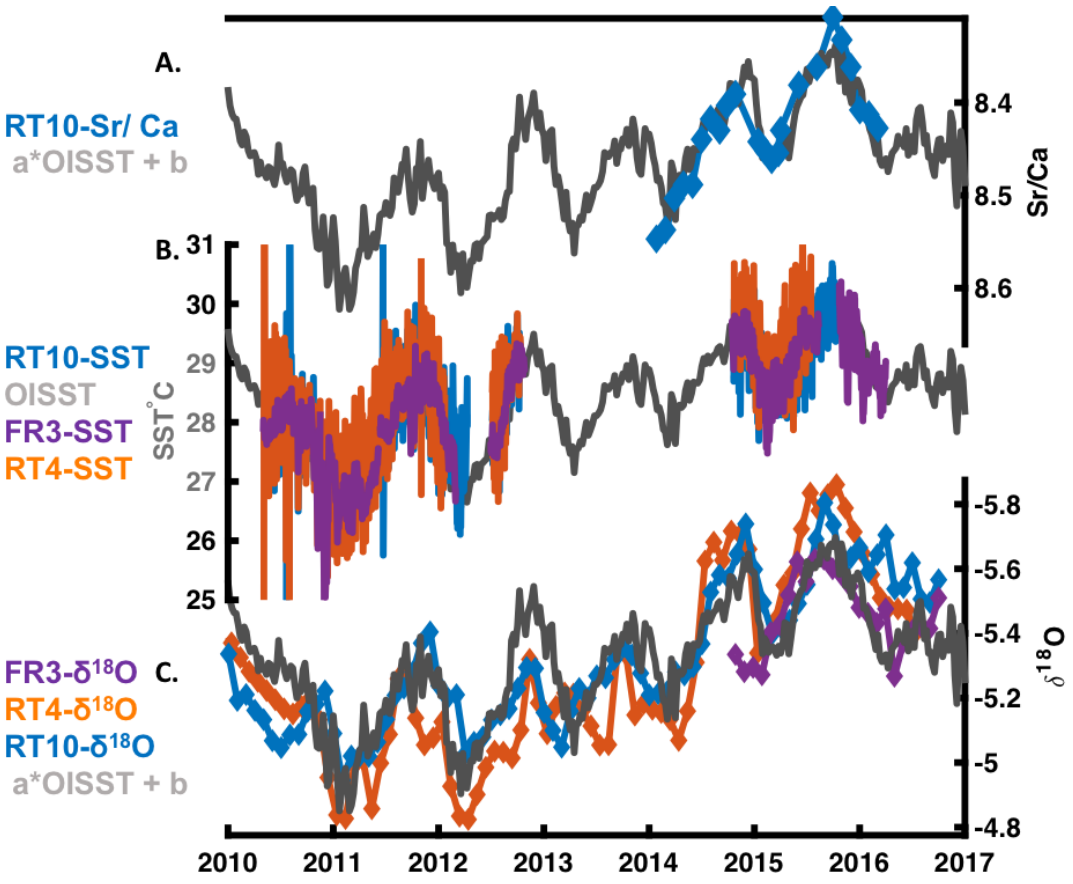

Figure 4.2 Timeseries of site characteristics. (A.) RT10 Sr/Ca and pseudo coral Sr/Ca record (black) using a*OISST + b, where a=-0.22‰ and b= an arbitrary constant.; **(B.)** OISST temperature (black) and temperature at each individual reef; **(C.)** $\delta^{18}O$ between sites and pseudo $\delta^{18}O$ (black) using a*OISST + b.

Cores from the three distinct sites were analyzed for boron isotope and trace metal composition, resulting in archives spanning two years from RT10, nine months from RT4 and eighteen months from the FR3 site (Figure 4.3). Over this interval, the *in situ* sensors document a relatively narrow pH range of 0.1-0.2 units, and although the time series at individual sites is discontinuous, there is little agreement among sites. The most continuous of sensor records, the Penguin Spit Middle Sensor (Figure 4.3A), documents a decrease in pH during the summer and maximum seawater pH in the winter over the 2014-2016 period. In general, the pH on most reefs must be controlled by the balance of net calcification and net respiration [Yeakel et al.

2015, Kline et al.2015, DeCarlo et al. 2016]. Thus, the lack of detailed agreement among sites must also point to reef-scale heterogeneity in these balances.

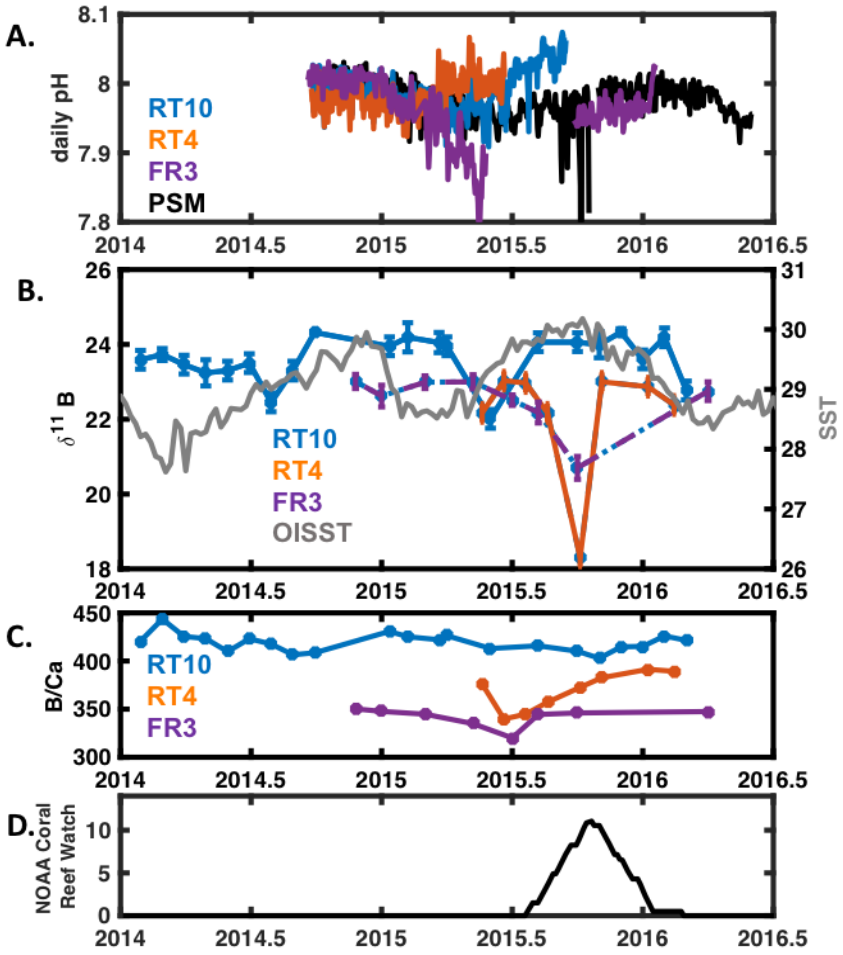

Figure 4.3 Observations of Palmyra carbonate chemistry. ***(A.)*** Smith Lab SeapHOx sensor data from the three coring sites, RT10 (blue), RT4 (purple), and FR3 (orange), as well as another more continuous reef terrace site, Penguin Spit Middle (black); data curated by Yui Takeshita, **(B.)** Coral $\delta^{11}B$, thought to be a proxy for extracellular calcifying fluid pH **(C.)** Coral B/Ca, thought to be a proxy for extracellular calcifying fluid carbonate ion concentration and ***(D.)*** NOAA Coral Reef Watch Degrees Heating Weeks bleaching index.

4.4.1 Boron chemistry

Despite the narrow range of sensor pH variability, the coral $\delta^{11}B$ records display considerable variability, both within a single site and in the mean composition between sites. In the mean, the $\delta^{11}B$ values of RT10 are significantly higher (~1.4 ‰) than those of RT4 and FR3. With existing calibrations of coral $\delta^{11}B$ to pH, an offset of 1.4‰ would imply higher seawater pH by ~0.2 units [Hönisch et al., 2004; Holcomb et al., 2014; McCulloch et al., 2012]. Since this offset is not observed in the sensor data, the offset towards higher $\delta^{11}B$ values in RT10 must be a physiological effect, implying different degrees of "upregulation" of calcifying fluid pH in corals from the same reef. Furthermore, the extremes in sensor pH are generally not associated with extremes in coral $\delta^{11}B$. There is a hint of a seasonal cycle in RT10 $\delta^{11}B$, evidenced by excursions to ~2‰ lower values (albeit captured with one point) during early fall in each year. Excursions of ~2‰ imply a pH decrease of ~0.26 unit, which is approximately the seasonal cycle in the sensor data. But more data is required to evaluate the consistency of the annual cycle.

The most prominent decreases in $\delta^{11}B$ in the RT4 and FR3 cores occur in conjunction with the severe bleaching event of September 2015. Sea surface temperatures around Palmyra surpassed a bleaching threshold for an extended amount of time; peaking at 10.6 Degree Heating Weeks. As reference, the threshold linked to highest likelihood of coral bleaching is 8 Degree Heating weeks. Additionally, each sampled site has photographic evidence of bleaching from a field excursion to Palmyra in September of 2015, (photoquad/personal communication, See Table 1.). The severe decline in $\delta^{11}B$ coeval with the bleaching event at Palmyra is not observed in the RT10 site.

The concentration of boron in corals is also meaningful, given that it is taken as a measure of the carbonate ion concentration of the calcifying fluid (e.g. [McCulloch et al. 2017, Yu and Elderfield 2007, Rae et al. 2011]). Absolute boron concentrations were notably separated in all cores. RT10 again had the largest offset, with a high mean B/Ca of 419 umol/mol. RT4 and FR3 were in a similar range again, with mean B/Ca concentrations of 369 umol/mol and 340 umol/mon, respectively. Local extremes of B/Ca concentration do not correspond with any $\delta^{11}B$ extremes within the cores.

4.4.2 Carbon isotope chemistry

The network of Palmyra cores displays marked offsets in the mean $\delta^{13}C$ composition of individual cores. Cores with most direct sunlight, RT10 and RT4, have heavier mean $\delta^{13}C$, but RT4S and FR3 have lighter, more depleted $\delta^{13}C$ values. A decrease in coral skeletal $\delta^{13}C$ with depth has been observed in many studies and attributed to the difference in the directness of sunlight, which is likely the case for the FR3 core (e.g. [Weber et al., 1976; Bosscher, 1992; Carriquiry et al., 1994; Grottoli, 1999]). The large offset in RT4 and RT4S is particularly notable as both cores were collected from the same coral head, confirming that the observed difference in mean skeletal $\delta^{13}C$ must be due to metabolic activity caused by photosynthetic activity rather than local seawater properties. This offset is in line with conventional ideas of photosynthetic fractionation; $\delta^{13}C$ is driven to higher values with increased light availability, presumably because of increased zooxanthellae photosynthetic activity would sequester more of the isotopically light carbon from the available pool for skeletal formation (e.g. [Fairbanks and Dodge, 1979], and many others). Interestingly, the mean isotopic composition of the "RT4S" core does not have a constant offset from the RT4 top core; at interannual timescales, the carbon

isotope composition converges, particularly at year 2003, 2008, and 2012. There are no obvious reasons for this convergence.

Variations in skeletal $\delta^{13}C$ composition are dominated by a semi-annual cycle, synchronous with the semi-annual seasonal variations in light, regardless of mean $\delta^{13}C$ composition or coral location. At all sites, heavier $\delta^{13}C$ is associated with decreased light availability, or increased cloud cover (as described in Fairbanks and Dodge, 1979) is observed in the rainy seasons in April/May and October/November during the annual passage of the ITCZ (Appendix C., Figure C.1). While all sites experience the same atmospheric cloud conditions, it is possible that the enhanced mixing or turbidity within the reef could play a role in this seasonality at individual locations. Increased nutrient supply from physical oceanographic forcing can also influence coral calcification by increasing rates of photosynthesis [Grottoli et al. 2002]. Oceanographic flow around Palmyra could also be influential on this semi-annual signal; in particular, buoyancy driven flows from the inner lagoon, waves, and tides have been shown to be influential on the Palmyra reefs [Rogers et al. 2016].

No clear relationship between $\delta^{11}B$ and $\delta^{13}C$ is found in the Palmyra cores, despite the fact that both tracers should be influenced by the same set of processes. When considering the full network of Palmyra records, there is a weak positive correlation between $\delta^{11}B$ and $\delta^{13}C$ values (Figure 4.4A); however, the relationship between the two isotopes within in each individual coral core is much more complex (Figure 4.4B-D). Furthermore, there is no clear relationship during the extreme minima in boron isotope concentration (as in Hemming et al. 1998). The FR3 core is predominantly responsible for the positive relationship between $\delta^{11}B$ and $\delta^{13}C$, and, to a lesser extent, the positive relationship is found in the RT4 (top) core. In the RT10 core, no clear trend is found when considering all points; the least squares linear regression slope

between $\delta^{11}B$ and $\delta^{13}C$ is 0.00. However, two distinct trends are observed when identifying the points by the season of year using the oxygen isotopic composition (Figure 4.5). A positive slope is found during cooler, drier periods, accompanied with a higher oxygen isotopic composition, while a no trend to a very weak positive trend is observed during the warmer, wetter periods accompanied by a lower oxygen isotopic composition. This bifurcation in the relationship between $\delta^{11}B$ and $\delta^{13}C$ is loosely supported when considering other previously published coral records (Figure 4.5). Further measurements are necessary to determine the validity (and statistical significance) of these possible trends.

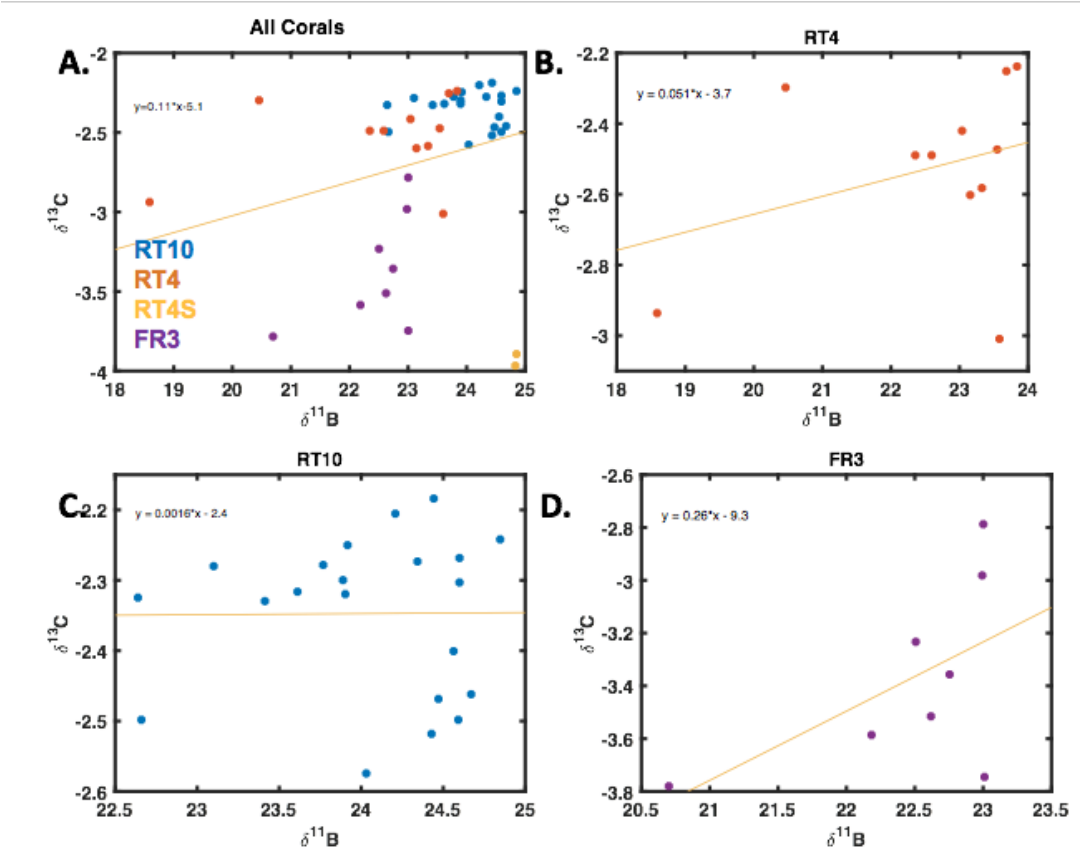

Figure 4.4 Relationship between $\delta^{13}C$ and $\delta^{11}B$ in the Palmyra cores, with the linear regression slope plotted in yellow. There are less points here than in Figure 5 due to data quality control checks. **(A.)** $\delta^{11}B$ vs $\delta^{13}C$ for all Palmyra coral records is plotted; **(B.)** $\delta^{11}B$ vs $\delta^{13}C$ in the RT4 (top) core; **(C.)** $\delta^{11}B$ vs $\delta^{13}C$ in the RT10 core; $\delta^{11}B$ vs $\delta^{13}C$ in the FR3 core.

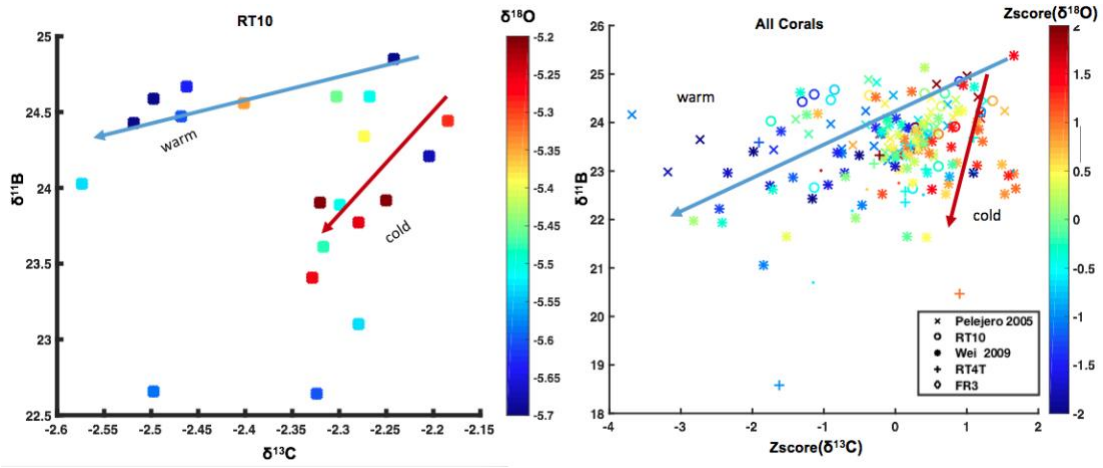

Figure 4.5. Potential role of temperature in relationship between $\delta^{13}C$ and $\delta^{11}B$. **(A.)** RT10 $\delta^{13}C$ and $\delta^{11}B$, as in 4.4C. Colors indicate oxygen isotopic composition of the same samples. **(B.)** Same as 4.5A, but using multiple coral records, from this study, Pelejero et al. 2005, and Wei et al. 2009. Cores are indicated by the shape of the marker.

4.4.3 Other Tracers

The longest record, RT10, is assessed for possible physical drivers influential on the observed geochemical variability. I take advantage of the suite of trace metal measurements to assess potential physical drivers influential to the RT10 coral (Figure 4.6 of RT10 with time). Perhaps the most obvious of physical drivers is the role of sea surface temperature. As previously mentioned, the $\delta^{11}B$ record in RT10 features prominent minima during maximal SST rise over the two years of observation. Sea surface temperature has a pronounced influence on the RT10 $\delta^{18}O$ and Sr/Ca concentration. B/Ca also notably follows the trend of SST (as expected from Hart and Cohen 1996 and Sinclair et al. 1998). Surprisingly, Mg/Ca and Li/Mg do not track particularly well with SST; Mg/Ca concentrations include some extra variability which complicates the SST driven signal.

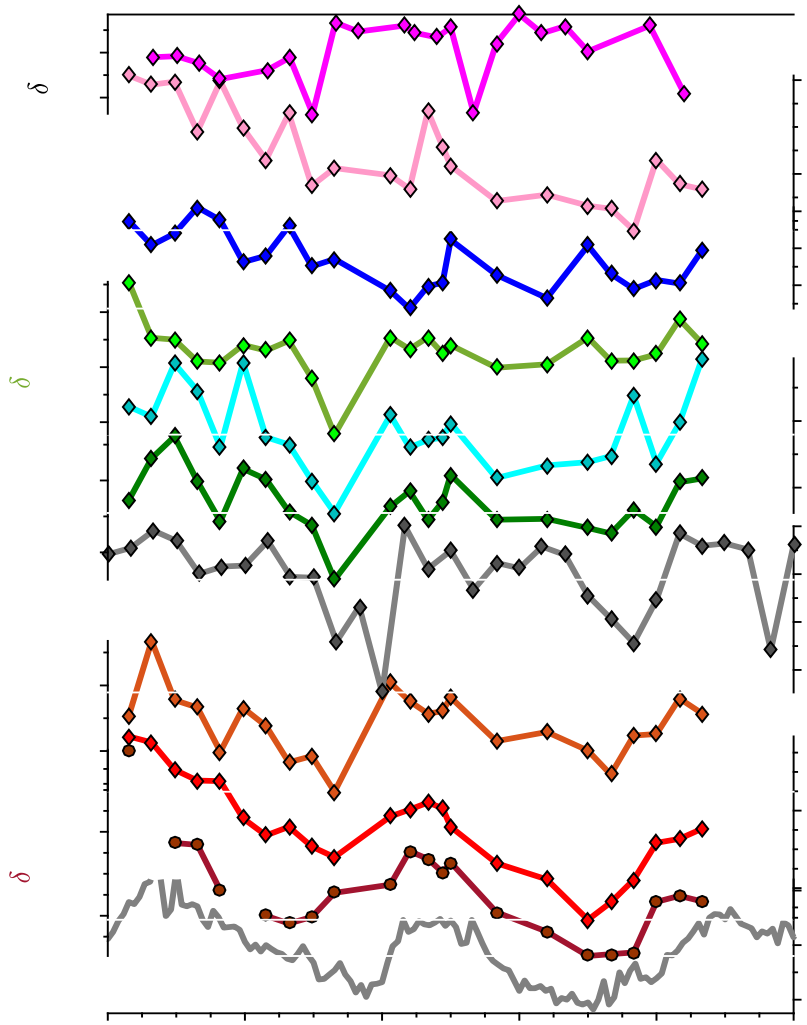

Figure 4.6 The suite of geochemical measurements in RT10 including (bottom to top) SST (OISST, grey), $\delta^{18}O$ (dark red), Sr/Ca (red), B/Ca (orange), precipitation from CPC-CMAP (grey), Na/Ca (dark green), Li/Ca (turquoise), $\delta^{13}C$ (light green), Ba/Ca (blue), U/Ca (pale pink), and $\delta^{11}B$ (magenta).

A strong semiannual cycle is notable in the trace metal data, particularly in the Na/Ca, Li/Ca, Ba/Ca. Due to the coherence with $\delta^{13}C$, it is possible that this periodicity reflects a biological response to the physical conditions related to the annual tracking of the ITCZ.

Several trace elemental ratios do not appear to purely respond to any of these physical variables. Perhaps the most noticeable is that of U/Ca. U/Ca is interesting for several reasons. It is thought to respond to sea surface temperature and carbonate ion concentration ion

concentrations in seawater; however, the timeseries of RT10 U/Ca variability seems thoroughly independent of SST and other proxies for carbonate ion here.

Despite uncertainty in the physical mechanisms responsible for all of the trace metal variability in the RT10 core, strong relationships in trace metal compositions between all collection sites are observed. These relationships in coral geochemistry are likely the result of the local reef environment, coral metabolism, and/or kinetic effects. The mechanisms behind trace metal incorporation and differences in biomineralization processes is further investigated in the Palmyra corals by comparing the coral records from the three sites, RT10, RT4, FR3, and include a fourth core from RT4. This fourth core, RT4S, is distinct as it was drilled into the side of the core, perpendicular to the traditional "top to bottom" approach to coring, as represented in the traditional RT4 coral record. This core will have experienced the same seawater conditions as RT4, but possibly very different vital effects due to differences in the intensity of solar radiation. Figure 4.7A highlights the variety of trace element relationships between sites in a "trace element matrix," including a Pearson correlation coefficient between all coral samples.

Figure 4.7. Top Right: Relationship between trace metals, colors represent core analyzed (RT10 (blue), RT4(orange), RT4S(yellow), FR3(purple)), number in upper left is Pearson correlation coefficient (N=48). Relationships between Li/Ca, B/Ca, Na/Ca, Mg/Ca, Sr/Ca, Ba/Ca, and U/Ca, $\delta^{13}C$, $\delta^{18}O$, $\delta^{11}B$ are investigated. Bottom Left: Theoretical Rayleigh fractionation curve compared with raw data for Li/Ca, Na/Ca relationship using partition coefficients as in RoillonBard et al. 2005 ($Li_{sw} = 25*10^{-6}$,$Na_{sw} = 0.459$, $D_{Na}= 0.000384$, $D_{Li}= 0.00198$). Using established coefficients yield large offsets from the data, most noticeable at more enriched trace element concentrations.

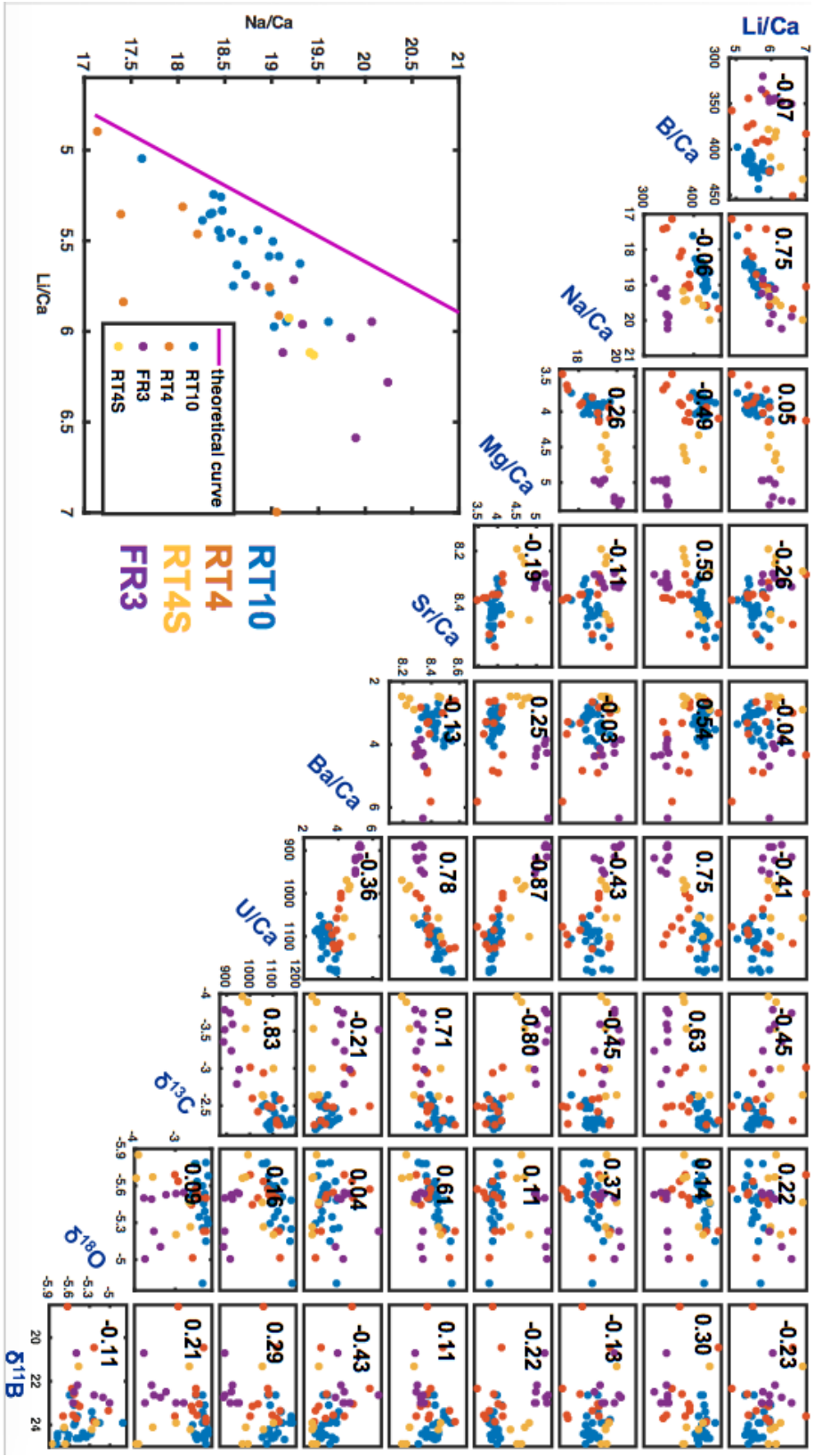
Li/Ca
B/Ca
Na/Ca
Mg/Ca
Sr/Ca
Ba/Ca
U/Ca
δ13C
δ18O
δ11B
-0.07
0.75
0.05
-0.26
-0.04
-0.41
-0.45
0.22
-0.23
-0.06
-0.49
0.26
-0.11
0.59
-0.19
0.54
-0.03
0.25
-0.13
0.75
-0.87
-0.43
0.63
-0.80
-0.45
0.14
0.37
0.30
-0.22
-0.18
-0.36
0.78
0.83
-0.21
0.71
0.09
0.16
0.04
0.61
0.11
-0.43
0.29
0.21
-0.11
Na/Ca
Li/Ca
theoretical curve
RT10
RT4
FR3
RT4S
RT10
RT4
RT4S
FR3

Four distinct patterns stand out in the tracer-tracer plots, highlighted here. (1.) Some trace element relationships feature a linear correlation within each individual coral core, but a seemingly small correlation when all cores are plotted together (for example the Li/Ca and B/Ca slopes). (2.) In some trace element relationships, there is a significant linear correlation, despite a lack of obvious physical mechanism of causing the covariance (Ex. Li/Ca and Na/Ca). (3.) For other trace element relationships, there is no intra-coral linear relationship, but strong inter-coral linear trends (Ex. Most elements plotted with U/Ca). (4.) Finally, there are some trace element relationships for which individual core values occupy a unique quadrant of the scatter plot, but no clear trend is discernible collectively (Ex. Mg/Ca vs B/Ca).

Between the Palmyra corals, the $\delta^{13}C$ composition has strong linear relationship with several trace metal variables; U/Ca, Mg/Ca, and Sr/U all exhibit a strongly linear relationship (Figure 4.7). This relationship is not observable within a single core, but rather observable when assessing multiple cores. The reason for this relationship not presently known. Coral U/Ca is thought to be influenced by SST (Min et al. 1995) and carbonate ion concentration [DeCarlo et al. 2015, Inoue et al. 2011]. Mg/Ca has been used as an SST proxy in corals [Mitsuguchi et al. 1996], but it is recognized that there are strong biological controls on Mg incorporation in the coral skeleton [Reynaud et al. 2007, Inoue et al. 2007]. In the Palmyra cores, Mg/Ca is not purely driven by SST (Figure 4.6). Additionally, Sr/U has gained attention as an SST proxy that minimizes the influence of Rayleigh fractionation on coral Sr/Ca composition [DeCarlo et al. 2016], however this proxy is not purely influenced by SST in the Palmyra corals. It is perhaps enlightening that this relationship would be maintained with $\delta^{13}C$, which is strongly influenced by kinetic effects.

4.5 Discussion

Boron isotopic and trace metal composition were measured in a network of *Porites* corals from multiple monitored reef sites during a period of anomalously high sea surface temperatures and pronounced bleaching. Coral boron isotopic composition was found to be independent of local seawater pH, but rather dependent upon the pH of the coral's internal calcifying fluid. This work suggests that corals are capable of different kinds of biomineralization processes, especially during periods of environmental stress. This work is not the first to suggest that the pH of the calcifying fluid does not strictly respond to variations in the pH of seawater [Georgiou et al. 2015, Wall et al. 2015, Comeau et al. 2017, McCulloch et al. 2016, Wu et al. 2017]. However, this study is the first to document natural $\delta^{11}B$ variability at multiple reef sites monitored with pH sensors. This work uniquely investigates means in which geochemical records might differ between reef systems in response to environmental stressors.

4.5.1 Coral bleaching of 2015

Over the 2014-2016 analysis period, the coral samples captured the growth and deterioration of one of the largest El Nino events, and subsequent global bleaching events. Both the NOAA Coral Reef Watch Satellite Virtual Station's bleaching metrics (Degree Heating Weeks and Hotspot Indices) and ecological transect characterization (Adi Khen, in prep) document contemporaneous mass bleaching at Palmyra, where bleaching peaked in September 2015. During this period of widespread documented bleaching, a negative spike in $\delta^{11}B$ is observed at two of the Palmyra sites; RT4 and FR3 (Figure 4.3). Site surveys during September 2015 document the RT4 and FR3 sites to have 16% and 20% bleached coral cover, respectively,

(Adi Khen, personal communication). The coral geochemistry from the third site, RT10, does not document any sharp decline in $\delta^{11}B$ at this time.

To date, no reliable paleo-bleaching proxy has been discovered, but abrupt declines in coral boron isotopic composition are thought to be related to coral bleaching. Depletions of 2.2-3.7‰ were observed in *Porites* sp. corals during bleaching in Dishon et al. 2015, and depletions of up to 5.1‰ were observed in *Stylophora pistillata* in Nir et al 2014. However, $\delta^{11}B$ is not a reliable bleaching proxy in corals; Schoepf et al. 2014 demonstrated that coral bleaching is not necessarily accompanied by a characteristic drop in $\delta^{11}B$. Furthermore, work by D'Olivo and McCulloch et al. 2017 documents a variety of responses of $\delta^{11}B$ to coral bleaching, even within the same coral. The study suggested that corals were capable of highly heterogeneous and individualized responses to stress.

Coral bleaching is primarily driven by extreme anomalous sea surface temperatures [Glynn, 1993; Brown, 1997; Hoegh-Guldberg, 1999], but other influential variables have been noted, as well as differences in sensitivity of individual coral species [Williams et al. 2010]. At Palmyra, bleaching susceptibility has been found to primarily respond to mean immediate temperature anomalies, and, to a lesser extent turbidity, sand cover, and depth [Williams et al. 2010]. The relatively stable $\delta^{11}B$ concentration at RT10 could possibly be due to its relatively protected environment and/or ability to maintain a much higher $\delta^{11}B$ of calcifying fluid.

4.5.2 Paired carbon and boron isotopes

Other geochemical clues indicate that the RT10 core could be capable of more homeostatic regulation of calcifying fluid chemistry. The RT10 core not only has a less variable, higher $\delta^{11}B$ concentration, it also has a distinctly higher B/Ca concentration, a proxy for

carbonate ion concentration [D'Olivo and McCulloch et al. 2017]. The largest variations in the $\delta^{11}B$ of the RT10 core seems to be due to a seasonal cycle. This work indicates that this coral from the clearer (less turbid) RT10 site has more control over its internal calcifying fluid chemistry. If this is the case, this implies that coral geochemistry could be used to assess the health and resilience of individual colonies.

Another proxy commonly used when assessing the influences on the coral calcification process is carbon isotopes. The interpretation of carbon isotopes in tropical, zooxanthellae bearing corals is notoriously complex as the calcification process is subject to both physical and biological interactions. However, the relationship between $\delta^{13}C$ and other tracers may help illuminate the mechanisms behind the coral calcification process. Skeletal carbon isotopic composition within the coral can reflect metabolic and diffusive carbon incorporation processes such as a direct leak from seawater activity of an ion transporter, or coral feeding. Skeletal $\delta^{13}C$ has been thought to be influenced the $\delta^{13}C$ of the ambient seawater [Swart et al. 2005], $\delta^{13}C$ of metabolic CO2 via zooxanthellae photosynthesis [Dodge and Fairbanks 1979, Erez et al. 1978] or food source [Grottoli et al. 2002], SST (ex. [Zhang et al. 1995]), non-equilibrium fractionation [McConnaughey (1989a, 2003)], and calcification site pH [Adkins et al. 2003].

The RT10 coral maintains distinction amongst the network of Palmyra corals when considering carbon isotopic composition. The mean carbon isotopic composition of RT10 is higher than the other cores. Additionally, the RT10 coral records a seasonal cycle in $\delta^{13}C$, as do the other cores, yet the variability has a much diminished magnitude (Appendix C., Figure C.1). Finally, the RT10 core appears to display a distinctly different relationship between $\delta^{11}B$ and $\delta^{13}C$.

Measurements of $\delta^{13}C$ in conjunction with measurements of calcifying fluid pH could offer valuable insight into the coral calcification process. Perhaps not surprisingly, the Palmyra cores suggest a complicated relationship between $\delta^{11}B$ and $\delta^{13}C$. The complexity of this relationship is likely due to multiple factors such as 1.) reef processes, 2.) organismal processes, 3.) kinetic effects. The likelihood of each of these factors influencing the $\delta^{11}B$ and $\delta^{13}C$ relationship in the Palmyra corals is addressed here.

At interannual to decadal timescales, seawater pH and seawater $\delta^{13}C$ could be influenced by variations in bulk seawater chemistry due to variations in local physical oceanography and variations in Community Net Ecosystem Production (NEP = gross primary production – autotrophic and heterotrophic respiration) and Net Ecosystem Calcification ((NEC = gross calcification – gross $CaCO_3$ dissolution) [Fowell et al. 2018, DeCarlo et al. 2017, Yeakel et al. 2015]. These reef scale processes could influence the skeletal $\delta^{13}C$ and $\delta^{11}B$ in the Palmyra cores, however if such a process was dominant, it would likely result in a similar relationship in $\delta^{13}C$ and $\delta^{11}B$ in all the sampled corals. This is not observed.

In *Porites,* positive correlations between $\delta^{13}C$ and $\delta^{11}B$ have been observed due to coral primary productivity [Hemming et al. 1998, Dissard et al. 2012, Reynaud et al. 2004]. According to this hypothesis, during periods of enhanced primary productivity and CO_2 fixation, $\delta^{12}C$ is preferentially utilized. This process leaves behind an enriched $\delta^{13}C$, and high pH, or elevated $\delta^{11}B$ in the extracellular calcifying fluid. In direct contradiction, other studies have documented no relationship between $\delta^{13}C$ and $\delta^{11}B$ has been found, particularly in situations where $\delta^{13}C$ is principally driven by variations in the $\delta^{13}C$ composition of metabolic CO_2 rather than by the abundance of metabolic CO_2 [Allison and Finch 2012]. Further work has shown that boron isotopes did not vary with light intensity or feeding in laboratory experiment [Honisch et al.

2004]. The Palmyra corals document both behaviors; RT4 and FR3 are associated with positive correlations, while the RT10 core shows no constant correlation between $\delta^{13}C$ and $\delta^{11}B$. The RT10 samples appear to have two distinct relationships between $\delta^{13}C$ and $\delta^{11}B$ related to SSTs. A high correlation between $\delta^{13}C$ and $\delta^{11}B$ is observed during higher SSTs, while a weaker correlation is found in association with cooler SSTs. It is unclear if this trend would be observable in the FR3 and RT4 cores with additional measurements.

Kinetic fractionation could also influence trends between $\delta^{13}C$ and $\delta^{11}B$ [McConneaughy et al. 1989a, Allison and Finch 2010, etc], but $\delta^{13}C$ and $\delta^{18}O$ are uncorrelated in the Palmyra corals, suggesting that they do not vary in response to a single factor. This lack of correlation suggests that $\delta^{13}C$ is not controlled by the photosynthetic fractionation, or fractionation due to the relative rate of CO_2 hydration and hydroxylation, which would also influence $\delta^{18}O$ [McConnaughey 1989a, McConnaughey, 2003]). Furthermore, $\delta^{13}C$ has no clear relationship with the previously validated temperature proxies (eg. Sr/Ca, or $\delta^{18}O$).

Taken together, the results from the Palmyra cores indicate a complex relationship between $\delta^{11}B$ and $\delta^{13}C$, dependent on multiple influences. One of the most intriguing aspects of this relationship is distinctly different relationships between $\delta^{11}B$ and $\delta^{13}C$ by sampling site. The difference in the relationship between $\delta^{11}B$ and $\delta^{13}C$ in the cores might be merely due to the limited measurements of the RT4 and FR3 cores, or it could be due to the potentially enhanced degree of internal upregulation in the RT10 coral. If the former is correct, this would suggest that the relationship between skeletal $\delta^{11}B$ and $\delta^{13}C$ varies throughout the year, and would be apparent with longer records from the RT4 and FR3 cores. This result suggests that the relationship between $\delta^{11}B$ and $\delta^{13}C$ varies in synchrony with temperature, or even perhaps reef scale NEP and NEC. Warmer temperatures would be associated with enhanced primary

productivity (using $\delta^{12}C$) and CO_2 fixation. If the difference in the relationship between $\delta^{11}B$ and $\delta^{13}C$ is due entirely to the enhanced regulation of the calcifying fluid in the RT10 core, this would suggest that corals with less internal upregulation can experience greater variations in the abundance of metabolic CO_2 within their calcifying fluid. This could account for different relationship between $\delta^{11}B$ and $\delta^{13}C$ between the different cores.

4.5.3 Environmental clues from aggregated tracers

Despite differences in reef environments of the sampled sites, the full network of Palmyra cores still has many consistencies that can be used to assess environmental change. For example, the $\delta^{18}O$ in all coral records is still in excellent agreement with SST. Additionally, strong correlations between various trace metal concentrations are observed at all sites. Several studies have addressed the occurrence of surprisingly high correlations between various trace elements and have cited a variety of potential mechanisms as the source of variability [Sinclair et al. 2005, Rollion Bard et al. 2015]. A variety of kinetic and metabolic processes may be responsible for the strong correlations in the trace metal data; mechanisms include Rayleigh fractionation [Cohen et al. 2006, Gagnon et al. 2007], temperature [Sinclair et al. 2005], pH of the calcifying fluid [Adkins et al., 2003; Holcomb et al., 2009], and the influence of specific ion pumps vs direct seawater transport [Gagnon et al., 2012]. As illustrated in Figure 4.6, many of the trace metals express similar variability within the RT10 core. These results suggest that Rayleigh distillation cannot be the cause of variability in the Li/Ca and Na/Ca relationship (Figure 4.7B). Additionally, temperature cannot be responsible for such agreement as many of these elements have clear biannual cycles, while temperature maintains a well-defined annual cycle. I also discard variations in the pH of the calcifying fluid as a potential mechanism as extremes in boron

isotope composition are not associated with significant extremes in the trace metal material in all corals. The potential role of specific ion pumps or an undescribed mechanism cannot be discounted. The mechanism(s) behind these strong correlations and offsets is unknown, but again highlights the important role of unique local environmental features on the coral calcification process.

The multi-site approach allows this work to emphasize the importance of spatial heterogeneity in small scale environmental features that might otherwise be overlooked in a coarsely resolved, global modelling analysis. Despite the close proximity of the Palmyra sites, there are important differences at much smaller spatial scales such as propensity for seawater turbidity, temperature variability, benthic cover, sedimentation, algae cover, currents, and relative protection from external forcing [Williams et al. 2010, Rogers et al. 2016]. These small scale features could have profound impacts on coral resilience and that these differences might manifest themselves in the geochemistry of the coral skeleton. This work provides a new assessment of coral geochemical proxies and their ability to address coral resilience in paleoclimate studies.

This work highlights wide variability in the community response to extreme environmental stressors. Regions that are reasonably well protected might be more resilient in the face of extreme events like the 2015-2016 El Nino. Management plans should consider that the ecosystem response could be moderated average level of background stressors. Within the Palmyra sites, the RT10 coral seemingly had the ability to upregulate internal chemistry over the length of the analysis, and did not record a shock associated with the 2015 bleaching event. The combination of greenhouse induced warming and progressive acidification of the ocean poses an

ominous threat coral reefs, but advances in damage mitigation might be made by understanding the factors that give rise to the reduced sensitivity exhibited by the RT10 coral.

4.6 References

Adkins, J. F., Boyle, E. A., Curry, W. B., & Lutringer, A. (2003). Stable isotopes in deep-sea corals and a new mechanism for "vital effects". *Geochimica et Cosmochimica Acta*, *67*(6), 1129-1143.

Allison, N., & Finch, A. A. (2012). A high resolution δ13C record in a modern Porites lobata coral: Insights into controls on skeletal δ13C. *Geochimica et Cosmochimica Acta*, *84*, 534-542.

Alpert, A. E., Cohen, A. L., Oppo, D. W., DeCarlo, T. M., Gove, J. M., & Young, C. W. (2016). Comparison of equatorial Pacific sea surface temperature variability and trends with Sr/Ca records from multiple corals. *Paleoceanography*, *31*(2), 252-265.

Andersson, A.J. and Gledhill, D., 2013. Ocean acidification and coral reefs: effects on breakdown, dissolution, and net ecosystem calcification. *Annual Review of Marine Science*, *5*, 321-348.

Barott, K.L., Barron, M.E. and Tresguerres, M., 2017. Identification of a molecular pH sensor in coral. *Proc. R. Soc. B*, *284*(1866), p.20171769.

Barott, K.L., Helman, Y., Haramaty, L., Barron, M.E., Hess, K.C., Buck, J., Levin, L.R. and Tresguerres, M., 2013. High adenylyl cyclase activity and in vivo cAMP fluctuations in corals suggest central physiological role. *Scientific reports*, *3*, p.1379.

Bates, N.R., Amat, A. and Andersson, A.J., 2010. Feedbacks and responses of coral calcification on the Bermuda reef system to seasonal changes in biological processes and ocean acidification. *Biogeosciences*, *7*(8), 2509-2530.

Banzon, V., Smith, T. M., Chin, T. M., Liu, C., and Hankins, W., 2016: A long-term record of blended satellite and in situ sea-surface temperature for climate monitoring, modeling and environmental studies. *Earth Syst. Sci. Data*, **8**, 165–176, doi:10.5194/essd-8-165-2016

Blackford, J. C., & Gilbert, F. J. (2007). pH variability and CO< sub> 2</sub> induced acidification in the North Sea. Journal of Marine Systems, 64(1), 229-241.

Bresnahan Jr, P. J., Martz, T. R., Takeshita, Y., Johnson, K. S., & LaShomb, M. (2014). Best practices for autonomous measurement of seawater pH with the Honeywell Durafet. *Methods in Oceanography*, *9*, 44-60.

Bopp, L., Resplandy, L., Orr, J.C., Doney, S.C., Dunne, J.P., Gehlen, M., Halloran, P., Heinze, C., Ilyina, T., Seferian, R. and Tjiputra, J., 2013. Multiple stressors of ocean ecosystems in the 21st century: projections with CMIP5 models. *Biogeosciences*, *10*, 6225-6245.

Bosscher, H. (1992). Growth potential of coral reefs and carbonate platforms.

Bryant, D., L. Burke, J. McManus, and M. Spalding. 1998. Reefs at Risk: A Map-based Indicator of Threats to the World's Coral Reefs. World Resources Institute. 56 pp. http://www.wri.org/wri/reefsatrisk/.

Carriquiry, J. D., Risk, M. J., & Schwarcz, H. P. (1994). Stable isotope geochemistry of corals from Costa Rica as proxy indicator of the El Niño/Southern Oscillation (ENSO). *Geochimica et Cosmochimica Acta*, *58*(1), 335-351.

Costanza, R., R. de Groot, P. Sutton, S. van der Ploeg, S. J. Anderson, I. Kubiszewski, S. Farber, and R. K. Turner (2014), Changes in the global value of ecosystem services, *Global Environ. Change*, 26, 152–158, doi:10.1016/j.gloenvcha.2014.04.002.

Comeau, S., Tambutté, E., Carpenter, R.C., Edmunds, P.J., Evensen, N.R., Allemand, D., Ferrier-Pagès, C., Tambutté, S. and Venn, A.A., 2017. Coral calcifying fluid pH is modulated by seawater carbonate chemistry not solely seawater pH. *Proc. R. Soc. B*, *284*(1847), p.20161669.

Cyronak, T., Schulz, K.G., Santos, I.R. and Eyre, B.D., 2014. Enhanced acidification of global coral reefs driven by regional biogeochemical feedbacks. *Geophysical Research Letters*, *41*(15), 5538-5546.

Cyronak, T., Andersson, A.J., Langdon, C., Albright, R., Bates, N.R., Caldeira, K., Carlton, R., Corredor, J.E., Dunbar, R.B., Enochs, I. and Erez, J., 2018. Taking the metabolic pulse of the world's coral reefs. *PloS one*, *13*(1), p.e0190872.

DeCarlo, T. M., Gaetani, G. A., Holcomb, M., & Cohen, A. L. (2015). Experimental determination of factors controlling U/Ca of aragonite precipitated from seawater: Implications for interpreting coral skeleton. *Geochimica et cosmochimica acta*, *162*, 151-165.

DeCarlo, T. M., Gaetani, G. A., Cohen, A. L., Foster, G. L., Alpert, A. E., & Stewart, J. A. (2016). Coral Sr-U thermometry. *Paleoceanography*, *31*(6), 626-638.

DeCarlo, T.M., Cohen, A.L., Wong, G.T., Shiah, F.K., Lentz, S.J., Davis, K.A., Shamberger, K.E. and Lohmann, P., 2017. Community production modulates coral reef pH and the sensitivity of ecosystem calcification to ocean acidification. *Journal of Geophysical Research: Oceans*, *122*(1), 745-761.

De Groot, R., Brander, L., Van Der Ploeg, S., Costanza, R., Bernard, F., Braat, L., Christie, M., Crossman, N., Ghermandi, A., Hein, L. and Hussain, S., 2012. Global estimates of the value of ecosystems and their services in monetary units. *Ecosystem services*, *1*(1), 50-61.

Dinsdale, E.A., Pantos, O., Smriga, S., Edwards, R.A., Angly, F., Wegley, L., Hatay, M., Hall, D., Brown, E., Haynes, M., Krause, L., Sala, E., Sandin, S.A., Thurber, R.V., Willis, B.L., Azam, F., Knowlton, N., Rohwer, F., 2008. Microbial ecology of four coral Atolls in the Northern Line Islands. PLoS ONE 3, e1584.

Dishon, G., Fisch, J., Horn, I., Kaczmarek, K., Bijma, J., Gruber, D.F., Nir, O., Popovich, Y. and Tchernov, D., 2015. A novel paleo-bleaching proxy using boron isotopes and high-resolution laser ablation to reconstruct coral bleaching events. *Biogeosciences 12 (2015), Nr. 19*, *12*(19), 5677-5687.

Dissard, D., Douville, E., Reynaud, S., Juillet-Leclerc, A., Montagna, P., Louvat, P., & McCulloch, M. (2012). Light and temperature effects on [delta] 11B and B/Ca ratios of the zooxanthellate coral Acropora sp.: results from culturing experiments. *Biogeosciences*, *9*(11), 4589.

D'olivo, J. P., & McCulloch, M. T. (2017). Response of coral calcification and calcifying fluid composition to thermally induced bleaching stress. *Scientific reports*, *7*(1), 2207.

Doney, S. C., Fabry, V. J., Feely, R. A., & Kleypas, J. A. (2009). Ocean acidification: the other CO2 problem.

Erez, J. (1978). Vital effect on stable-isotope composition seen in foraminifera and coral skeletons. *Nature*, *273*(5659), 199.

Fairbanks, R. G., & Dodge, R. E. (1979). Annual periodicity of the 18O16O and 13C12C ratios in the coral Montastrea annularis. *Geochimica et Cosmochimica Acta*, *43*(7), 1009-1020.

Feely, R.A., Sabine, C.L., Lee, K., Berelson, W., Kleypas, J., Fabry, V.J. and Millero, F.J., 2004. Impact of anthropogenic CO2 on the CaCO3 system in the oceans. *Science*, *305*(5682), 362-366.

Feely, R. A., Sabine, C. L., Hernandez-Ayon, J. M., Ianson, D., & Hales, B. (2008). Evidence for upwelling of corrosive" acidified" water onto the continental shelf. science, 320(5882), 1490-1492.

Feely, R.A., Sabine, C.L., Byrne, R.H., Millero, F.J., Dickson, A.G., Wanninkhof, R., Murata, A., Miller, L.A. and Greeley, D., 2012. Decadal changes in the aragonite and calcite saturation state of the Pacific Ocean. *Global Biogeochemical Cycles*, *26*(3).

Fowell, S., Foster, G.L., Ries, J., Castillo, K.D., De La Vega, E., Tyrrell, T., Donald, H.K. and Chalk, T.B., 2018. Historical trends in pH and carbonate biogeochemistry on the Belize Mesoamerican Barrier Reef System. *Geophysical Research Letters*.

Gagnon, A. C. (2013). Coral calcification feels the acid. Proceedings of the National Academy of Sciences, 110(5), 1567-1568.

Georgiou, L., Falter, J., Trotter, J., Kline, D.I., Holcomb, M., Dove, S.G., Hoegh-Guldberg, O. and McCulloch, M., 2015. pH homeostasis during coral calcification in a free ocean CO2 enrichment (FOCE) experiment, Heron Island reef flat, Great Barrier Reef. *Proceedings of the National Academy of Sciences*, *112*(43), 13219-13224.

Grottoli, A. G. (1999). Variability of stable isotopes and maximum linear extension in reef-coral skeletons at Kaneohe Bay, Hawaii. *Marine Biology*, *135*(3), 437-449.

Grottoli, A. G. (2002). Effect of light and brine shrimp on skeletal δ13C in the Hawaiian coral Porites compressa: a tank experiment. *Geochimica et Cosmochimica Acta*, *66*(11), 1955-1967.

Hart, S. R., & Cohen, A. L. (1996). An ion probe study of annual cycles of Sr/Ca and other trace elements in corals. *Geochimica et Cosmochimica Acta*, *60*(16), 3075-3084.

Hemming, N. G., Guilderson, T. P., & Fairbanks, R. G. (1998). Seasonal variations in the boron isotopic composition of coral: A productivity signal?. *Global biogeochemical cycles*, *12*(4), 581-586.

Hemming, N. G., & Hanson, G. N. (1992). Boron isotopic composition and concentration in modern marine carbonates. *Geochimica et Cosmochimica Acta*, *56*(1), 537-543.
McCulloch, M., Falter, J., Trotter, J., & Montagna, P. (2012). Coral resilience to ocean acidification and global warming through pH up-regulation. *Nature Climate Change*, *2*(8), 623.

Hofmann, G.E., Smith, J.E., Johnson, K.S., Send, U., Levin, L.A., Micheli, F., Paytan, A., Price, N.N., Peterson, B., Takeshita, Y. and Matson, P.G., 2011. High-frequency dynamics of ocean pH: a multi-ecosystem comparison. *PloS one*, *6*(12), p.e28983.

Holcomb, M. *et al*. Coral calcifying uid pH dictates response to ocean acidi cation. *Scienti c Reports* **4**, 5207 (2014).

Hönisch, B., Hemming, N., Grottoli, A. G., Amat, A., Hanson, G. N., & Bijma, J. (2004). Assessing scleractinian corals as recorders for paleo-pH: Empirical calibration and vital effects. *Geochimica et Cosmochimica Acta*, *68*(18), 3675-3685.

Huang, B., V.F. Banzon, E. Freeman, J. Lawrimore, W. Liu, T.C. Peterson, T.M. Smith, P.W. Thorne, S.D. Woodruff, and H.-M. Zhang, 2014: Extended Reconstructed Sea Surface Temperature version 4 (ERSST.v4): Part I. Upgrades and intercomparisons. Journal of Climate, 28, 911-930, doi:10.1175/JCLI-D-14-00006.1

Hughes, T.P., Baird, A.H., Bellwood, D.R., Card, M., Connolly, S.R., Folke, C., Grosberg, R., Hoegh-Guldberg, O., Jackson, J.B., Kleypas, J. and Lough, J.M., 2003. Climate change, human impacts, and the resilience of coral reefs. *science*, *301*(5635), 929-933.

Hughes, T.P., Kerry, J.T., Álvarez-Noriega, M., Álvarez-Romero, J.G., Anderson, K.D., Baird, A.H., Babcock, R.C., Beger, M., Bellwood, D.R., Berkelmans, R. and Bridge, T.C., 2017. Global warming and recurrent mass bleaching of corals. *Nature*, *543*(7645), p.373.

Hughes, T.P., Anderson, K.D., Connolly, S.R., Heron, S.F., Kerry, J.T., Lough, J.M., Baird, A.H., Baum, J.K., Berumen, M.L., Bridge, T.C. and Claar, D.C., 2018. Spatial and temporal patterns of mass bleaching of corals in the Anthropocene. *Science*, *359*(6371), 80-83.

Inoue, M., Suzuki, A., Nohara, M., Hibino, K., & Kawahata, H. (2007). Empirical assessment of coral Sr/Ca and Mg/Ca ratios as climate proxies using colonies grown at different temperatures. *Geophysical Research Letters*, *34*(12).

Inoue, M., Suwa, R., Suzuki, A., Sakai, K., & Kawahata, H. (2011). Effects of seawater pH on growth and skeletal U/Ca ratios of Acropora digitifera coral polyps. *Geophysical Research Letters*, *38*(12).

Karl, David M., and Roger Lukas. "The Hawaii Ocean Time-series (HOT) program: Background, rationale and field implementation." *Deep Sea Research Part II: Topical Studies in Oceanography* 43.2-3 (1996): 129-156.

Keeling, C. D. (1979). The Suess effect: 13Carbon-14Carbon interrelations. *Environment International*, *2*(4-6), 229-300.

Kiss, E. (1988). Ion-exchange separation and spectrophotometric determination of boron in geological materials. *Analytica Chimica Acta*, *211*, 243-256.

Kline, D.I., Teneva, L., Hauri, C., Schneider, K., Miard, T., Chai, A., Marker, M., Dunbar, R., Caldeira, K., Lazar, B. and Rivlin, T., 2015. Six month in situ high-resolution carbonate chemistry and temperature study on a coral reef flat reveals asynchronous pH and temperature anomalies. *PloS one*, *10*(6), p.e0127648.

Krief, S., Hendy, E. J., Fine, M., Yam, R., Meibom, A., Foster, G. L., & Shemesh, A. (2010). Physiological and isotopic responses of scleractinian corals to ocean acidification. *Geochimica et Cosmochimica Acta*, *74*(17), 4988-5001.

Kubota, K., Yokoyama, Y., Ishikawa, T., Suzuki, A., & Ishii, M. (2017). Rapid decline in pH of coral calcification fluid due to incorporation of anthropogenic CO 2. *Scientific reports*, *7*(1), 7694.

Martz, T. R., Connery, J. G., & Johnson, K. S. (2010). Testing the Honeywell Durafet® for seawater pH applications. *Limnology and Oceanography: Methods*, *8*(5), 172-184.

McConnaughey, T. (1989). 13C and 18O isotopic disequilibrium in biological carbonates: II. In vitro simulation of kinetic isotope effects. *Geochimica et Cosmochimica Acta*, *53*(1), 163-171.

McConnaughey, T. A. (2003). Sub-equilibrium oxygen-18 and carbon-13 levels in biological carbonates: carbonate and kinetic models. *Coral Reefs*, *22*(4), 316-327.

McCulloch, M. T., D'Olivo, J. P., Falter, J., Holcomb, M., & Trotter, J. A. (2017). Coral calcification in a changing World and the interactive dynamics of pH and DIC upregulation. *Nature communications*, *8*, 15686.

McCulloch, M., Trotter, J., Montagna, P., Falter, J., Dunbar, R., Freiwald, A., Försterra, G., Correa, M.L., Maier, C., Rüggeberg, A. and Taviani, M., 2012. Resilience of cold-water scleractinian corals to ocean acidification: Boron isotopic systematics of pH and saturation state up-regulation. *Geochimica et Cosmochimica Acta*, *87*, 21-34.

Min, G. R., Edwards, R. L., Taylor, F. W., Recy, J., Gallup, C. D., & Beck, J. W. (1995). Annual cycles of UCa in coral skeletons and UCa thermometry. *Geochimica et Cosmochimica Acta*, *59*(10), 2025-2042.

Mitsuguchi, T., Matsumoto, E., Abe, O., Uchida, T., & Isdale, P. J. (1996). Mg/Ca thermometry in coral skeletons. *Science*, *274*(5289), 961-963.

Moberg, F., & Folke, C. (1999). Ecological goods and services of coral reef ecosystems. *Ecological economics*, *29*(2), 215-233.

Okai, T., Suzuki, A., Kawahata, H., Terashima, S., & Imai, N. (2002). Preparation of a New Geological Survey of Japan Geochemical Reference Material: Coral JCp-1. *Geostandards and Geoanalytical Research*, *26*(1), 95-99.

Pelejero, C., Calvo, E., McCulloch, M. T., Marshall, J. F., Gagan, M. K., Lough, J. M., & Opdyke, B. N. (2005). Preindustrial to modern interdecadal variability in coral reef pH. Science, 309(5744), 2204-2207.

Price, N. N., Martz, T. R., Brainard, R. E., & Smith, J. E. (2012). Diel variability in seawater pH relates to calcification and benthic community structure on coral reefs. *PloS one*, *7*(8), e43843.

Rae, J. W., Foster, G. L., Schmidt, D. N., & Elliott, T. (2011). Boron isotopes and B/Ca in benthic foraminifera: proxies for the deep ocean carbonate system.Earth and Planetary Science Letters, 302(3), 403-413.

Reynaud, S., Hemming, N. G., Juillet-Leclerc, A., & Gattuso, J. P. (2004). Effect of pCO 2 and temperature on the boron isotopic composition of the zooxanthellate coral Acropora sp. *Coral Reefs*, *23*(4), 539-546.

Reynaud, S., Ferrier-Pages, C., Meibom, A., Mostefaoui, S., Mortlock, R., Fairbanks, R., & Allemand, D. (2007). Light and temperature effects on Sr/Ca and Mg/Ca ratios in the scleractinian coral Acropora sp. *Geochimica et Cosmochimica Acta*, *71*(2), 354-362.

Ries, J. B. Skeletal mineralogy in a high-CO_2 world. *J. Exp. Mar. Biol. Ecol.* **403**, 54–64 (2011).

Rivest, E. B., & Hofmann, G. E. (2014). Responses of the Metabolism of the Larvae of Pocillopora damicornis to Ocean Acidification and Warming. PloS one, 9(4), e96172.

Roemmich, D. H., Davis, R. E., Riser, S. C., Owens, W. B., Molinari, R. L., Garzoli, S. L., & Johnson, G. C. (2003). *The argo project. global ocean observations for understanding and prediction of climate variability*. SCRIPPS INSTITUTION OF OCEANOGRAPHY LA JOLLA CA.

Rogers, J. S., Monismith, S. G., Koweek, D. A., Torres, W. I., & Dunbar, R. B. (2016). Thermodynamics and hydrodynamics in an atoll reef system and their influence on coral cover. *Limnology and Oceanography*, *61*(6), 2191-2206.

Rogers, J. S., Monismith, S. G., Fringer, O. B., Koweek, D. A., & Dunbar, R. B. (2017). A coupled wave-hydrodynamic model of an atoll with high friction: Mechanisms for flow, connectivity, and ecological implications. *Ocean Modelling*, *110*, 66-82.

Rollion-Bard, C., & Blamart, D. (2015). Possible controls on Li, Na, and Mg incorporation into aragonite coral skeletons. *Chemical Geology*, *396*, 98-111.

Salisbury, J., Green, M., Hunt, C., & Campbell, J. (2008). Coastal acidification by rivers: a threat to shellfish?. Eos, Transactions American Geophysical Union,89(50), 513-513.

Sandin, S.A., Smith, J.E., DeMartini, E.E., Dinsdale, E.A., Donner, S.D., Friedlander, A.M., Konotchick, T., Malay, M., Maragos, J.E., Obura, D., Pantos, O., Paulay, G., Richie, M., Rohwer, F., Schroeder, R.E., Walsh, S., Jackson, J.B.C., Knowlton, N., Sala, E., 2008. Baselines and degradation of Coral Reefs in the Northern Line Islands. PLoS ONE 3, e1548.

Sanyal, A., Bijma, J., Spero, H., & Lea, D. W. (2001). Empirical relationship between pH and the boron isotopic composition of Globigerinoides sacculifer: Implications for the boron isotope paleo-pH proxy. *Paleoceanography*, *16*(5), 515-519.

Schoepf, V., Jury, C. P., Toonen, R. J., & McCulloch, M. T. (2017, December). Coral calcification mechanisms facilitate adaptive responses to ocean acidification. In *Proc. R. Soc. B*(Vol. 284, No. 1868, p. 20172117). The Royal Society.

Shamberger, K.E., Cohen, A.L., Golbuu, Y., McCorkle, D.C., Lentz, S.J. and Barkley, H.C., 2014. Diverse coral communities in naturally acidified waters of a Western Pacific reef. *Geophysical Research Letters*, *41*(2), 499-504.

Shaw, E.C., McNeil, B.I. and Tilbrook, B., 2012. Impacts of ocean acidification in naturally variable coral reef flat ecosystems. *Journal of Geophysical Research: Oceans*, *117*(C3).

Suess, H. E. (1955). Radiocarbon concentration in modern wood. *Science*, *122*(3166), 415-417.

Shinjo, R., Asami, R., Huang, K. F., You, C. F., & Iryu, Y. (2013). Ocean acidification trend in the tropical North Pacific since the mid-20th century reconstructed from a coral archive. Marine Geology, 342, 58-64.

Silverman, J., Lazar, B., Cao, L., Caldeira, K., & Erez, J. (2009). Coral reefs may start dissolving when atmospheric CO2 doubles. *Geophysical Research Letters*, *36*(5).

Sinclair, D. J., Williams, B., & Risk, M. (2006). A biological origin for climate signals in corals—Trace element "vital effects" are ubiquitous in Scleractinian coral skeletons. *Geophysical Research Letters*, *33*(17).

Sinclair, D. J. (2005a), Correlated trace element 'vital effects' in tropical corals: A new tool for probing biomineralization chemistry, *Geochim. Cosmochim. Acta*, 69, 3265–3284.

Sinclair, D. J., L. P. J. Kinsley, and M. T. McCulloch (1998), High resolution analysis of trace elements in corals by laser-ablation ICP-MS, *Geochim. Cosmochim. Acta*, 62, 1889–1901.

Sinclair, D. J., and M. J. Risk (2006), A numerical model of trace-element coprecipitation in a physicochemical calcification system: Application to coral biomineralization and trace-element 'vital effects', *Geochim. Cosmochim. Acta*, 70(15), 3855–3868.

Spivack, A. J., & Edmond, J. M. (1986). Determination of boron isotope ratios by thermal ionization mass spectrometry of the dicesium metaborate cation. *Analytical Chemistry*, *58*(1), 31-35.

Stevenson, Charlotte, Laure S. Katz, Fiorenza Micheli, Barbara Block, Kimberly W. Heiman, Chris Perle, Kevin Weng, Robert Dunbar, and Jan Witting. "High apex predator biomass on remote Pacific islands." *Coral reefs* 26, no. 1 (2007): 47-51.

Stewart, J. A., Anagnostou, E., & Foster, G. L. (2016). An improved boron isotope pH proxy calibration for the deep-sea coral Desmophyllum dianthus through sub-sampling of fibrous aragonite. *Chemical Geology*, *447*, 148-160.

Swart, P. K., Szmant, A., Porter, J. W., Dodge, R. E., Tougas, J. I., & Southam, J. R. (2005). The isotopic composition of respired carbon dioxide in scleractinian corals: implications for cycling of organic carbon in corals. *Geochimica et Cosmochimica Acta*, *69*(6), 1495-1509.

Takeshita, Y., McGillis, W., Briggs, E.M., Carter, A.L., Donham, E.M., Martz, T.R., Price, N.N. and Smith, J.E., 2016. Assessment of net community production and calcification of a coral reef using a boundary layer approach. *Journal of Geophysical Research: Oceans*, *121*(8), 5655-5671.

Taylor, S. R., & McLennan, S. M. (1985). The continental crust: Its evolution and composition. *Lon on: Blackwell*.

Trotter, J. A. et al. Quantifying the pH 'vital effect' in the temperate zooxanthellate coral Cladocora caespitosa: Validation of the boron seawater pH proxy. Earth Planet. Sci. Lett. 303, 163–173 (2011).

Venn, A., Tambutté, E., Holcomb, M., Allemand, D., & Tambutté, S. (2011). Live tissue imaging shows reef corals elevate pH under their calcifying tissue relative to seawater. *PloS one*, *6*(5), e20013.

Venn, A. A. *et al*. Impact of seawater acidi cation on pH at the tissue–skeleton interface and calcification in reef corals. *Proc. Natl. Acad. Sci. USA* **110**, 1634–1639 (2013).

Wall, M., Fietzke, J., Schmidt, G. M., Fink, A., Hofmann, L. C., De Beer, D., & Fabricius, K. E. (2016). Internal pH regulation facilitates in situ long-term acclimation of massive corals to end-of-century carbon dioxide conditions. *Scientific reports*, *6*, 30688.

Weber, J. N., Deines, P., Weber, P. H., & Baker, P. A. (1976). Depth related changes in the 13C12C ratio of skeletal carbonate deposited by the Caribbean reef-frame building coral Montastrea annularis: further implications of a model for stable isotope fractionation by scleractinian corals. *Geochimica et Cosmochimica Acta*, *40*(1), 31-39.

Wei, G., McCulloch, M. T., Mortimer, G., Deng, W., & Xie, L. (2009). Evidence for ocean acidification in the Great Barrier Reef of Australia. Geochimica et cosmochimica acta, 73(8), 2332-2346.

Williams, G. J., Knapp, I. S., Maragos, J. E., & Davy, S. K. (2010). Modeling patterns of coral bleaching at a remote Central Pacific atoll. *Marine Pollution Bulletin*, *60*(9), 1467-1476.

Williams, G. J., Smith, J. E., Conklin, E. J., Gove, J. M., Sala, E., & Sandin, S. A. (2013). Benthic communities at two remote Pacific coral reefs: effects of reef habitat, depth, and wave energy gradients on spatial patterns. *PeerJ*, *1*, e81.

Wu, H. C., Dissard, D., Le Cornec, F., Thil, F., Tribollet, A., Moya, A., & Douville, E. (2017). Primary Life Stage Boron Isotope and Trace Elements Incorporation in Aposymbiotic Acropora millepora Coral under Ocean Acidification and Warming. *Frontiers in Marine Science*, *4*, 129.

Yates, K. K., & Halley, R. B. (2006). CO 2− 3 concentration and pCO 2 thresholds for calcification and dissolution on the Molokai reef flat, Hawaii.Biogeosciences Discussions, 3(1), 123-15

Yeakel, K. L., Andersson, A. J., Bates, N. R., Noyes, T. J., Collins, A., & Garley, R. (2015). Shifts in coral reef biogeochemistry and resulting acidification linked to offshore productivity. *Proceedings of the National Academy of Sciences*, *112*(47), 14512-14517.

4.7 Acknowledgements

Portions of Chapter 4 are being prepared for submission for publication.

Sanchez, Sara; Charles, Chris; Rae, James; Stewart, Joseph; Smith, Jennifer; Takeshita, Yui. The dissertation author was the primary investigator and author of this paper.

Additional elements of this submission can be found in Appendix C.

Appendix A. Supplementary Materials for Chapter 2. Two centuries of coherent decadal climate variability across the Pacific North American region

A.1 Introduction

This appendix contains supplementary information for (1.) a more complete comparison with published data (Figure A.1); (2.) the analysis and interpretation of the coral oxygen isotopic record (Figure A.2); and (3.) additional regressions of the NADA PDSI anomalies with useful indices (Figure A.3); (4.) cross spectral analysis of the paleorecords used in this analysis (Figure A.4); (5.) 500mb geopotential height anomalies associated with the NPGO (Figure A.5).

A.2 Known modes of variability

Hartman 2015 discusses two modes of primarily decadal variability in the Pacific: EOF2 and EOF3 (using NOAA ERSST v3b SST domains from 30S to 65N, from 1900 to the present). EOF3 was dubbed the "North Pacific Mode" in light of its similarity to the mode described in Deser et al. 1995. The link between this EOF3 mode and the seasonal footprinting mechanism [Vimont et al. 2001, Vimont et al. 2003] was made in contrast to the link between EOF2 and an atmospheric bridge-type mechanism [Lau 1996, Alexander et al. 2002]. Most traditional modes of Pacific decadal climate variability are described within the confines of 20N to 60N, and thus are not explicitly identical to the modes in the Hartman paper. Here, however, EOF3 bears strong

similarity to the North Pacific Gyre Oscillation, while EOF2 greatly resembles the Pacific Decadal Oscillation. The NPGO is the oceanic component of the North Pacific Oscillation [DiLorenzo et al. 2008, DiLorenzo et al. 2010, Furtado et al. 2012]. The NPGO is defined as the second most dominant mode of sea surface height in the North Pacific, and physically represents the strengthening and weakening of the subtropical gyre ([DiLorenzo et al. 2008], Figure A.1A). The NPGO is very important for ecosystem function as this mode best explains salinity and nutrient variability along the eastern Pacific [DiLorenzo et al. 2009]. While the relative power of the NPGO is less than the Pacific Decadal Oscillation (PDO), the NPGO has been strengthening in the last several decades to the oscillation's relationship with central Pacific warming events [DiLorenzo et al. 2008, DiLorenzo et al. 2010]. Figure A.1A shows the spatial representation of the Hartman EOF3 (directly comparable with the spatial expression of the NPGO in Figure 1), Figure 1B compares the timeseries of the NPGO and the principal component of EOF 3. The strong similarities in the spatial representation, and timeseries coherence suggest that these different indices represent the different faces (SSH and SST) of the same physical oscillation.

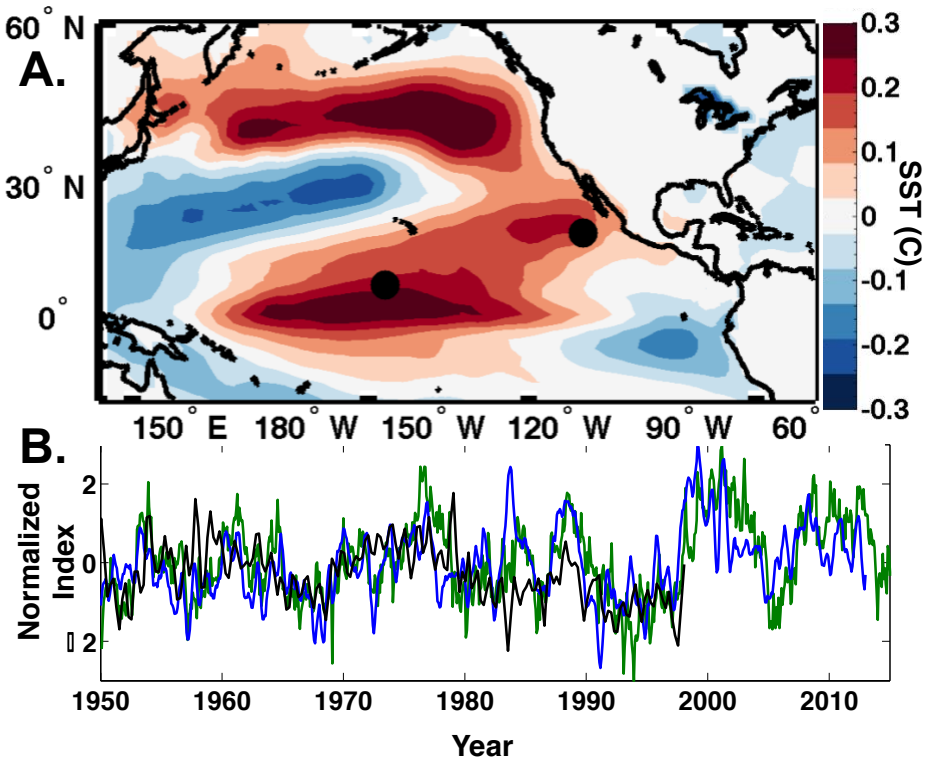

Figure A.1 Relationship between NPGO, Clarion coral $\delta^{18}O$, and Hartmann 2015 index. **(A.)** Linear regression of monthly mean SST anomalies (ERSST v3b) with the 1900-present principal component of EOF3 of Pacific sea surface temperatures, from 20S to 60N, as described by Hartmann 2015; locations of Palmyra and Clarion are indicated with a black circle. **(B.)** Time series from 1950-2013 of the normalized principal component of EOF (blue) with normalized Clarion coral $\delta^{18}O$ (black) and NPGO index (green)

A.3 Interpreting the Clarion coral oxygen isotopic composition

In corals, the isotopic fractionation of oxygen reflects a linear combination of sea surface temperatures and the oxygen isotopic composition of seawater ($\delta^{18}O_{sw}$, representing local precipitation- evaporation, which relates directly to salinity). This combination can be utilized as a proxy for sea surface height, making Clarion Island a particularly effective region to reconstruct North Pacific Gyre Oscillation dynamics (Figure A.2). The relationship between temperature, salinity, and oxygen isotopes can be written as:

$$\Delta\delta^{18}O_{coral} = a_1\Delta SST + a_2\Delta SSS + \text{noise} \quad (1)$$

Using a_1=-0.22**‰/°C, a_2=0.44‰/PSU, typical values for Porites genus corals in the Northeastern Pacific [Evans et al. 2000, Lough 2004, Legrande and Schmidt 2006, Thompson et al. 2011, Brown et al. 2006]. The relative role of sea surface temperature and salinity in the coral $\delta^{18}O$ can be estimated with a known SST or SSS variable. SST measurements are fairly ubiquitous throughout the latter half of the twentieth century, although large, gridded products may differ from micro-scale reef variability possibly recorded in the coral skeleton. Thus, another coral derived geochemical tool at our disposal is the ratio of strontium to calcium (Sr/Ca) in the coral skeleton; this ratio corresponds linearly with ambient sea surface temperature. The exact magnitude of the relationship is found by linearly regressing the Sr/Ca signal with known SST. The relationship between previously analyzed Sr/Ca variability (by JDC and JAV) and SST was found using least squares linear regression to be (Sr/Ca= -0.0295(SSTA) + 9.19, R= -0.63 on using annual timescales anomalies from 1900-1998; slightly improved relative to the relationship at seasonal timescales (Sr/Ca=-.024*SSTA+ 9.19, R=-0.43) using ERSSTv3b data from 1900-1998 with the annual cycle removed. The Kaplan and Hadley products provided similar results. While the Sr/Ca- SST regression coefficient is less than a typical Porites (0.04-0.08 mmol/mol per 1°C, [Gagan et al. 2012]); this could be due to the slow 4-6mm/year growth rate of the Clarion coral. Converting SST to $\delta^{18}O$ on annual timescales from 1900-1998 yields the following relationship: $\delta^{18}O$ = SSTA*-0.22-4.1, R=-0.5423. Gagan et al. 2012 ascribe standard regression coefficients for Porites corals of SST-Sr/Ca:-0.084 mmol/mol per 1°C, and for SST-$\delta^{18}O$: -0.23 ‰ per 1°C; this difference suggests that our temperature conversions might amplify the expected role of temperature on the coral geochemistry.

The pseudo-coral analysis is limited by complicated oceanic dynamics and a lack of continuous salinity records from this region. Kessler 2006, Figure 5b highlights the regions

where the interconnections between the prevailing patterns of oceanic circulation remain unknown, including the termination of the California Current System. Advection of salinity anomalies from the California Current System, Gulf of California, or the inner gyre all have the potential to alter salinity in the Clarion region [Roden 1972]. Additionally, alterations in precipitation-evaporation, likely due to shifts in the ITCZ, or changes in upwelling can also have a strong imprint on the salinity of waters surrounding the Revillagigedos Archipelago (Roden 1972). Long, continuous salinity datasets are sparse in the Eastern Tropical North Pacific; data products from the NASA Aquarius satellite, or the ARGO surface drifters [Roemmich et al. 2011] are still too brief to capture decadal variations prior to the mid 2000s. Other reanalysis products, such as SODA[Carton and Giese 2008], or Delcroix [Delcroix et al. 2011] suffer from sparse sampling. Regional Ocean Model (ROMs) hindcasts are used in many of the papers describing the effects of the NPGO, yet this analysis is limited to the North Pacific and does not extend into the tropics, or even the Revillagigedos Island region. Figure A.2 illustrates the difficulties in using instrumental data from this region: while there is good instrumental agreement of temperature variability (Figure A. 2A, poor instrumental salinity agreement (Figure A.2B) creates large uncertainties when creating a pseudocoral record using Equation 1 (Figure A.2C).

Because of the complications with the salinity measurements in the period overlapping the coral geochemical record, I rely on the Sr/Ca measurements and the estimated influence of temperature on oxygen isotopes to interpret the variability of the oxygen isotopes of seawater. I transform both temperature indicators (both the coral Sr/Ca and NOAA's Extended Reconstruction SST Version 3b) into a pseudo-coral $\delta^{18}O$ record to show the $\delta^{18}O$ variability expected if the values depended only on sea surface temperature.

Figure A.2D scales all temperature metrics to an expected oxygen isotopic anomaly. The figure shows that while the true oxygen isotopic signal from Clarion Island coral displays strong decadal variability, the expected influence of temperature on oxygen isotopes provides weak decadal variability, though still in phase with the observed oxygen isotopic signal. The strong decadal variability seen in the coral record is interpreted to be strongly influenced by changes in the $\delta^{18}O$ of seawater. When using the standard regression coefficients from Gagan et al. 2012, the estimated influence of salinity at decadal timescales is further amplified. This interpretation is reasonable as the North Pacific Gyre Oscillation is the dominant control over salinity variations in the California Current System on decadal timescales ([DiLorenzo et al. 2008, Chhak et al. 2009, DiLorenzo et al. 2009], roughly +/-0.2 PSU).

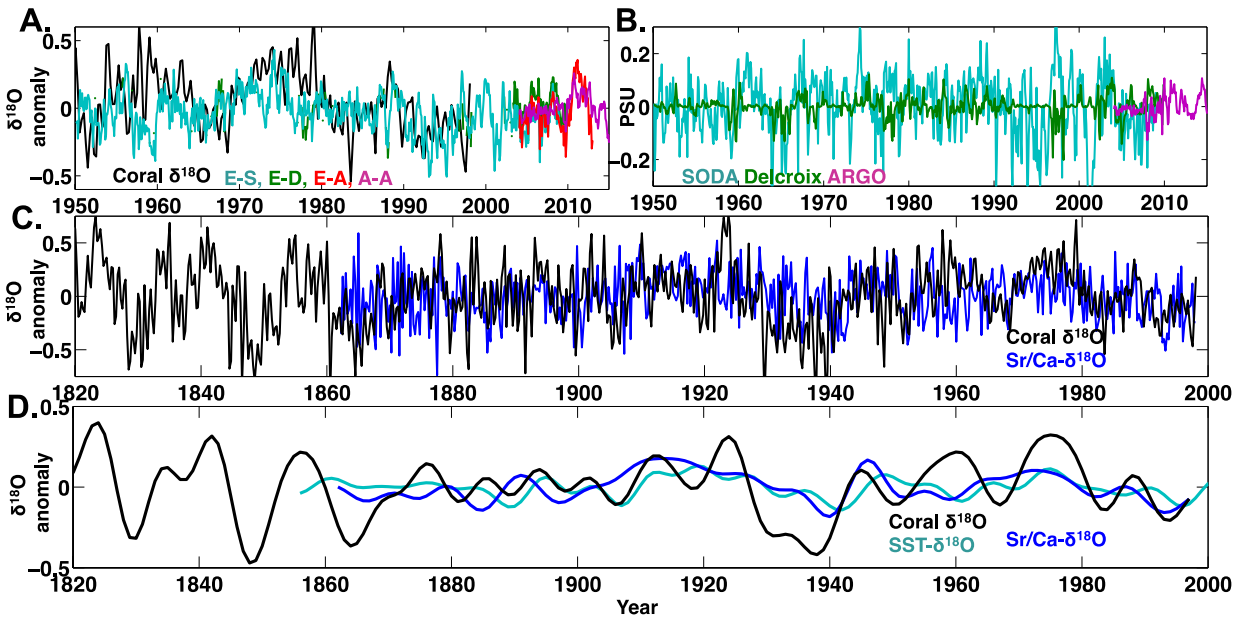

Figure A.2 Forward modeling of Clarion coral $\delta^{18}O$.
Clarion location temperature indices converted to expected oxygen isotopic anomalies where positive values indicate cooler, drier/more saline conditions, while lower values indicate warmer, wetter/fresher conditions. **(A.)** Clarion location combined temperature and salinity indices converted to expected oxygen isotopic anomalies where positive values indicate cooler, drier/more saline conditions, while lower values indicate warmer, wetter/fresher conditions. Using equation and the regression coefficients of: $\Delta\delta^{18}O_{coral} = 0.22\ \delta^{18}O/C * SST + 0.44\ \delta^{18}O/PSU * SSS$ for monthly anomalies. Clarion coral $\delta^{18}O$ (black), NOAA's ERSST v3b and SODA SSS (E-S, turquoise), NOAA's ERSST v3b and Delcroix SSS (E-D, green, the Delcroix salinity reconstruction was filtered for periods with at least 40% confidence in the observations), NOAA's ERSST v3b and ARGO SSS (E-A, red), ARGO SST and ARGO SSS (A-A, magenta). **(B.)** Annual anomalies of Clarion coral $\delta^{18}O$ (black) and expected anomalies derived from available SST and SSS products. from ERSST v3b(blue) multiplied by the regression coefficient of -0.22 $\delta^{18}O$ /C **(C.)** Clarion location gridbox's salinity timeseries, monthly means removed. SODA (turquoise), Delcroix(green), ARGO SSS (magenta). **(D.)** Seasonal anomalies of Clarion coral $\delta^{18}O$ (black) and coral Sr/Ca (blue) multiplied by the regression coefficient of -0.22 $\delta^{18}O$ /C *-0.0295 C/Sr/Ca. **(E.)** Clarion coral $\delta^{18}O$ (black) and estimated coral $\delta^{18}O$ from SST(turquoise, SST from ERSST v3b(blue) multiplied by the regression coefficient of -0.22 $\delta^{18}O$ /C) and Sr/Ca (blue) with an eight year lowpass filter. Note the actual coral oxygen isotopic record has much larger magnitude decadal variation than expected from sea surface temperatures alone.

A.4 North American Drought Atlas: proxy time series comparisons

Figure A.3A shows the regression the NADA PDSI [Cook et al. 1999, Cook et al. 2004] with the MacDonald Case Index [MacDonald Case 2005] over the years 1800-2005. Stippling indicates a 95% statistical significance using a student's two-sided t-test accounting for autocorrelation by changing the number of effective degrees of freedom [Bretherton et al. 1999] and multiple hypothesis testing through a control using the False Discovery Rate [Wilks 2016]. Figure A.3B shows the regression the NADA PDSI with the NPGO index from 1950-2005.

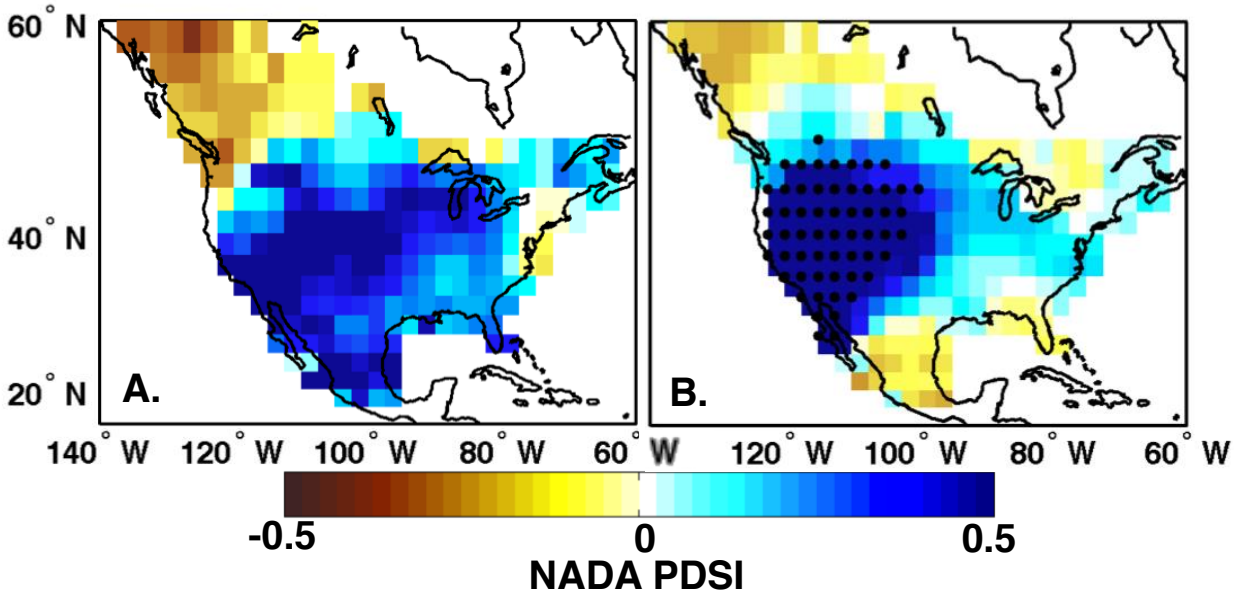

Figure A.3 Linear regression of the NADA- PDSI data (Cook et al. 1999, Cook et al. 2004). Regression of the NADA- PDSI data with **(A.)** Annual anomalies of the NPGO index (1950-2006) (negative NPGO, so that dry-warm conditions (red) are associated with warm sea surface temperatures in the eastern tropical north Pacific). Stippling indicates significance at 95% using a two-sided student's t-test. Annual anomalies were calculated over the May-April ENSO year. **(B.)** Griffin and Anchukaitis tree ring series (1800-1996) (1790-1990) monitoring PDSI in south central California.

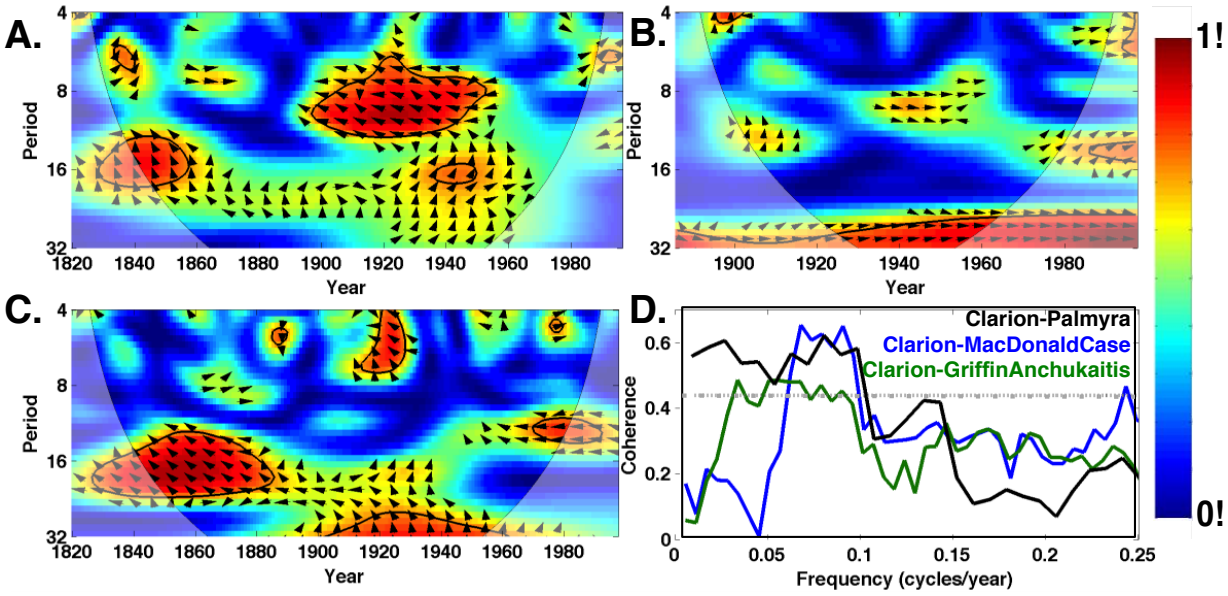

Figure A.4 Squared wavelet coherence between the standardized paleo timeseries, as in Grinstead et al. 2004. The thick black line denotes a 5% significance level against red noise. The relative phase relationship is shown in arrows (in-phase points right, anti-phase left, and Clarion leading the series by 90 degrees pointing up). **(A.)** Clarion coral $\delta^{18}O$ and MacDonald-Case Pacific Decadal Variability reconstruction over years 1820-1998, antiphased where significant. **(B.)** Clarion coral $\delta^{18}O$ and Palmyra coral $\delta^{18}O$ over years 1886-1998, in phase where significant. **(C.)** Clarion coral $\delta^{18}O$ and Griffin Anchukaitis NADA PDSI compilation over years 1820-1998, antiphased where significant. **(D.)** Multi-taper coherence estimate using eight windows in the Matlab routine of Peter Huybers (http://www.people.fas.harvard.edu/~phuybers/Mfiles/). Dashed line shows 95% confidence interval highlighting the coherence at 10-17 years band throughout the length of the Clarion coral $\delta^{18}O$ record. The analysis highlights the coherency found throughout the last two centuries in the 9-26 year band. In both tree ring reconstructions, a statistically significant relationship is found with Clarion Island prior to 1860.

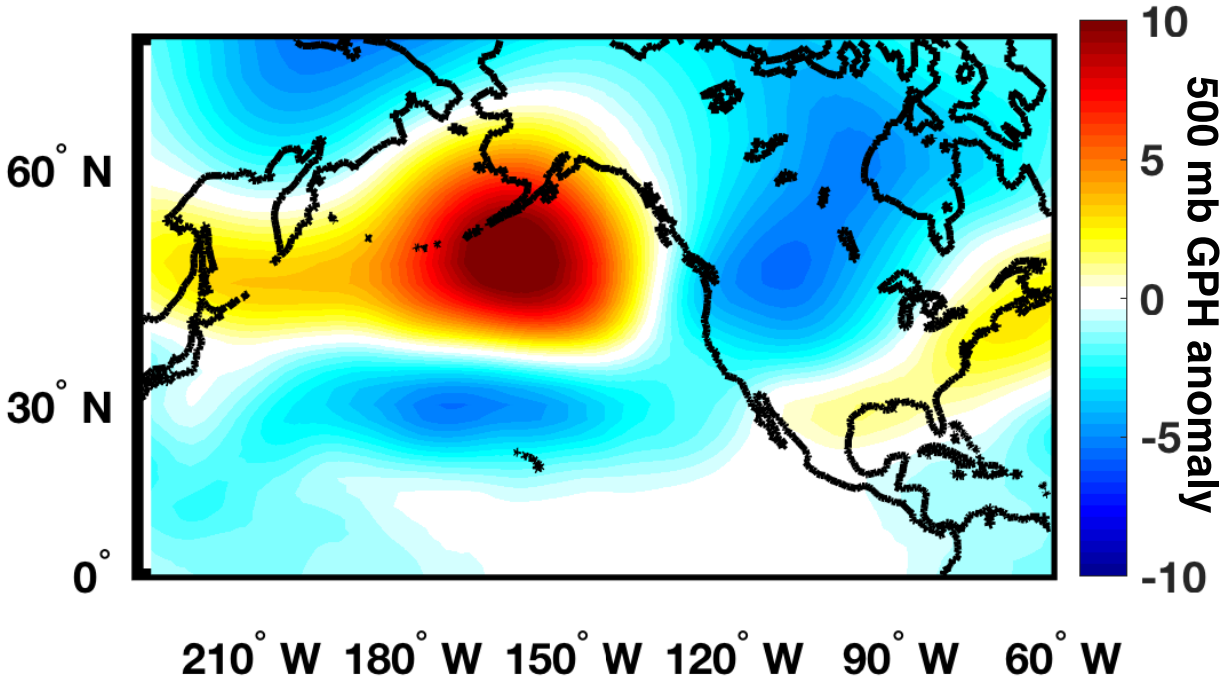

Figure A.5 Regression of NDJFM field of 500mb geopotential height (NCEP NCAR Reanalysis (S20)) with negative NDJFM NPGO Index.

A.5 References

Alexander, M. A., Bladé, I., Newman, M., Lanzante, J. R., Lau, N. C., & Scott, J. D. (2002), The atmospheric bridge: The influence of ENSO teleconnections on air-sea interaction over the global oceans, J Clim, 15(16): 2205-2231,doi:10.1175/1520-0442(2002)015<2205:TABTIO>2.0.CO;2.

Bretherton, C. S., Widmann, M., Dymnikov, V. P., Wallace, J. M., & Bladé, I. (1999), The effective number of spatial degrees of freedom of a time-varying field, J Clim, 12(7):1990-2009,doi:10.1175/1520-0442(1999)012<1990:TENOSD>2.0.CO;2.

Brown, J., Simmonds, I., & Noone, D. (2006), Modeling δ18O in tropical precipitation and the surface ocean for present-day climate, J Geophys Res: Atmos, 111(D5): D05105, doi:10.1029/2004JD005611.

Carton, J.A. and Giese, B.S.. (2008), A reanalysis of ocean climate using Simple Ocean Data Assimilation (SODA), Mon Weather Rev, 136, 2999 3017, doi: http://dx.doi.org/10.1175/2007MWR1978.1.

Chhak, K. C., E. Di Lorenzo, N. Schneider and P. F. Cummins, (2009), Forcing of Low-Frequency Ocean Variability in the Northeast Pacific, J Clim, 22(5) 1255-1276, doi:10.1175/2008jcli2639.1.

Cook, E.R., C.A. Woodhouse, C.M. Eakin, D.M. Meko and D.W. Stahle (2004), Long-Term Aridity Changes in the Western United States, Science, 306 (5698): 1015-1018, doi:10.1126/science.1102586.

Cook, E.R., D.M. Meko, D.W. Stahle, and M.K. Cleaveland (1999), Drought reconstructions for the continental United States, J Clim, 12:1145-1162, doi:10.1175/1520-0442(1999)012<1145:DRFTCU>2.0.CO;2.

Delcroix, T., Alory, G., Cravatte, S., Corrège, T., & McPhaden, M. J. (2011). A gridded sea surface salinity data set for the tropical Pacific with sample applications (1950–2008). Deep-Sea Res Pt I,58(1), 38-48, DOI: 10.1016/j.dsr.2010.11.002.

Deser, C., & Blackmon, M. L. (1995), On the relationship between tropical and North Pacific sea surface temperature variations, J Clim, 8(6): 1677-1680, doi:10.1175/1520-0442(1995)008<1677:OTRBTA>2.0.CO;2.

Di Lorenzo, E., Cobb, K. M., Furtado, J. C., Schneider, N., Anderson, B. T., Bracco, A., Alexander, M.A., & Vimont, D. J. (2010). Central Pacific El Niño and decadal climate change in the North Pacific Ocean. Nature Geoscience, 3(11), 762-765.

Di Lorenzo, E., Fiechter, J., Schneider, N., Bracco, A., Miller, A.J., Franks, P.J.S., Bograd, S.J., Moore, A.M., Thomas, A.C., Crawford, W. and Peña, A., (2009). Nutrient and salinity decadal variations in the central and eastern North Pacific. *Geophysical Research Letters*, *36*(14).

Di Lorenzo, E., Schneider, N., Cobb, K.M., Franks, P.J.S., Chhak, K., Miller, A.J., McWilliams, J.C., Bograd, S.J., Arango, H., Curchitser, E. and Powell, T.M., (2008). North Pacific Gyre Oscillation links ocean climate and ecosystem change. *Geophysical Research Letters*, *35*(8).

Evans, M. N., Kaplan, A., & Cane, M. A. (2000), Intercomparison of coral oxygen isotope data and historical sea surface temperature (SST): Potential for coral-based SST field reconstructions, Paleoceanography, 15(5): 551-563.

Furtado, J. C., Di Lorenzo, E., Anderson, B. T., & Schneider, N. (2012), Linkages between the North Pacific Oscillation and central tropical Pacific SSTs at low frequencies, Cli Dyn, 39(12): 2833-2846, doi:10.1007/s00382-011-1245-4.

Gagan, M. K., Dunbar, G. B., & Suzuki, A. (2012), The effect of skeletal mass accumulation in Porites on coral Sr/Ca and δ18O paleothermometry, Paleoceanography, 27(1): PA1203, doi:10.1029/2011PA002215.

Grinsted, A., Moore, J. C., & Jevrejeva, S. (2004), Application of the cross wavelet transform and wavelet coherence to geophysical time series, Nonlinear Process Geophys, 11(5/6): 561-566, doi:10.5194/npg-11-561-2004.

Kalnay, E., Kanamitsu, M., Kistler, R., Collins, W., Deaven, D., Gandin, L., Iredell, M., Saha, S., White, G., Woollen, J. and Zhu, Y., 1996. The NCEP/NCAR 40-year reanalysis project. *Bulletin of the American meteorological Society*, *77*(3), 437-471.

Lau, N. C., & Nath, M. J. (1996), The role of the "atmospheric bridge" in linking tropical Pacific ENSO events to extratropical SST anomalies, J Clim, 9(9): 2036-2057, doi:10.1175/1520-0442(1996)009<2036:TROTBI>2.0.CO;2.

LeGrande, A. N., & Schmidt, G. A. (2006), Global gridded data set of the oxygen isotopic composition in seawater, Geophys Res Lett, 33(12): L12604,doi:10.1029/2006GL026011.

Lough, J. M. (2004), A strategy to improve the contribution of coral data to high-resolution paleoclimatology, Palaeogeogr Palaeoclimatol Palaeoecol, 204(1): 115-143, doi:10.1016/S0031-0182(03)00727-2.

MacDonald, G. M., & Case, R. A. (2005), Variations in the Pacific Decadal Oscillation over the past millennium, Geophys Res Lett, 32(8): L0873, doi:10.1029/2005GL022478.

Reynolds, R.W., N.A. Rayner, T.M. Smith, D.C. Stokes, and W. Wang. (2002): An Improved in situ and satellite SST analysis for climate, J. Clim, 15, 1609-1625, doi:10.1175/1520-0442(2002)015<1609:AIISAS>2.0.CO;2.

Roemmich, D., & Gilson, J. (2011), The global ocean imprint of ENSO.Geophys Res Lett, 38(13), doi: 10.1029/2011GL047992

Thompson, D. M., Ault, T. R., Evans, M. N., Cole, J. E., & Emile-Geay, J. (2011), Comparison of observed and simulated tropical climate trends using a forward model of coral δ18O, Geophys Res Lett, 38(14): L14706, doi:10.1029/2011GL048224.

Smith, T.M., R.W. Reynolds, T.C. Peterson, and J. Lawrimore. (2008), Improvements NOAAs Historical Merged Land–Ocean Temp Analysis (1880–2006), J Clim, 21, 2283–2296, doi: http://dx.doi.org/10.1175/2007JCLI2100.1.

Vimont, D. J., Battisti, D. S., & Hirst, A. C. (2001), Footprinting: A seasonal connection between the tropics and mid-latitudes, Geophyis Res Lett, 28(20): 3923-3926, doi:10.1029/2001GL013435.

Vimont, D. J., Wallace, J. M., & Battisti, D. S. (2003), The seasonal footprinting mechanism in the Pacific: implications for ENSO*, J Clim, 16(16): 2668-2675, doi:10.1175/1520-0442(2003)016<2668:TSFMIT>2.0.CO;2.

Wilks, D.S. (2016), "The stippling shows statistically significant gridpoints": How Research Results are Routinely Overstated and Over-interpreted, and What to Do About It. Bull. Amer. Meteor. Soc. , 0, doi: 10.1175/BAMS-D-15-00267.1.

Appendix B. Supplementary Materials for Chapter 3. Pacific Meridional Mode over the last millennium

B.1 Introduction

This appendix contains supplementary information for (1.) An evaluation of the role of the Samalas eruption on the average moving standard deviation of the Pacific Meridional Mode (Figure B.1); (2.) composites of the extremes in the Pacific Meridional Mode variance (Figure B.1); (3.) an evaluation of the diversity in the response to volcanic eruptions within single ensemble members (Figure B.3).

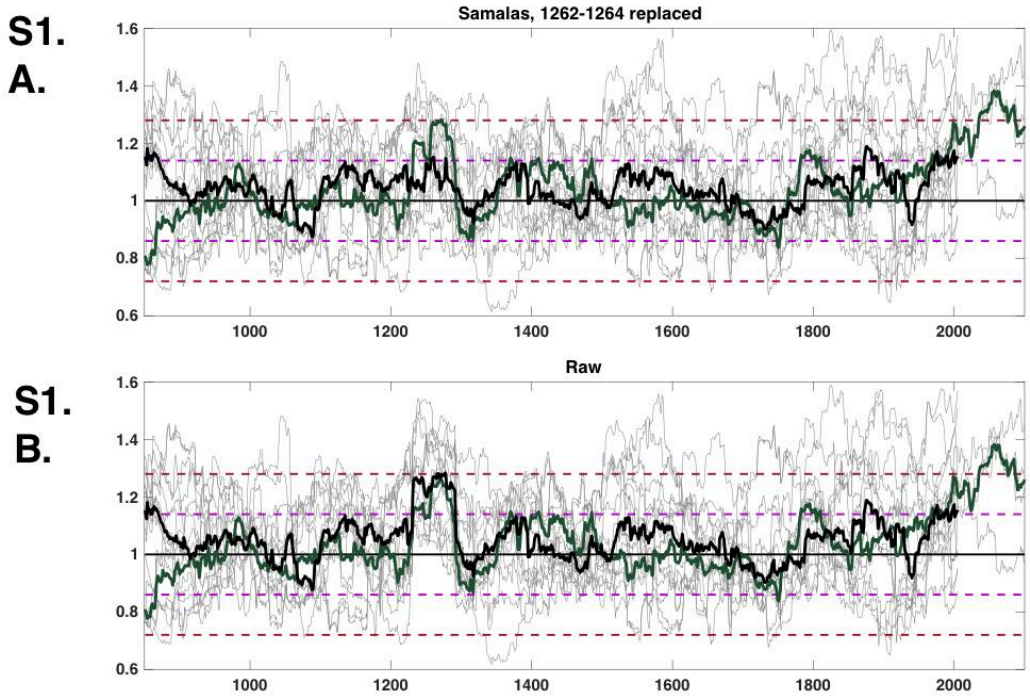

Figure B.1 Evaluation of 30 year moving standard deviation of PMM index (using the SST expansion coefficient) over the Samalas Volcanic eruption. Figure (**A.)** shows that when the three eruption response years (1261-1263) are replaced with random values within one sigma of the mean, there is no notable increase in variance during the 1230 to 1290 period. (**B.),** same as A, but calculated using all years highlights that the Samalas Volcanic eruption of 1258 creates an extremely short-lived anomaly that overwhelms the 30 year moving standard deviation methodology.

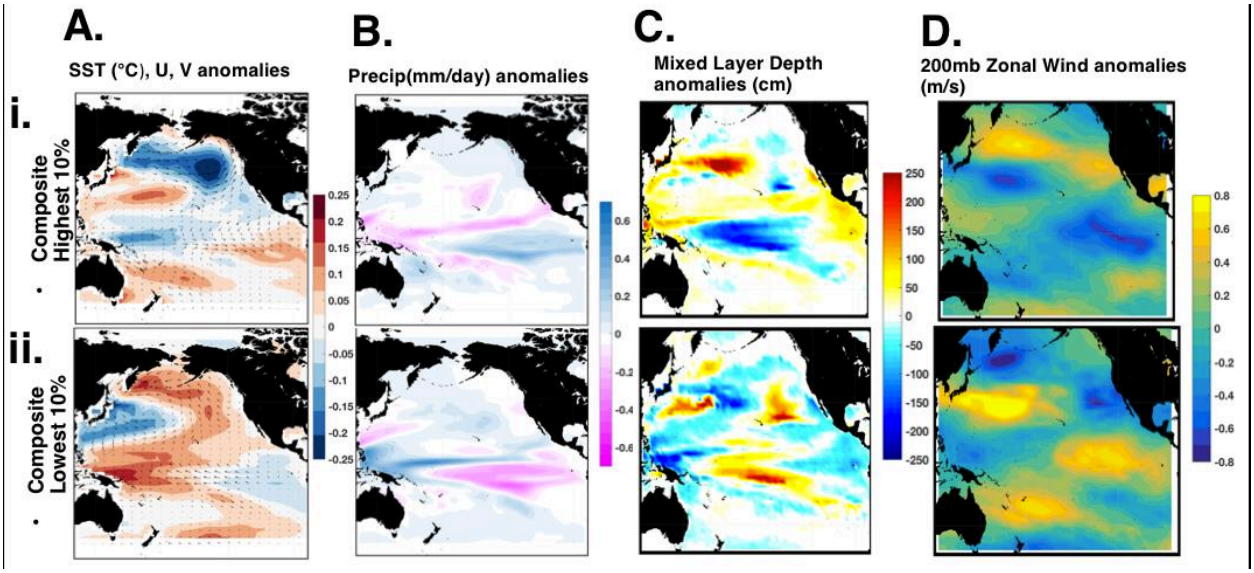

Figure B.2 We composite the highest 10% and lowest 10% of PMM variance years in each of the 12 "All Forcing" ensemble members (12 ensemble members of 1156 years. Similar and physically consistent patterns emerge between this and the linear regression approach in Figure 3.4. It should also be noted that the middle 80% of events from the composites average out to roughly zero anomaly. (**A.)** SST and wind vector composites (**B.)** Precipitation composites (**C.)** Mixed layer depth composites. (**D.)** 200mb zonal wind composites.

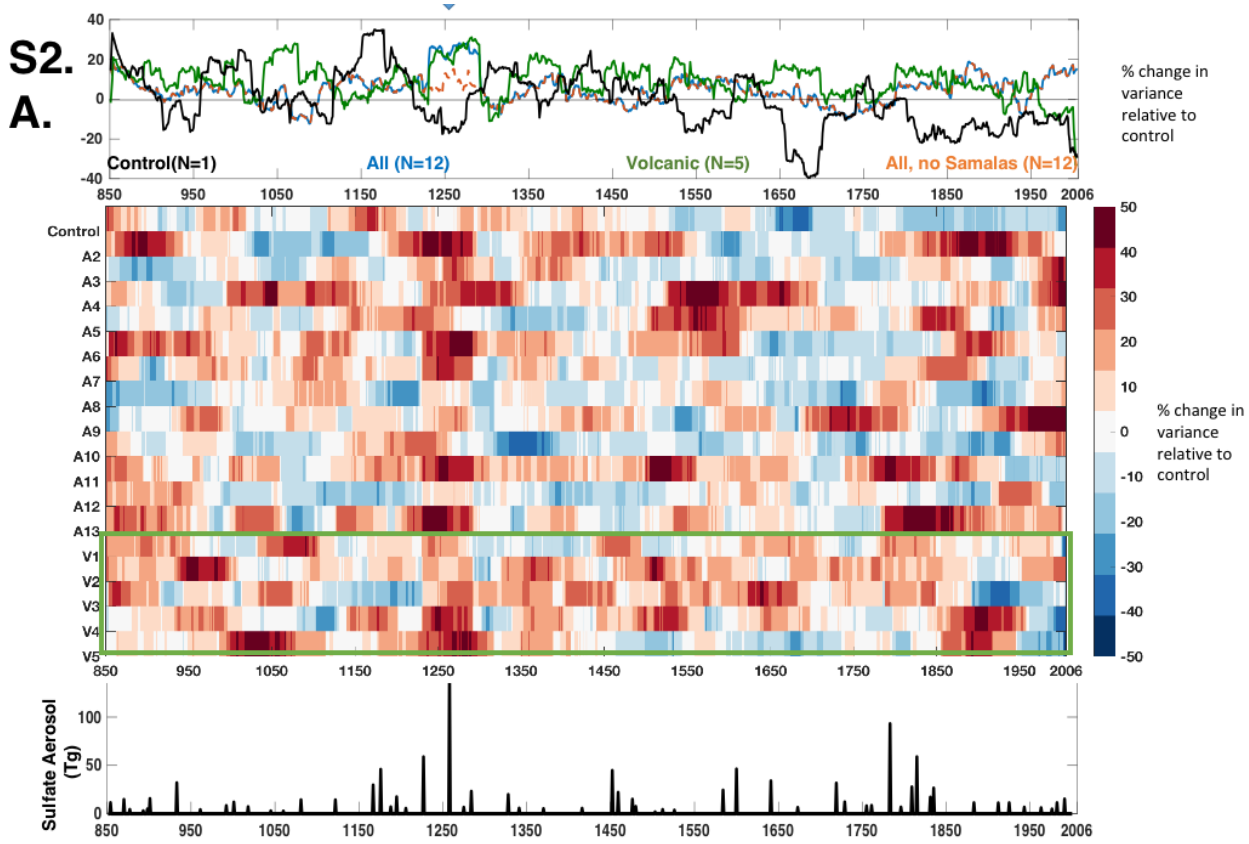

Figure B.3. Illustration of the diversity within ensemble members in response to volcanic eruptions. (**A).** The first portion features the timeseries of the 30 year moving standard deviation of the control run (black, single ensemble member), the all forcing experiment (blue, 12 ensemble members), the volcanic forcing only experiments (green, 5 ensemble members), and the all forcing experiment, excluding the 3 years of extreme variance post Samalas eruption (orange, 12 ensemble members) . The Y axis of this plot is slightly different from Figure 3. To convert the previous plots into this scale, merely subtract 1 and multiply by 100% to get a change in variance relative to the control. (**B).** The middle plot shows the relative increase or decrease in variance (relative to the control run) in each ensemble member. 18 Ensemble members are shown here; the Control at the top, the 12 All Forcing experiments, and 5 volcanic- forcing only experiments. (**C).** The bottom plot shows the volcanic eruptions used in this model from the Gao 2008 study. With the exception of the enormous Samalas eruption, no consistent PMM response to volcanoes is observed in the LME.

B.2 References

Gao, C., Robock, A. and Ammann, C., 2008. Volcanic forcing of climate over the past 1500 years: An improved ice core-based index for climate models. *Journal of Geophysical Research: Atmospheres*, *113*(D23).

APPENDIX

Appendix C. Supplementary Materials for Chapter 4. Constraining paleo carbonate chemistry: new insights from $\delta^{11}B$ and B/Ca measurements in monitored corals from Palmyra Atoll

C.1 Introduction

This appendix contains supplementary information for 1.) the seasonality of carbon isotopic composition and precipitation at Palmyra (Figure C.1).

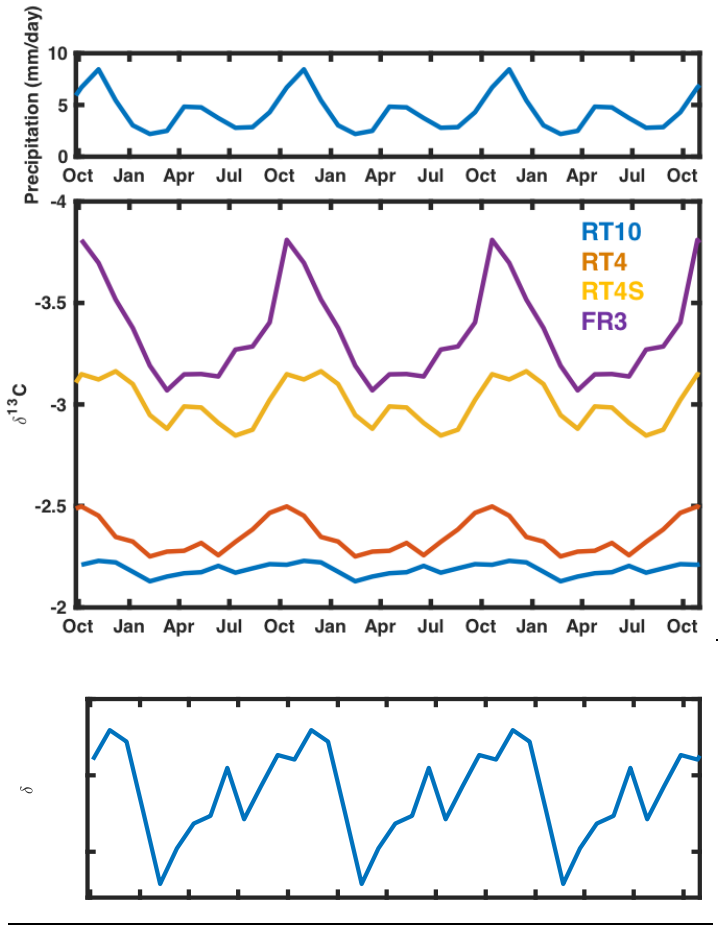

Figure C.1 Seasonality of carbon isotopic composition and precipitation. (**A).** precipitation (from CPC CMAP, in mm/day) carbon isotope variability and in **(B).** carbon isotopes using the annual average calculated over the length of each respective record. Colors represent core analyzed (RT10 (blue), RT4(orange), RT4S(yellow), FR3(purple)). (**C).** RT10 is plotted with a different Y axis to better observe the seasonal cycle.

APPENDIX

Appendix D. Coral collection and analysis

Coral Collection

Porites cores were collected using SCUBA and a hand-held, reversible pneumatic drill (Ingersoll-Rand 7803RA) following specifications from Dr. Jessica Carilli. Two different drilling configurations were employed throughout this dissertation: 1) a medium-sized drill (2.25in diameter, 6ft length), powered off of an air compressor and 2). a smaller (1.5 in diameter drill, 14 in length) powered off of scuba tanks.

Prior to each use, the coral drill was cleaned, and the drill bit was sterilized with a 10% bleach solution, and tested for mechanical problems before loading into the boat. Upon arrival the dive site, the dive team would identify both a sizeable *Porites lobata* and a safe place to store the equipment during the drilling process. In general, cores were collected by a single dive buddy team, using a handheld pneumatic drill. The drilling setup was compact enough to be able to fit all equipment into a single dive bag, plus a scuba tank (with a weight belt). The drill setup would be handed down from the boat to the dive team and then carefully placed in the identified spot to not disturb any of the surrounding coral. Short cores required roughly 30-45 minutes to drill (~1-2 tanks of air), but the longer cores could take several hours. In all but a single case, cores were drilled vertically to sample along the maximum growth axis. The RT4S core is the exception. In this instance, the core was drilled horizontally, 90 degrees off of normal, to assess vital effects.

All core holes were filled in with a nontoxic marine epoxy (Aquamend) to prevent damage

via infiltration by boring organisms and easily facilitate regrowth on the coral head. All equipment and samples were carefully returned to the boat.

After collection, coral samples were air dried and packed away to prepare for laboratory analysis once back in California. In Scripps Institution of Oceanography, the cores were slabbed using a doubled bladed table saw, or a hand saw (depending on the diameter of the coral). Cores were cleaned in de-ionized water and air-dried. Afterwards, the flat coral slabs were subject to X-ray scans at the Thornton Hospital and UV scans through the Avaatech X-Ray Flourescence at the Deep Sea Drilling lab's x-ray facility.

Coral analysis

The $\delta^{18}O$ and $\delta^{13}C$ stable isotopes of the coral carbonate samples were analyzed in the Charles lab at Scripps Institution of Oceanography. Roughly 0.4-0.7mg of carbonate powder was collected along the coral's primary growth axis using a microdrill press for stable isotope ($\delta^{18}O$ and $\delta^{13}C$) analysis. Samples were run on a Finnegan MAT253 gas source mass spectrometer with a Kiel IV carbonate device. Sample $\delta^{18}O$ and $\delta^{13}C$ are reported in delta notation, a standard format used to document the isotopic composition of a substance. Delta notation uses units of permil (‰) referenced against an international standard, here the Vienna Peedee belemnite standard(VPDB):

$$\delta^{H}X = \left(\frac{(R_x)sample}{(R_x)standard} - 1\right) * 1000$$

where X is the element of interest, the superscript H refers to the mass of the heavy isotope and R_X is the ratio of the heavy to light isotopes in either the sample or standard such that:

$$R_x = \frac{{}^{H}X}{{}^{L}X}$$

where L refers to “light” and H “heavy. As an example using $\delta^{18}O$:

$$\delta^{18}O_{coral} = \left(\frac{\left(\frac{^{18}O}{^{16}O} \right)_{coral}}{\left(\frac{^{18}O}{^{16}O} \right)_{PDB}} - 1 \right) \times 1000$$

Samples were run for every millimeter down the primary growth axis. The data presented in Appendices E-I has been fit to a seasonal or monthly cycle using linear interpolation.

Appendix E. Tabulated Clarion $\delta^{18}O$ isotopic data

Metadata for Clarion Island core
The *Porites* core was collected at 18.4°N, -114.8°W, 26ft depth in July, 1998 by Dr. Jose Carriquiry. The record spans one hundred seventy-eight years. Data can also be found online at https://www.ncdc.noaa.gov/paleo-search/study/21310

Table E.1 Clarion Island $\delta^{18}O$

Year	**Clarion $\delta^{18}O$‰**
1819.50	-3.70
1819.75	-3.11
1820.00	-3.24
1820.25	-3.60
1820.50	-4.07
1820.75	-4.04
1821.00	-3.93
1821.25	-4.00
1821.50	-4.03
1821.75	-3.73
1822.00	-3.50
1822.25	-3.73
1822.50	-3.80
1822.75	-3.50
1823.00	-3.24
1823.25	-3.14
1823.50	-3.37
1823.75	-3.33
1824.00	-3.25
1824.25	-3.41
1824.50	-3.60
1824.75	-3.56
1825.00	-3.52
1825.25	-3.71

Year	Clarion $\delta^{18}O$‰ (continued)
1825.50	-3.82
1825.75	-3.61
1826.00	-3.62
1826.25	-4.15
1826.50	-4.08
1826.75	-3.68
1827.00	-3.62
1827.25	-3.92
1827.50	-4.01
1827.75	-3.79
1828.00	-3.74
1828.25	-4.26
1828.50	-4.58
1828.75	-4.50
1829.00	-4.23
1829.25	-4.29
1829.50	-4.43
1829.75	-4.27
1830.00	-3.87
1830.25	-3.95
1830.50	-4.56
1830.75	-4.49
1831.00	-3.79
1831.25	-4.21
1831.50	-4.39
1831.75	-4.02
1832.00	-3.84
1832.25	-4.10
1832.50	-4.25
1832.75	-3.94
1833.00	-3.46
1833.25	-3.49
1833.50	-3.70
1833.75	-3.63

Year	Clarion $\delta^{18}O$‰ (continued)
1834.00	-3.49
1834.25	-3.63
1834.50	-3.83
1834.75	-3.45
1835.00	-3.22
1835.25	-3.83
1835.50	-4.33
1835.75	-4.02
1836.00	-3.76
1836.25	-4.07
1836.50	-4.19
1836.75	-3.90
1837.00	-3.90
1837.25	-4.32
1837.50	-4.24
1837.75	-3.88
1838.00	-3.63
1838.25	-3.52
1838.50	-3.81
1838.75	-3.80
1839.00	-3.71
1839.25	-4.03
1839.50	-4.02
1839.75	-3.74
1840.00	-3.37
1840.25	-3.45
1840.50	-3.66
1840.75	-3.62
1841.00	-3.28
1841.25	-3.46
1841.50	-3.70
1841.75	-3.47
1842.00	-3.43
1842.25	-3.56

Year	Clarion $\delta^{18}O$‰ (continued)
1842.50	-3.84
1842.75	-3.82
1843.00	-3.64
1843.25	-3.74
1843.50	-3.95
1843.75	-3.91
1844.00	-3.80
1844.25	-3.89
1844.50	-4.61
1844.75	-4.54
1845.00	-3.83
1845.25	-3.97
1845.50	-4.16
1845.75	-3.65
1846.00	-3.65
1846.25	-3.99
1846.50	-4.74
1846.75	-4.30
1847.00	-3.71
1847.25	-4.18
1847.50	-4.52
1847.75	-4.39
1848.00	-4.35
1848.25	-4.59
1848.50	-4.73
1848.75	-4.55
1849.00	-4.39
1849.25	-4.53
1849.50	-4.58
1849.75	-4.25
1850.00	-3.82
1850.25	-4.11
1850.50	-4.35
1850.75	-3.93

Year	Clarion $\delta^{18}O$‰ (continued)
1851.00	-3.92
1851.25	-4.16
1851.50	-4.31
1851.75	-4.24
1852.00	-4.22
1852.25	-4.40
1852.50	-4.29
1852.75	-3.81
1853.00	-3.68
1853.25	-3.76
1853.50	-4.04
1853.75	-3.61
1854.00	-3.41
1854.25	-3.57
1854.50	-3.65
1854.75	-3.43
1855.00	-3.38
1855.25	-3.79
1855.50	-4.05
1855.75	-4.02
1856.00	-3.97
1856.25	-4.11
1856.50	-4.04
1856.75	-3.62
1857.00	-3.47
1857.25	-3.72
1857.50	-3.94
1857.75	-3.74
1858.00	-3.69
1858.25	-4.20
1858.50	-3.88
1858.75	-3.70
1859.00	-3.54
1859.25	-3.78

Year	Clarion $\delta^{18}O$‰ (continued)
1859.50	-4.03
1859.75	-3.76
1860.00	-3.45
1860.25	-3.96
1860.50	-4.84
1860.75	-4.35
1861.00	-4.12
1861.25	-4.16
1861.50	-4.27
1861.75	-4.14
1862.00	-4.07
1862.25	-4.30
1862.50	-4.32
1862.75	-3.99
1863.00	-3.90
1863.25	-4.16
1863.50	-4.38
1863.75	-4.20
1864.00	-4.25
1864.25	-4.46
1864.50	-4.72
1864.75	-4.23
1865.00	-4.38
1865.25	-4.46
1865.50	-4.63
1865.75	-4.29
1866.00	-4.09
1866.25	-4.33
1866.50	-4.43
1866.75	-4.26
1867.00	-4.14
1867.25	-4.23
1867.50	-4.34
1867.75	-4.03

Year	Clarion $\delta^{18}O$‰ (continued)
1868.00	-3.78
1868.25	-3.83
1868.50	-3.90
1868.75	-3.67
1869.00	-3.71
1869.25	-4.01
1869.50	-4.27
1869.75	-4.38
1870.00	-4.25
1870.25	-3.98
1870.50	-4.08
1870.75	-4.30
1871.00	-4.10
1871.25	-4.08
1871.50	-4.23
1871.75	-3.83
1872.00	-3.77
1872.25	-4.11
1872.50	-4.15
1872.75	-4.05
1873.00	-3.82
1873.25	-3.83
1873.50	-4.01
1873.75	-3.92
1874.00	-3.78
1874.25	-3.89
1874.50	-4.03
1874.75	-3.93
1875.00	-3.73
1875.25	-3.78
1875.50	-3.93
1875.75	-3.84
1876.00	-3.81
1876.25	-4.12

Year	Clarion $\delta^{18}O$‰ (continued)
1876.50	-4.30
1876.75	-4.02
1877.00	-3.74
1877.25	-3.81
1877.50	-3.87
1877.75	-3.64
1878.00	-3.42
1878.25	-3.60
1878.50	-4.03
1878.75	-4.03
1879.00	-3.87
1879.25	-4.06
1879.50	-4.54
1879.75	-4.36
1880.00	-4.02
1880.25	-4.05
1880.50	-4.16
1880.75	-4.08
1881.00	-4.02
1881.25	-4.15
1881.50	-4.11
1881.75	-3.82
1882.00	-4.14
1882.25	-4.54
1882.50	-4.70
1882.75	-3.70
1883.00	-3.46
1883.25	-4.09
1883.50	-3.81
1883.75	-3.46
1884.00	-3.72
1884.25	-4.15
1884.50	-4.22
1884.75	-4.06

Year	Clarion $\delta^{18}O$‰ (continued)
1885.00	-3.89
1885.25	-4.02
1885.50	-4.32
1885.75	-4.27
1886.00	-3.88
1886.25	-3.99
1886.50	-4.28
1886.75	-4.22
1887.00	-3.87
1887.25	-4.10
1887.50	-4.15
1887.75	-3.85
1888.00	-3.74
1888.25	-3.55
1888.50	-4.31
1888.75	-3.84
1889.00	-3.82
1889.25	-3.99
1889.50	-4.30
1889.75	-4.14
1890.00	-3.83
1890.25	-4.36
1890.50	-4.26
1890.75	-3.79
1891.00	-3.97
1891.25	-4.06
1891.50	-4.75
1891.75	-4.13
1892.00	-3.84
1892.25	-4.10
1892.50	-4.41
1892.75	-3.96
1893.00	-3.49
1893.25	-3.67

Year	Clarion $\delta^{18}O$‰ (continued)
1893.50	-3.89
1893.75	-3.72
1894.00	-3.71
1894.25	-3.87
1894.50	-3.91
1894.75	-3.77
1895.00	-3.70
1895.25	-3.97
1895.50	-4.12
1895.75	-3.94
1896.00	-4.15
1896.25	-4.23
1896.50	-4.30
1896.75	-3.75
1897.00	-3.98
1897.25	-4.06
1897.50	-4.38
1897.75	-4.23
1898.00	-3.98
1898.25	-4.10
1898.50	-4.20
1898.75	-3.80
1899.00	-3.76
1899.25	-4.03
1899.50	-4.60
1899.75	-4.35
1900.00	-4.08
1900.25	-4.09
1900.50	-4.07
1900.75	-3.79
1901.00	-3.80
1901.25	-3.95
1901.50	-4.29
1901.75	-3.65

Year	Clarion $\delta^{18}O$‰ (continued)
1902.00	-3.47
1902.25	-3.96
1902.50	-4.06
1902.75	-3.92
1903.00	-4.10
1903.25	-4.21
1903.50	-4.11
1903.75	-3.93
1904.00	-3.49
1904.25	-3.99
1904.50	-4.31
1904.75	-4.24
1905.00	-4.25
1905.25	-4.55
1905.50	-4.49
1905.75	-4.12
1906.00	-4.31
1906.25	-4.45
1906.50	-4.51
1906.75	-4.18
1907.00	-3.90
1907.25	-4.03
1907.50	-4.34
1907.75	-4.15
1908.00	-4.03
1908.25	-3.79
1908.50	-3.79
1908.75	-4.02
1909.00	-3.94
1909.25	-4.05
1909.50	-4.08
1909.75	-3.72
1910.00	-3.48
1910.25	-3.74

Year	Clarion $\delta^{18}O$‰ (continued)
1910.50	-4.02
1910.75	-3.95
1911.00	-3.89
1911.25	-4.20
1911.50	-4.36
1911.75	-4.05
1912.00	-3.78
1912.25	-3.92
1912.50	-4.04
1912.75	-3.82
1913.00	-3.69
1913.25	-3.92
1913.50	-4.03
1913.75	-3.85
1914.00	-4.03
1914.25	-4.11
1914.50	-4.06
1914.75	-3.76
1915.00	-3.88
1915.25	-3.98
1915.50	-4.00
1915.75	-3.87
1916.00	-3.89
1916.25	-4.13
1916.50	-4.24
1916.75	-3.98
1917.00	-3.84
1917.25	-3.86
1917.50	-4.02
1917.75	-3.80
1918.00	-3.90
1918.25	-4.25
1918.50	-4.08
1918.75	-3.93

Year	Clarion $\delta^{18}O$‰ (continued)
1919.00	-4.13
1919.25	-4.43
1919.50	-4.35
1919.75	-4.27
1920.00	-3.94
1920.25	-4.35
1920.50	-4.40
1920.75	-4.02
1921.00	-3.90
1921.25	-3.81
1921.50	-4.43
1921.75	-4.00
1922.00	-3.68
1922.25	-3.88
1922.50	-3.86
1922.75	-3.51
1923.00	-3.36
1923.25	-3.49
1923.50	-3.54
1923.75	-3.34
1924.00	-3.45
1924.25	-4.07
1924.50	-4.17
1924.75	-3.78
1925.00	-3.77
1925.25	-3.92
1925.50	-4.29
1925.75	-4.14
1926.00	-4.13
1926.25	-4.30
1926.50	-4.25
1926.75	-4.00
1927.00	-3.62
1927.25	-4.18

Year	Clarion $\delta^{18}O$‰ (continued)
1927.50	-4.33
1927.75	-4.14
1928.00	-4.07
1928.25	-4.17
1928.50	-4.13
1928.75	-3.89
1929.00	-3.91
1929.25	-4.54
1929.50	-5.10
1929.75	-4.59
1930.00	-4.26
1930.25	-4.28
1930.50	-4.42
1930.75	-4.49
1931.00	-4.39
1931.25	-4.54
1931.50	-4.65
1931.75	-4.44
1932.00	-3.98
1932.25	-4.09
1932.50	-4.53
1932.75	-4.65
1933.00	-4.50
1933.25	-4.38
1933.50	-4.52
1933.75	-4.13
1934.00	-4.43
1934.25	-4.49
1934.50	-4.55
1934.75	-4.38
1935.00	-4.25
1935.25	-4.72
1935.50	-4.80
1935.75	-4.57

Year	Clarion $\delta^{18}O$‰ (continued)
1936.00	-4.40
1936.25	-4.38
1936.50	-4.62
1936.75	-4.14
1937.00	-4.21
1937.25	-4.58
1937.50	-4.91
1937.75	-4.89
1938.00	-4.15
1938.25	-4.44
1938.50	-4.67
1938.75	-4.48
1939.00	-4.61
1939.25	-5.13
1939.50	-4.84
1939.75	-3.87
1940.00	-3.96
1940.25	-4.55
1940.50	-4.66
1940.75	-4.33
1941.00	-4.18
1941.25	-4.20
1941.50	-4.35
1941.75	-4.22
1942.00	-4.08
1942.25	-4.14
1942.50	-4.18
1942.75	-4.09
1943.00	-4.12
1943.25	-4.27
1943.50	-4.26
1943.75	-3.95
1944.00	-3.84
1944.25	-4.34

Year	Clarion $\delta^{18}O$‰ (continued)
1944.50	-4.24
1944.75	-4.09
1945.00	-3.94
1945.25	-4.06
1945.50	-4.18
1945.75	-3.91
1946.00	-3.88
1946.25	-4.10
1946.50	-4.30
1946.75	-4.01
1947.00	-3.70
1947.25	-4.09
1947.50	-4.61
1947.75	-4.10
1948.00	-4.19
1948.25	-4.50
1948.50	-4.82
1948.75	-4.21
1949.00	-3.85
1949.25	-4.16
1949.50	-4.42
1949.75	-3.98
1950.00	-3.72
1950.25	-3.99
1950.50	-4.34
1950.75	-4.25
1951.00	-4.20
1951.25	-4.43
1951.50	-4.60
1951.75	-4.36
1952.00	-4.23
1952.25	-4.51
1952.50	-4.52
1952.75	-4.14

Year	Clarion $\delta^{18}O$‰ (continued)
1953.00	-4.14
1953.25	-4.31
1953.50	-4.25
1953.75	-3.71
1954.00	-3.70
1954.25	-4.00
1954.50	-4.14
1954.75	-4.14
1955.00	-4.04
1955.25	-3.86
1955.50	-4.04
1955.75	-3.95
1956.00	-4.11
1956.25	-4.37
1956.50	-4.35
1956.75	-4.16
1957.00	-3.93
1957.25	-4.17
1957.50	-4.07
1957.75	-3.56
1958.00	-3.79
1958.25	-4.27
1958.50	-4.27
1958.75	-3.87
1959.00	-3.66
1959.25	-3.87
1959.50	-3.92
1959.75	-3.82
1960.00	-3.96
1960.25	-4.16
1960.50	-4.19
1960.75	-4.01
1961.00	-3.89
1961.25	-4.00

Year	Clarion $\delta^{18}O$‰ (continued)
1961.50	-4.12
1961.75	-4.09
1962.00	-4.06
1962.25	-4.10
1962.50	-4.03
1962.75	-3.84
1963.00	-3.84
1963.25	-4.08
1963.50	-4.14
1963.75	-4.08
1964.00	-3.99
1964.25	-4.14
1964.50	-4.33
1964.75	-4.19
1965.00	-4.24
1965.25	-4.45
1965.50	-4.43
1965.75	-4.17
1966.00	-4.21
1966.25	-4.35
1966.50	-4.32
1966.75	-4.21
1967.00	-4.18
1967.25	-4.33
1967.50	-4.43
1967.75	-4.28
1968.00	-4.24
1968.25	-4.40
1968.50	-4.53
1968.75	-4.30
1969.00	-4.04
1969.25	-4.10
1969.50	-4.18
1969.75	-3.98

Year	Clarion $\delta^{18}O$‰ (continued)
1970.00	-3.99
1970.25	-4.15
1970.50	-4.18
1970.75	-4.07
1971.00	-4.02
1971.25	-4.05
1971.50	-4.03
1971.75	-3.89
1972.00	-3.85
1972.25	-3.99
1972.50	-4.00
1972.75	-3.84
1973.00	-3.87
1973.25	-3.96
1973.50	-3.92
1973.75	-3.78
1974.00	-3.76
1974.25	-3.92
1974.50	-4.04
1974.75	-3.89
1975.00	-3.80
1975.25	-3.97
1975.50	-4.19
1975.75	-4.06
1976.00	-3.78
1976.25	-3.78
1976.50	-3.99
1976.75	-3.91
1977.00	-3.70
1977.25	-3.99
1977.50	-4.13
1977.75	-4.01
1978.00	-3.97
1978.25	-4.11

Year	Clarion $\delta^{18}O$‰ (continued)
1978.50	-4.13
1978.75	-3.76
1979.00	-3.51
1979.25	-3.98
1979.50	-4.31
1979.75	-4.14
1980.00	-4.22
1980.25	-3.99
1980.50	-4.28
1980.75	-4.22
1981.00	-4.14
1981.25	-4.37
1981.50	-4.41
1981.75	-4.29
1982.00	-4.19
1982.25	-4.38
1982.50	-4.43
1982.75	-4.23
1983.00	-4.19
1983.25	-4.48
1983.50	-4.78
1983.75	-4.48
1984.00	-4.19
1984.25	-4.31
1984.50	-4.41
1984.75	-4.31
1985.00	-4.27
1985.25	-4.20
1985.50	-4.29
1985.75	-4.29
1986.00	-4.20
1986.25	-4.34
1986.50	-4.58
1986.75	-4.17

Year	Clarion $\delta^{18}O$‰ (continued)
1987.00	-4.15
1987.25	-4.23
1987.50	-4.18
1987.75	-4.24
1988.00	-4.01
1988.25	-3.90
1988.50	-4.05
1988.75	-4.09
1989.00	-4.07
1989.25	-4.11
1989.50	-4.32
1989.75	-4.54
1990.00	-4.38
1990.25	-4.27
1990.50	-4.21
1990.75	-4.21
1991.00	-4.17
1991.25	-4.43
1991.50	-4.54
1991.75	-4.46
1992.00	-4.47
1992.25	-4.62
1992.50	-4.63
1992.75	-4.43
1993.00	-4.39
1993.25	-4.49
1993.50	-4.50
1993.75	-4.34
1994.00	-4.24
1994.25	-4.41
1994.50	-4.55
1994.75	-4.36
1995.00	-4.29
1995.25	-4.39

Year	Clarion $\delta^{18}O‰$ (continued)
1995.50	-4.42
1995.75	-4.24
1996.00	-4.28
1996.25	-4.37
1996.50	-4.43
1996.75	-4.30
1997.00	-4.51
1997.25	-4.65
1997.50	-4.74
1997.75	-4.42
1998.00	-4.08

Appendix F. Tabulated Palmyra RT10 $\delta^{18}O$ isotopic data

Metadata for Palmyra RT10

The *Porites* core was collected at 5.89°N, -162.12°W, 18ft depth in September, 2016 by the dissertation author. The record spans twenty-one years. All data will be posted on NOAA NCDC after publication.

Table F.1 Palmyra RT10 $\delta^{18}O$

Year	RT10 $\delta^{18}O$‰
1995.75	-5.00
1995.83	-4.98
1995.92	-5.12
1996.00	-5.01
1996.08	-5.07
1996.17	-4.81
1996.25	-5.20
1996.33	-5.41
1996.42	-5.47
1996.50	-5.31
1996.58	-5.36
1996.67	-5.42
1996.75	-5.35
1996.83	-5.05
1996.92	-5.11
1997.00	-5.12
1997.08	-5.13
1997.17	-5.14
1997.25	-5.25
1997.33	-5.50
1997.42	-5.51
1997.50	-5.57
1997.58	-5.68
1997.67	-5.72

Year	RT10 $\delta^{18}O$‰ (continued)
1997.75	-5.76
1997.83	-5.69
1997.92	-5.35
1998.00	-5.25
1998.08	-5.32
1998.17	-5.37
1998.25	-5.29
1998.33	-5.24
1998.42	-5.22
1998.50	-5.28
1998.58	-5.41
1998.67	-5.27
1998.75	-5.24
1998.83	-5.23
1998.92	-5.05
1999.00	-4.99
1999.08	-5.04
1999.17	-5.02
1999.25	-4.97
1999.33	-5.04
1999.42	-5.00
1999.50	-5.00
1999.58	-5.05
1999.67	-5.07
1999.75	-5.06
1999.83	-5.03
1999.92	-4.95
2000.00	-4.88
2000.08	-4.82
2000.17	-4.78
2000.25	-4.94
2000.33	-4.86
2000.42	-4.99
2000.50	-5.04

Year	RT10 $\delta^{18}O$‰ (continued)
2000.58	-5.11
2000.67	-5.09
2000.75	-5.12
2000.83	-5.18
2000.92	-5.20
2001.00	-5.08
2001.08	-4.96
2001.17	-4.96
2001.25	-4.87
2001.33	-4.89
2001.42	-5.03
2001.50	-5.18
2001.58	-5.22
2001.67	-5.31
2001.75	-5.36
2001.83	-5.25
2001.92	-5.19
2002.00	-5.27
2002.08	-5.19
2002.17	-5.08
2002.25	-5.32
2002.33	-5.53
2002.42	-5.64
2002.50	-5.53
2002.58	-5.58
2002.67	-5.64
2002.75	-5.55
2002.83	-5.46
2002.92	-5.40
2003.00	-5.29
2003.08	-5.41
2003.17	-5.40
2003.25	-5.31
2003.33	-5.31

Year	RT10 $\delta^{18}O$‰ (continued)
2003.42	-5.34
2003.50	-5.49
2003.58	-5.52
2003.67	-5.49
2003.75	-5.58
2003.83	-5.47
2003.92	-5.35
2004.00	-5.28
2004.08	-5.23
2004.17	-5.23
2004.25	-5.20
2004.33	-5.21
2004.42	-5.31
2004.50	-5.39
2004.58	-5.30
2004.67	-5.44
2004.75	-5.61
2004.83	-5.67
2004.92	-5.62
2005.00	-5.55
2005.08	-5.48
2005.17	-5.42
2005.25	-5.35
2005.33	-5.24
2005.42	-5.10
2005.50	-5.11
2005.58	-5.21
2005.67	-5.22
2005.75	-5.30
2005.83	-5.37
2005.92	-5.17
2006.00	-5.16
2006.08	-5.08
2006.17	-4.95

Year	RT10 $\delta^{18}O$‰ (continued)
2006.25	-4.98
2006.33	-5.07
2006.42	-5.17
2006.50	-5.26
2006.58	-5.36
2006.67	-5.34
2006.75	-5.35
2006.83	-5.42
2006.92	-5.16
2007.00	-5.01
2007.08	-5.02
2007.17	-4.96
2007.25	-4.86
2007.33	-4.83
2007.42	-4.95
2007.50	-4.98
2007.58	-5.07
2007.67	-5.07
2007.75	-5.00
2007.83	-4.90
2007.92	-4.77
2008.00	-4.76
2008.08	-4.80
2008.17	-4.75
2008.25	-4.94
2008.33	-4.95
2008.42	-4.73
2008.50	-4.98
2008.58	-5.15
2008.67	-5.18
2008.75	-5.25
2008.83	-5.34
2008.92	-5.37
2009.00	-5.25

Year	RT10 $\delta^{18}O$‰ (continued)
2009.08	-4.98
2009.17	-4.77
2009.25	-4.75
2009.33	-4.80
2009.42	-4.85
2009.50	-4.90
2009.58	-5.02
2009.67	-5.16
2009.75	-5.21
2009.83	-5.34
2009.92	-5.41
2010.00	-5.37
2010.08	-5.33
2010.17	-5.28
2010.25	-5.25
2010.33	-5.22
2010.42	-5.19
2010.50	-5.17
2010.58	-5.15
2010.67	-5.17
2010.75	-5.20
2010.83	-5.13
2010.92	-4.95
2011.00	-4.84
2011.08	-4.83
2011.17	-4.99
2011.25	-5.01
2011.33	-4.86
2011.42	-5.00
2011.50	-5.09
2011.58	-5.26
2011.67	-5.29
2011.75	-5.14
2011.83	-5.05

Year	RT10 $\delta^{18}O$‰ (continued)
2011.92	-5.08
2012.00	-5.13
2012.08	-4.93
2012.17	-4.83
2012.25	-4.82
2012.33	-4.90
2012.42	-4.99
2012.50	-5.04
2012.58	-5.03
2012.67	-5.01
2012.75	-5.10
2012.83	-5.32
2012.92	-5.18
2013.00	-5.09
2013.08	-5.17
2013.17	-5.22
2013.25	-5.21
2013.33	-5.16
2013.42	-5.11
2013.50	-5.05
2013.58	-5.06
2013.67	-5.34
2013.75	-5.33
2013.83	-5.15
2013.92	-5.18
2014.00	-5.17
2014.08	-5.16
2014.17	-5.13
2014.25	-5.07
2014.33	-5.16
2014.42	-5.31
2014.50	-5.62
2014.58	-5.68
2014.67	-5.63

Year	RT10 $\delta^{18}O$‰ (continued)
2014.75	-5.72
2014.83	-5.71
2014.92	-5.66
2015.00	-5.34
2015.08	-5.38
2015.17	-5.44
2015.25	-5.55
2015.33	-5.59
2015.42	-5.72
2015.50	-5.83
2015.58	-5.78
2015.67	-5.83
2015.75	-5.86
2015.83	-5.79
2015.92	-5.71
2016.00	-5.65
2016.08	-5.58
2016.17	-5.51
2016.25	-5.48
2016.33	-5.48
2016.42	-5.47
2016.50	-5.40

Appendix G. Tabulated Palmyra RT4 $\delta^{18}O$ isotopic data

Metadata for Palmyra RT4

The *Porites* core was collected at 5.88°N, -162.12°W, 18ft depth in September, 2016 by the dissertation author. The record spans seventeen years. All data will be posted on NOAA NCDC after publication.

Table G.1 Palmyra RT4 $\delta^{18}O$

Year	RT4 $\delta^{18}O$‰
1999.42	-4.82
1999.50	-5.02
1999.58	-5.05
1999.67	-5.25
1999.75	-5.02
1999.83	-4.90
1999.92	-4.82
2000.00	-4.76
2000.08	-4.85
2000.17	-4.77
2000.25	-4.75
2000.33	-4.96
2000.42	-5.08
2000.50	-5.15
2000.58	-5.17
2000.67	-5.10
2000.75	-5.12
2000.83	-4.95
2000.92	-5.05
2001.00	-4.99
2001.08	-4.83
2001.17	-4.94
2001.25	-5.05
2001.33	-4.93

Year	RT4 $\delta^{18}O$‰ (continued)
2001.42	-5.01
2001.50	-5.15
2001.58	-5.21
2001.67	-5.25
2001.75	-5.30
2001.83	-5.27
2001.92	-5.19
2002.00	-5.14
2002.08	-5.17
2002.17	-5.07
2002.25	-4.98
2002.33	-4.84
2002.42	-4.90
2002.50	-4.79
2002.58	-4.86
2002.67	-4.87
2002.75	-5.12
2002.83	-5.34
2002.92	-5.09
2003.00	-5.03
2003.08	-4.96
2003.17	-4.92
2003.25	-4.99
2003.33	-4.87
2003.42	-5.11
2003.50	-5.13
2003.58	-5.27
2003.67	-5.27
2003.75	-5.32
2003.83	-5.15
2003.92	-5.13
2004.00	-5.00
2004.08	-4.86
2004.17	-4.66

Year	RT4 $\delta^{18}O$‰ (continued)
2004.25	-4.81
2004.33	-5.00
2004.42	-5.07
2004.50	-5.18
2004.58	-5.14
2004.67	-5.27
2004.75	-5.23
2004.83	-5.32
2004.92	-5.17
2005.00	-5.25
2005.08	-5.29
2005.17	-5.01
2005.25	-4.87
2005.33	-4.84
2005.42	-4.92
2005.50	-5.13
2005.58	-5.13
2005.67	-5.02
2005.75	-4.92
2005.83	-4.84
2005.92	-4.85
2006.00	-4.82
2006.08	-4.84
2006.17	-4.88
2006.25	-4.75
2006.33	-4.93
2006.42	-4.94
2006.50	-4.83
2006.58	-5.18
2006.67	-5.36
2006.75	-5.53
2006.83	-5.42
2006.92	-5.44
2007.00	-5.29

Year	RT4 $\delta^{18}O$‰ (continued)
2007.08	-5.05
2007.17	-5.06
2007.25	-5.17
2007.33	-5.22
2007.42	-5.08
2007.50	-4.95
2007.58	-5.05
2007.67	-5.33
2007.75	-5.31
2007.83	-5.11
2007.92	-5.02
2008.00	-4.88
2008.08	-4.83
2008.17	-4.88
2008.25	-4.95
2008.33	-4.97
2008.42	-4.92
2008.50	-4.93
2008.58	-5.01
2008.67	-5.09
2008.75	-5.07
2008.83	-5.02
2008.92	-5.04
2009.00	-5.00
2009.08	-4.95
2009.17	-4.94
2009.25	-4.93
2009.33	-4.99
2009.42	-5.03
2009.50	-5.07
2009.58	-5.13
2009.67	-5.29
2009.75	-5.46
2009.83	-5.46

Year	RT4 $\delta^{18}O$‰ (continued)
2009.92	-5.40
2010.00	-5.34
2010.08	-5.19
2010.17	-5.21
2010.25	-5.16
2010.33	-5.13
2010.42	-5.07
2010.50	-5.05
2010.58	-5.09
2010.67	-5.09
2010.75	-5.16
2010.83	-5.18
2010.92	-5.22
2011.00	-5.09
2011.08	-4.95
2011.17	-5.02
2011.25	-5.02
2011.33	-5.02
2011.42	-5.06
2011.50	-5.13
2011.58	-5.21
2011.67	-5.23
2011.75	-5.28
2011.83	-5.37
2011.92	-5.40
2012.00	-5.24
2012.08	-5.20
2012.17	-5.21
2012.25	-5.03
2012.33	-5.06
2012.42	-5.08
2012.50	-5.13
2012.58	-5.15
2012.67	-5.17

Year	RT4 $\delta^{18}O$‰ (continued)
2012.75	-5.23
2012.83	-5.29
2012.92	-5.29
2013.00	-5.15
2013.08	-5.10
2013.17	-5.05
2013.25	-5.16
2013.33	-5.23
2013.42	-5.20
2013.50	-5.27
2013.58	-5.26
2013.67	-5.32
2013.75	-5.36
2013.83	-5.33
2013.92	-5.28
2014.00	-5.21
2014.08	-5.21
2014.17	-5.22
2014.25	-5.28
2014.33	-5.27
2014.42	-5.30
2014.50	-5.37
2014.58	-5.53
2014.67	-5.58
2014.75	-5.57
2014.83	-5.65
2014.92	-5.74
2015.00	-5.60
2015.08	-5.49
2015.17	-5.40
2015.25	-5.42
2015.33	-5.44
2015.42	-5.49
2015.50	-5.55

Year	RT4 $\delta^{18}O$‰ (continued)
2015.58	-5.69
2015.67	-5.80
2015.75	-5.74
2015.83	-5.60
2015.92	-5.64
2016.00	-5.67
2016.08	-5.59
2016.17	-5.64
2016.25	-5.70
2016.33	-5.54
2016.42	-5.54
2016.50	-5.62
2016.58	-5.51
2016.67	-5.50
2016.75	-5.57

Appendix H. Tabulated Palmyra FR3 $\delta^{18}O$ isotopic data

Metadata for Palmyra FR3

The *Porites* core was collected at 5.87°N, -162.11°W, 42ft depth in September, 2016 by the dissertation author. The record spans two years. All data will be posted on NOAA NCDC after publication.

Table H.1 Palmyra FR3 $\delta^{18}O$

Year	**$\delta^{18}O$‰**
2014.83	-5.33
2014.92	-5.28
2015.00	-5.29
2015.08	-5.27
2015.17	-5.40
2015.25	-5.43
2015.33	-5.52
2015.42	-5.62
2015.50	-5.56
2015.58	-5.63
2015.67	-5.63
2015.75	-5.60
2015.83	-5.58
2015.92	-5.55
2016.00	-5.48
2016.08	-5.46
2016.17	-5.43
2016.25	-5.48
2016.33	-5.27
2016.42	-5.37
2016.50	-5.41
2016.58	-5.42
2016.67	-5.42
2016.75	-5.51

Appendix I. Tabulated Palmyra RT4S $\delta^{18}O$ isotopic data

Metadata for Palmyra RT4S

The *Porites* core was collected at 5.88°N, -162.12°W, 18ft depth in September, 2016 by the dissertation author. Notably, this core was drilled horizontally into the coral; 90 degrees off of the standard drilling configuration. The record spans thirteen years. All data will be posted on NOAA NCDC after publication.

Table I.1 Palmyra RT4S $\delta^{18}O$

Year	RT4TS $\delta^{18}O$‰
2003.00	-5.00
2003.08	-4.91
2003.17	-4.91
2003.25	-5.09
2003.33	-4.94
2003.42	-5.09
2003.50	-5.27
2003.58	-5.30
2003.67	-5.21
2003.75	-5.25
2003.83	-5.35
2003.92	-5.29
2004.00	-5.30
2004.08	-5.30
2004.17	-5.32
2004.25	-5.35
2004.33	-5.18
2004.42	-5.16
2004.50	-5.31
2004.58	-5.34
2004.67	-5.56
2004.75	-5.57
2004.83	-5.63
2004.92	-5.54

Year	RT4S $\delta^{18}O$‰ (continued)
2005.00	-5.48
2005.08	-5.41
2005.17	-5.36
2005.25	-5.20
2005.33	-5.19
2005.42	-5.20
2005.50	-5.11
2005.58	-5.14
2005.67	-5.27
2005.75	-5.47
2005.83	-5.35
2005.92	-5.27
2006.00	-5.19
2006.08	-5.05
2006.17	-4.99
2006.25	-5.04
2006.33	-5.15
2006.42	-5.20
2006.50	-5.26
2006.58	-5.32
2006.67	-5.39
2006.75	-5.40
2006.83	-5.38
2006.92	-5.37
2007.00	-5.37
2007.08	-5.23
2007.17	-5.10
2007.25	-4.97
2007.33	-4.99
2007.42	-4.99
2007.50	-4.84
2007.58	-5.17
2007.67	-5.26
2007.75	-5.21

Year	RT4S $\delta^{18}O$‰ (continued)
2007.83	-5.12
2007.92	-5.04
2008.00	-4.92
2008.08	-4.77
2008.17	-4.90
2008.25	-4.93
2008.33	-4.95
2008.42	-4.82
2008.50	-4.83
2008.58	-5.05
2008.67	-5.32
2008.75	-5.41
2008.83	-5.21
2008.92	-5.29
2009.00	-5.16
2009.08	-4.98
2009.17	-5.02
2009.25	-4.89
2009.33	-4.83
2009.42	-4.82
2009.50	-5.08
2009.58	-5.02
2009.67	-5.04
2009.75	-5.39
2009.83	-5.45
2009.92	-5.45
2010.00	-5.44
2010.08	-5.42
2010.17	-5.33
2010.25	-5.26
2010.33	-5.18
2010.42	-5.10
2010.50	-5.15
2010.58	-5.12

Year	RT4S $\delta^{18}O$‰ (continued)
2010.67	-5.23
2010.75	-5.30
2010.83	-5.08
2010.92	-5.08
2011.00	-5.01
2011.08	-4.90
2011.17	-4.91
2011.25	-4.96
2011.33	-4.93
2011.42	-5.00
2011.50	-5.08
2011.58	-5.12
2011.67	-5.05
2011.75	-5.02
2011.83	-5.00
2011.92	-4.94
2012.00	-5.05
2012.08	-5.13
2012.17	-5.14
2012.25	-5.12
2012.33	-5.01
2012.42	-5.13
2012.50	-5.15
2012.58	-5.10
2012.67	-5.33
2012.75	-5.24
2012.83	-5.19
2012.92	-5.11
2013.00	-4.99
2013.08	-4.99
2013.17	-4.98
2013.25	-5.00
2013.33	-5.05
2013.42	-5.15

Year	RT4S $\delta^{18}O$‰ (continued)
2013.50	-5.28
2013.58	-5.22
2013.67	-5.21
2013.75	-5.29
2013.83	-5.37
2013.92	-5.29
2014.00	-5.19
2014.08	-5.10
2014.17	-5.03
2014.25	-5.13
2014.33	-5.27
2014.42	-5.20
2014.50	-5.21
2014.58	-5.35
2014.67	-5.50
2014.75	-5.64
2014.83	-5.75
2014.92	-5.75
2015.00	-5.67
2015.08	-5.45
2015.17	-5.30
2015.25	-5.41
2015.33	-5.49
2015.42	-5.35
2015.50	-5.62
2015.58	-5.76
2015.67	-5.69
2015.75	-5.77
2015.83	-5.71
2015.92	-5.81
2016.00	-5.70
2016.08	-5.66
2016.17	-5.75
2016.25	-5.72

Year	RT4S $\delta^{18}O$‰ (continued)
2016.33	-5.56
2016.42	-5.38
2016.50	-5.44
2016.58	-5.50
2016.67	-5.55
2016.75	-5.61